THE UNIVERSITY OF CHICAGO

MICROBIOME ASSEMBLY PROCESSES IN *ARABIDOPSIS THALIANA*

A DISSERTATION SUBMITTED TO
THE FACULTY OF THE DIVISION OF THE BIOLOGICAL SCIENCES
AND THE PRITZKER SCHOOL OF MEDICINE
IN CANDIDACY FOR THE DEGREE OF
DOCTOR OF PHILOSOPHY

DEPARTMENT OF ECOLOGY AND EVOLUTION

BY
CAROLINE ANNE OLDSTONE-JACKSON

CHICAGO, ILLINOIS
DECEMBER 2023

This work is dedicated to Nick, Gabriel, and Grandpop.

carry me through,

anchor me here and

ignite

TABLE OF CONTENTS

LIST OF FIGURES

LIST OF TABLES

ACKNOWLEDGMENTS

ABSTRACT

Plants are colonized by a diverse community of bacteria, fungi, and other microorganisms. This community, or microbiome, impacts numerous plant traits including growth rate, reproductive yield, abiotic stress tolerance, and disease resistance. Disentangling the processes that govern plant microbiome assembly will provide insight into plant-microbe interactions and reveal strategies to effectively engineer microbiomes to achieve ecological or agricultural goals.

In this dissertation, I explored microbiome assembly processes in Arabidopsis thaliana from several angles, First, I evaluated if plant pattern recognition receptors, one arm of the plant immune system, affect plant microbiome structure in the field. These receptors detect microbe-associated molecular patterns (MAMPs), which are prevalent across diverse microbial taxa and trigger a broad-spectrum antimicrobial response that regulates microbial growth in single microbe infections. I found that the loss of MAMP-detecting pattern recognition receptors had little effect on the structure of bacterial and fungal communities residing within the tissues of A. thaliana, despite evaluating several tissue types over four developmental stages. Next, I tested if disease induced by two native bacterial pathogens, Pseudomonas syringae NP29.1a and Pseudomonas viridiflava RMX3.1b, altered resistance phenotypes in future generations of A. thaliana. In contrast to previous work that used high intensity infections, I found no evidence that these native pathogens triggered transgenerational induced resistance; bacterial growth and disease symptoms were not significantly different between plants derived from lineages with or without historic pathogen exposure. Finally, I explored how microbial dispersal affects plant and soil microbiome assembly. Using a synthetic bacterial community in a closed, peat-based microcosm, I found that variation in bacterial through-soil dispersal rates significantly affected microbiome structure in both plants and soil for more than five weeks. Bacterial dispersal patterns generated pervasive, long-lasting priority effects over time and spatial scales highly relevant to plants in the field.

Together, this dissertation provides a deeper understanding of plant-microbe interactions and the forces that influence microbiome assembly. This work demonstrates the challenges of predicting plant interactions with complex microbial communities and/or native pathogens using results obtained from high-intensity, single-microbe infections. Thus, to understand plant microbiome assembly and function, experiments in the field, or experimental designs that mimic conditions in the field, are required. Additionally, I found that bacterial dispersal has a substantial impact on plant and soil microbiome assembly, illustrating that microbial dispersal dynamics warrant increased consideration in microbiome studies.

CHAPTER 1

INTRODUCTION

Plants are colonized by diverse microbial communities comprised of bacteria, fungi, oomycetes, and other microorganisms. This community, or microbiome, is composed of beneficial, commensal, and pathogenic microbes. The microbiome inhabits the intercellular space within plant structures (endosphere), the external surfaces of roots (rhizoplane) and aerial tissues, and the soil immediately surrounding the roots (rhizosphere). The microbiome influences numerous plant traits including growth (Vessey, 2003), phenology (Lau and Lennon, 2011; Wagner et al., 2014), abiotic stress tolerance (Rodriguez et al., 2008), and disease resistance (Vannier et al., 2019). Disentangling plant microbiome assembly rules will deepen our understanding of forces impacting plant ecology and evolution, and guide efforts to engineer plant microbiomes to improve crop performance.

In this dissertation, I investigate plant microbiome assembly rules from several angles. In recent decades, there have been considerable efforts to delineate the processes governing microbiome assembly. Abiotic conditions, soil type, host effects, and microbe-microbe interactions all shape plant microbiome structure (Hassani et al., 2018; Fitzpatrick et al., 2020; Sohrabi et al., 2023). Defining the causative agents underlying these observations, such as the specific plant genes and traits that cause host effects, is an active area of research. Importantly, even when all of the factors above are considered, significant portions of microbiome variation observed in the field remain unexplained, suggesting other relatively unexplored community assembly processes such as microbial dispersal patterns (Vannette and Fukami, 2017; Debray et al., 2022) and ecological drift (Ramoneda et al., 2020) are important components of plant microbiome assembly.

1.0.1 Community ecology in the plant microbiome

Community assembly processes that have long been studied in macroscopic communities of plants and/or animals are an excellent starting point to investigate microbiome assembly. Vellend (2010) groups the mechanisms underpinning community assembly into four classes: selection, dispersal, drift and speciation. In Vellend's (2010) conceptual synthesis, the processes governing ecological community assembly are analogous to the forces affecting population genetics, but act at the level of species rather than alleles within populations. There is evidence that all four community assembly processes, selection, dispersal, drift, and speciation, act on microbial communities. Selection acts on the fitness disparities between different species (Vellend, 2010). For example, microbe-microbe interactions in the plant rhizosphere could determine the relative abundance of species observed in a community (Durán et al., 2018). Dispersal, or the movement of individuals across space, determines if and when a given species arrives to a microbial community. Studies have demonstrated that reducing global microbial dispersal rates affects microbiome composition (Vannette and Fukami, 2017). Ecological drift is defined as the random fluctuation of species' population sizes (Hubbell, 2001; Vellend, 2010), and can be an important determinant of plant microbiome structure variation in some systems. For example, ecological drift is sufficient to explain a large portion of variation in rooibos root nodule microbiomes when grown in wild soil collected from several locations (Ramoneda et al., 2020). The final assembly process is speciation, or the generation of new species. Interestingly, evolution and speciation may play an observable role in microbial community assembly because many bacteria have short generation times and a high capacity for rapid evolution through both mutation and horizontal gene transfer. Importantly, selection, dispersal, drift and speciation do not act in isolation; these processes interact in complex ways to structure ecological communities. For example the arrival order and timing of a species to a community (dispersal) can affect the outcome of species interactions (selection) (Chase, 2003). This phenomenon, called priority effects,

has been observed in many ecological systems and can have long-term effects on community structure (Fukami, 2015). In this dissertation, I investigate how two community assembly processes, selection acting on microbes and microbial dispersal, affect members of the plant microbiome and overall assembly patterns in the model plant, *Arabidopsis thaliana*.

1.0.2   Study system

A. thaliana is an excellent model to explore plant microbiome assembly processes both in controlled laboratory experiments and in the field. *A. thaliana* is an annual plant native to Europe and Asia that was introduced to North America several hundred years ago (O'Kane and Al-Shehbaz, 1997). In the Midwestern United States, *A. thaliana* germinates in the fall, overwinters as rosettes, and then flowers and produces a large seed set in the spring. *A. thaliana* typically self-pollinates and has a relatively small, diploid genome (The Arabidopsis Genome Initiative, 2000). Overall, its rapid lifecycle, copious seed set, small genome, and large, public repositories of genetic mutants (e.g. the Arabidopsis Biological Resource Center) make *A. thaliana* a powerful genetic tool. In nature, *A. thaliana* hosts a complex microbiome (Kniskern et al., 2007; Traw et al., 2007; Bodenhausen et al., 2013; Horton et al., 2014; Beilsmith et al., 2021; Brachi et al., 2022). Importantly, many of the bacterial species that associate with *A. thaliana* can be cultured, which allows experimental reconstruction and manipulation of these communities in a laboratory setting, (Kniskern et al., 2007; Traw et al., 2007; Bodenhausen et al., 2013; Bai et al., 2015), as *A. thaliana* grows well in many conditions, including several sterile growth systems. Throughout this dissertation, I capitalize on these useful traits to investigate the role of plant genetics and microbial dispersal in plant microbiome assembly.

1.0.3   Selection and dispersal in plant microbiome assembly

Selection on the plant microbiome can be divided into three primary categories: abiotic conditions, host-effects, and microbe-microbe interactions. There are examples of all three of these factors contributing to plant microbiome structure. Abiotic conditions such as temperature, humidity, soil salinity, phosphorus availability and drought impact microbiome composition (Cheng et al., 2013; Castrillo et al., 2017; Naylor et al., 2017; Santos-Medellín et al., 2017; Berens et al., 2019; Chen et al., 2020; Karasov et al., 2022). The plant also exerts host-specific effects on microbiome assembly. Microbiome structure varies by plant species (Naylor et al., 2017; Tkacz et al., 2020; Wippel et al., 2021), genotype within species (Bulgarelli et al., 2012; Lundberg et al., 2012; Horton et al., 2014; Bergelson et al., 2019; Brachi et al., 2022), and tissue type within each individual plant (Bodenhausen et al., 2013; Beilsmith et al., 2021). Finally, both laboratory- and field-based experiments have revealed that microbe-microbe interactions structure plant microbiomes (Agler et al., 2016; Hassani et al., 2018; Durán et al., 2018; Bergelson et al., 2019; Brachi et al., 2022). In Chapter 2 and 3, I investigate how host effects, specifically two arms of the plant immune system, impact endosphere microbiome members and community assembly. In Chapter 4, I investigate how microbial dispersal dynamics affect microbiome assembly and impact selection by the host and/or microbe-microbe interactions.

Microbial dispersal likely plays a pivotal role in plant microbiome assembly (Vannette and Fukami, 2017; Baltrus, 2020; Custer et al., 2022). Dispersal patterns can influence microbiome structure by determining which microbes reach the plant and the timing of their arrival. Indeed, priority effects have been experimentally demonstrated to affect plant microbiome structure, although this is largely limited to artificial regulation of microbial arrival order (Toju et al., 2018; Carlström et al., 2019; Debray et al., 2022, but see Boynton and Peterson, 2019 for natural variation in fungal dispersal affecting microbiome structure). Despite the putative importance of microbial dispersal in community assembly, natural vari-

ation in microbial dispersal rates is largely unexplored (Barbour et al., 2023). Furthermore, it is unknown if dispersal rate variation in microbes is likely to generate priority effects, and if they do, if they have transient or long-term consequences on plant microbiome structure. In Chapter 4, I address these questions by exploring the effect of bacterial dispersal on plant microbiome assembly using a synthetic bacterial community in a closed microcosm.

1.0.4   Chapter summaries

The three chapters in my dissertation investigate different components of plant microbiome assembly with experiments in natural and controlled settings. Exploring microbiome assembly from multiple angles is necessary to fully comprehend how plant-associated communities establish. Together, these chapters paint a more complete picture of microbiome assembly rules in *A. thaliana*.

In Chapter 2, I test how one arm of plant immunity, pattern recognition receptors (PRRs) that detect widespread, non-self microbe associated molecular patterns (MAMPs), affect endophytic bacterial and fungal microbiome assembly in *A. thaliana* in the field. Four lineages of *A. thaliana* with a knockout mutation in a MAMP-detecting PRR (*fls2, efr, lore* and *lyk4*) were planted alongside congenic wild-type plants in the field in Southwest Michigan in Fall 2017. Plants germinated in the fall and overwintered as rosettes, as is typical for local *A. thaliana* populations. Several tissue types (roots, rosettes, stems, cauline leaves, flowers, and siliques) were collected at four developmental stages (vegetative, flowering, immature siliques, and mature siliques). The endophytic microbiomes of each tissue were characterized by sequencing the 799F-1193R region of 16S rRNA and the ITS1 region of the internal transcribed spacer to target bacteria and fungi, respectively. I found little effect of PRR knockout on endophytic microbiome assembly. β-diversity of fungal microbiomes were subtly shifted in *lore* mutants compared to wild-type plants in one developmental stage, suggesting that in addition to its characterized role detecting bacterial lipids, LORE may function in

regulating plant-fungal interactions. Bacterial communities were unaffected by the loss of any PRR tested. I speculate that PRRs work in collectives, are maintained through epistasis or are important in regulating specific plant-pathogen and/or plant-beneficial interactions rather than generally structuring the commensal microbiome.

In Chapter 3, I investigate if two natural pathogens isolated from *A. thaliana* in the field trigger transgenerational induced resistance phenotypes. Post-doctoral fellow Jacob Herman infected *A. thaliana* with *Pseudomonas syringae* NP29.1, *P. viridiflava* RMX3.1b, a co-infection of the two bacteria, or no bacteria over two generations. I challenged the uninfected, third-generation progeny of these lineages with either *P. syringae NP29.1* or *P. viridiflava* RMX3.1b and measured microbial growth and disease symptoms. I found no evidence of transgenerational induced resistance; infections in previous generations had no effect on bacterial growth or disease symptoms induced by infection in either trial. This suggests that the intensity of most pathogen encounters in *A. thaliana* are insufficient to trigger transgenerational induced resistance, and are thus unlikely to affect microbial growth in future generations.

In Chapter 4, I tested how microbial dispersal affects microbiome assembly in *A. thaliana* using a bacterial synthetic community (SynCom) in a closed microcosm. With the help of several undergraduates, I generated a complex, synthetic bacterial community of 83 isolates from the rhizospheres of wild-grown *A. thaliana*. I also developed a closed, sterilized-peat microcosm to test the effect of bacterial movement through soil on microbiome assembly. *A. thaliana* was planted at one end of the microcosm and bacteria were released using each of two inoculation methods. The first method required the SynCom to move through the microcosm to colonize the plant, and was achieved by inoculating the SynCom into the soil on the opposite side of the microcosm from the plant. In contrast, in the other inoculation method, the SynCom was evenly distributed throughout the microcosm, including directly onto plant tissues, and thus no movement was necessary to reach the plant. Community assembly in

plant tissues and the soil was characterized by sequencing a fragment of DNA gyrase B over the course of five weeks. I found that both plant and soil microbiomes were affected by microbial dispersal treatment and that these effects persisted for at least five weeks. Further experiments revealed that differences in plant microbiome structure were largely due to widespread priority effects. Priority effects in soil community assembly had several important effects. I found that increasing distance from the inoculation site augmented the disparity between the inoculation site community and the colonized site community. Interestingly, several microbial species that persisted in the inoculation site were unable to colonize distant sites in both the soil and plant when released as part of a SynCom, despite being able to colonize the soil microcosm when released alone. Thus, I inferred that priority effects in soil communities generated "biological barriers" that effectively prevented some bacteria from dispersing through the soil and colonizing the plant. Additionally, my work demonstrates a large range of motility rates across bacterial isolates.

CHAPTER 2

MICROBE-ASSOCIATED MOLECULAR PATTERN RECOGNITION RECEPTORS HAVE LITTLE EFFECT ON ENDOPHYTIC MICROBIOME ASSEMBLY IN *A. THALIANA* IN THE FIELD

The content of this chapter was published as: Oldstone-Jackson, Caroline; Huang, Feng; and Bergelson, Joy. *Microbe-associated molecular pattern recognition receptors have little effect on endophytic Arabidopsis thaliana microbiome assembly in the field.* Frontiers in Plant Science, (2023).

2.1   Introduction

Plants closely associate with complex microbial communities composed of bacteria, fungi, oomycetes, and other microorganisms. This community, or microbiome, colonizes the soil surrounding the roots (rhizosphere), external plant surfaces, and the spaces within plants (endosphere). The microbiome affects plant growth (Vessey, 2003), phenology (Lau and Lennon, 2011; Wagner et al., 2014), abiotic stress tolerance (Rodriguez et al., 2008) and disease resistance (Vannier et al., 2019). These observations have sparked a major effort to engineer plant microbiomes to improve crop yields and tolerance to abiotic and biotic stress, thus reducing dependency on chemical fertilizers and pesticides and increasing crop resiliency to the mounting challenges of climate change. To harness the microbiome to achieve these agricultural goals, the rules governing plant microbiome assembly processes must be elucidated.

Plant microbiomes are primarily composed of microbes derived from the environment. Only a subset of environmental microbes associate with plants, suggesting that selective filtering processes prevent certain microbes from joining the plant microbiome (Bulgarelli

et al., 2012; Lundberg et al., 2012; Vorholt, 2012). Numerous factors, including abiotic conditions, microbe-microbe interactions, and host effects, underpin this selective filtering (Fitzpatrick et al., 2020). Selectivity typically increases in the endosphere; the microbial communities within plant tissues are generally less diverse than those of external plant surfaces (Bulgarelli et al., 2012; Lundberg et al., 2012; Bodenhausen et al., 2013; Coleman-Derr et al., 2016; Chen et al., 2020; Mina et al., 2020). This filtering effect is also tissue-specific (Beilsmith et al., 2021) and host genetics likely play a role in filtering environmental microbes, as plant microbiomes are typically more similar within species than between species, even when grown in common environments (Naylor et al., 2017; Tkacz et al., 2020; Wippel et al., 2021). Within-species genotype can also affect microbiome composition (Bulgarelli et al., 2012; Lundberg et al., 2012; Horton et al., 2014; Brachi et al., 2022).

How are microbes selected from the environment during colonization of plant tissues? The plant immune system is an obvious candidate, as host-microbe interactions often involve the host's immune system. The plant immune system recognizes non-self and modified-self molecules via two main classes of receptor proteins (Jones and Dangl, 2006; Dodds and Rathjen, 2010). One class, transmembrane pattern recognition receptors (PRRs), detects microbe-associated molecular patterns (MAMPs) and endogenous signals caused by damage to plant cells, known as damage-associated molecular patterns (DAMPs). MAMPs are non-self molecules commonly found across broad taxonomic classes of microbes that contribute to microbial fitness in numerous environments, such as flagellin, elongation factor Tu, chitin, peptidoglycan, and lipid metabolites (Boller and Felix, 2009; Tang et al., 2017; Kutschera et al., 2019; Schellenberger et al., 2021). Indeed, genomic surveys reveal that most, if not all, plant-associated bacteria produce immunogenic MAMPs (Garrido-Oter et al., 2018; Teixeira et al., 2019). In addition to PRRs, plants employ Resistance (R) receptors to detect effectors, molecules secreted by microbes to suppress plant immunity and/or manipulate the plant environment to promote microbial growth (Cui et al., 2015). R proteins can also detect the

modified plant targets of these effectors.

Upon detection of MAMPs, plants respond with a multifaceted response including ion fluxes, reactive oxygen species bursts, and massive transcriptional reprogramming (Boller and Felix, 2009; Macho and Zipfel, 2014). This response, pattern-triggered immunity (PTI), moderates pathogen growth and is thought to control the majority of plant-microbe interactions (Hacquard et al., 2017). If R proteins are stimulated in conjunction with PRRs, the plant can generate an amplified immune response called effector-triggered immunity (Jones and Dangl, 2006). While PTI can generate robust immunity independently of effector-triggered immunity, effector-triggered immunity requires PTI to mount meaningful resistance (Ngou et al., 2021; Yuan et al., 2021). Furthermore, PTI and effector-triggered immunity can have systemic, long-term effects on plant physiology by inducing systemic resistance (Mishina and Zeier, 2007; Pieterse et al., 2014). This causes distal, unexposed tissues to exhibit enhanced resistance to pathogen infection; a phenotype that can persist over many weeks and potentially into future generations (Luna et al., 2012).

Since MAMPs of numerous microbes are reactive with plant PRRs (Yu et al., 2019) and PTI is a central component in plant immune responses that affect microbial growth, MAMP-detecting PRRs may affect the structure of plant microbiomes. Experimental evidence from plant-microbe pairs supports the hypothesis. For example, single knockouts of many well-characterized plant MAMP-detecting PRRs in *A. thaliana* allow increased pathogen growth and/or increased disease severity (Zipfel et al., 2004; Wan et al., 2008; Nekrasov et al., 2009; Willmann et al., 2011; Wan et al., 2012; Ranf et al., 2015), likewise, transforming plants with non-native PRRs can reduce pathogen growth and disease symptoms (Lacombe et al., 2010; Liu et al., 2021). In addition to suppressing pathogen growth, plant PRRs can also mediate the interaction between plants and beneficial microbes. For example, plant beneficial *Bacillus velezensis* requires PTI induced by the PRR EF-TU RECEPTOR (EFR), which detects a small fragment of bacterial elongation-factor Tu, to efficiently colonize the *A. thaliana* root

surface (Tzipilevich et al., 2021). Similarly, beneficial arbuscular mycorrhizal fungi requires stimulation of the PRR OsCERK1, which detects fungal chitin, to effectively colonize rice (Miyata et al., 2014).

Although MAMP-detecting PRRs clearly regulate the interactions of many plant-microbe pairs, how they sculpt the complex plant microbiome is less clear. In a complex community, the effect of the plant immune system on a given microbe may depend on the activity of other community members, including immunosuppression (Ma et al., 2021; Teixeira et al., 2021). Furthermore, plants respond in a distinct manner to particular types of MAMPs (Vetter et al., 2016). The baseline expression of MAMP-detecting PRRs and their downstream signaling pathways depends on the PRR in question, tissue type and developmental stage (Millet et al., 2010; Wan et al., 2012; Wyrsch et al., 2015; Rich-Griffin et al., 2020; Emonet et al., 2021; Verbon et al., 2023), thus the influence of PRRs on microbiome assembly may be specific to the present MAMPs and localized within an individual plant. Experiments evaluating the role of MAMP-detecting PRRs in *A. thaliana* microbiome assembly using synthetic microbial communities have yielded mixed results. Colaianni et al. (2021) found that root and shoot microbiomes were depleted in bacteria carrying immunogenic versions of the MAMP flagellin compared to microbial communities in surrounding agar. On the other hand, lab-based studies using complex synthetic communities rarely observe differences in microbiome structure in MAMP-detecting PRRs knockout lines compared to wild-type plants (Bodenhausen et al., 2014; Chen et al., 2020; Wippel et al., 2021; Wolinska et al., 2021). However, the synthetic communities used in these experiments were derived from microbes that closely associate with wild-type plants, potentially bypassing the filtering of environmental microbes mediated by PRRs. Other greenhouse-based experiments found evidence of small effects of PRRs on plant microbiome structure using soil collected from the field (Wolinska et al., 2021; Fonseca et al., 2022). Fonseca et al. (2022) found that *A. thaliana fls2* mutant plants, which are unable to detect an epitope MAMP derived from

11

flagellin, assembled distinct rhizosphere communities compared to wild-type plants, but the rhizospheres of other PRR knockout lines (*efr* and *cerk1*, respectively) were indistinguishable from wild-type plants. Wolinska *et al.* (2021) found minor changes in endophytic (within tissue) bacterial root communities in the triple *fls2 efr cerk1* mutants compared to wild-type plants. Curiously, the triple mutant *bak1 bkk1 cerk1*, with dysfunctional coreceptors of these PRRs, had no apparent effect on bacterial community structure. Additionally, experiments using wild-soil and a synthetic community derived from the wild soil identified only partially overlapping PRRs/PRR coreceptors as important factors in structuring microbial communities (Wolinska et al., 2021).

Several key questions remain concerning the role of PRRs in microbiome assembly. When exposed to the immense microbial diversity present in the field, do MAMP-detecting PRRs modulate microbiome structure? If so, is the effect specific to certain tissues or developmental stages? To address these questions, we grew wild-type *A. thaliana* Columbia-0 and four single knockout lines of MAMP-targeting PRRs, *fls2*, *efr*, *lore* and *lyk4*, in the field in southwest Michigan. Mutant plants were prevented or impaired from detecting various well-characterized MAMPS: epitopes from bacterial flagellin or elongation factor-Tu, certain bacterial lipids (medium-chain 3-hydroxy fatty acids and 3-hydroxyalkanoates), or fungal chitin (Table 2.1). Mutant lines were also previously shown to affect the growth of at least one microbe (Zipfel et al., 2004; Nekrasov et al., 2009; Wan et al., 2012; Ranf et al., 2015). Surface sterilized seeds were planted in flats filled with field soil in Fall 2017. Flats were placed into the field, where plants germinated, overwintered as rosettes, and bolted in the spring as is typical for local, wild *A. thaliana*. At four developmental stages (Vegetative, Flowering, Unripe Siliques, Ripe Siliques) all present plant tissues, including roots, rosettes, stems, cauline leaves, flowers, and siliques (seed pods), were harvested. We characterized the endophytic microbiome of each tissue because the microbial filtering effect is strongest in internal plant spaces. This experiment reveals a comprehensive picture of if, when, and

where MAMP-detecting PRRs influence *A. thaliana* endosphere microbiome structure in the field.

Receptor Name	MAMP detected	Microbes affected	References
FLAGELLIN-SENSITIVE 2 (FLS2)	flg22 epitope from flagellin	bacteria	Zipfel et al. 2004
EF-TU RECEPTOR (EFR)	elf18 epitope from EF-Tu	bacteria	Zipfel et al. 2006, Nekrasov et al. 2009
LIPOOLIGOSACCHARIDE-SPECIFIC REDUCED ELICITATION (LORE)	medium-chain 3-hydroxy fatty acid metabolites	bacteria	Ranf et al. 2015, Kutschera et al. 2019, Schellenberger et al. 2021
LYSM-CONTAINING RECEPTOR-LIKE KINASE 4 (LYK4)	chitin/ ?	fungi/ bacteria	Wan et al. 2012

Table 2.1
Pattern recognition receptors evaluated in this experiment. Knockout lines of each of these receptors was planted in the field alongside wild-type plants. Bacterial and fungal microbiome composition was characterized across tissues and developmental stages.

2.2   Methods

2.2.1   Plant Materials

Wild-type *A. thaliana* Columbia-0 (Col-0) and four PRR T-DNA insertion lines in the Col-0 background were used. The mutants *lore* (SAIL_857_E06) and *lyk4* (WISCDSLOX297300_01C) were obtained from the Arabidopsis Biological Resource Center.

fls2 (SALK_141277) was a gift from J. Greenberg and *efr* (SALK_044334) was a gift from S. Robatzek. All lines were previously confirmed to be null mutants and affect microbial growth *in planta* (Zipfel et al., 2004; Zipfel et al., 2006; Nekrasov et al., 2009; Wan et al., 2012; Ranf et al., 2015). Mutant lines were confirmed homozygous mutants by T-DNA amplification with the primers listed in Appendix 6.2.1.

2.2.2   Study site and planting

The field experiment occurred from October 2017 - May 2018 at the University of Chicago Warren Woods Ecological Field Station in southwest Michigan (41.837155, -86.631). Seeds were surface sterilized with 50% bleach and stratified in sterile DI water for three days at 4°C. In late September, soil was collected from the field site and sifted with a 2 mm sieve to remove large debris. 36-cell flats were filled with the sifted soil and soil was soaked with tap water. A plastic washer was placed in the center of each cell to mark target plants, and a single stratified seed was pipetted into the center of the washer. Plant genotypes were randomized across flats. Flats were placed in shallow holes in the field site and spaces between each cell loosely packed with soil. Drainage holes in the bottom of each cell allowed contact with the surrounding soil. Until the first true leaves emerged, flats were covered with plastic domes during rainstorms to prevent seeds from washing away, but otherwise left uncovered. Flats were initially watered daily with tap water for several weeks if required. In total, 35 flats with 1250 plants (250 replicates of each genotype) were planted. Plants germinated and overwintered as rosettes as is typical for local *A. thaliana* populations.

2.2.3 Sample collection and processing

Stage	Tissues Present	Harvest Dates	n
Vegetative	root, rosette	March 9-10, 2018	40 (8 per genotype)
Flowering	root, rosette, stems, cauline leaves, flowers	April 21-23, 2018	40 (8 per genotype)
Unripe Siliques	root, rosette, stems, cauline leaves, flowers, immature siliques	May 6-15, 2018	90 (17-19 per genotype)
Ripe Siliques	root, rosette, stems, cauline leaves, flowers, immature siliques, mature siliques	May 15 - 23, 2018	40 (7-9 per genotype)

Table 2.2
Tissues and developmental stages harvested. Plants were harvested in sets of five
(one of each genotype). Developmental stages were defined as follows: Vegetative = no
reproductive tissues, Flowering = flowers present, but no siliques present, Unripe Siliques
= siliques present but immature, Ripe Siliques = at least some are ripe siliques are present.

Five soil samples spanning the experimental plot (the four corners and the center) were
collected each day plants were harvested. Flame-sterilized tweezers were pressed 5 cm deep
into the soil to extract a narrow core. Soil cores were placed into plastic storage tubes and
immediately frozen at -80°C.

Plants tissues were randomly selected for harvesting at several developmental stages
described in Table 2.2. Plants were harvested in sets of five (one of each genotype) and
immediately processed. Siliques of each plant were counted if present. Excess soil was
removed by gently patting roots with a flame-sterilized metal spatula. Roots and aerial

15

tissues were separated with a flame-sterilized razor blade and placed into a 50 mL conical tube with 25 mL of surfactant buffer (6.33 g $NaH_2PO_4\cdot H_2O$, 16.5 g $Na_2HPO_4\cdot 7H_2O$, per 1 L, autoclaved then 200 µL Silwet L-77 added) (Lundberg et al., 2012). Epiphytes were removed based on protocols described in Lundberg *et al.* (2012) and Perisin (2016). Briefly, tubes were vortexted for 15 seconds, transferred to a fresh tube of buffer, and vortexed again for 15 seconds. Any remaining clumps of soil attached to plant tissues were removed by gently rinsing with additional surfactant buffer and/or using flame-sterilized tweezers. Aerial plant parts were separated using a flame-sterilize razor blade. The entire plant was retained, and replicate parts were combined into a single tube (e.g. all cauline leaves of an individual were combined into a single sample). Separated plant parts were transferred to fresh tubes of surfactant buffer; large plant parts in 50 mL conical tubes (25 mL surfactant buffer) and small plant parts in 1.7 mL Eppendorf tubes (1 mL surfactant buffer) and sonicated for total of 5 minutes with 30 second on/off cycles. Plant parts were transferred to storage tubes and immediately placed at -80°C until further processing. If samples were too large to fit into a single tube, they were spread across additional tubes.

2.2.4 Spike-in sequences and design

Plasmids containing synthetic sequences that coamplify with ITS1 region of the fungal internal transcribed spacer region were acquired from Addgene (Tkacz et al., 2018), and synthetic sequences that coamplify the 799F - 1193R region of 16S were designed in-house (Appendix 6.7). Plasmids were grown in *E. coli* and purified using QIAGEN MiniPrep kits. Known amounts of purified plasmid were added to the initial PCR reaction to allow absolute quantitation of microbial load across samples as described in (Tkacz et al., 2018).

2.2.5   DNA extraction

Sample preparation and DNA extraction was performed as in (Perisin, 2016). Briefly, samples were lyophilized (LABCONCO FreeZone 4.5), weighed, and randomized across plates. Negative controls (TES: 10 mM Tris-Cl, 1 mM EDTA, 100 mM NaCl) and a synthetic control community composed of 10 microbes (ZymoBIOMICS Microbial Community Standard, D6300) were included in each extraction plate. Samples were homogenized by bead beating; 2-3 sterilized 2.3 mm silica beads were added to each tube, and samples were homogenized over two, 2.5 minute cycles at 1750 RPM (2010 Geno/Grinder, SPEX). Samples that were not adequately homogenized were subjected to additional bead beating cycles using several 2.3 mm steel beads and/or manual grinding. Samples were suspended in TES at 0.05 mg sample per μL, with a minimum volume of 250 μL TES. Samples were homogenized once more at 1750 PRM for 2.5 minutes, and DNA was extracted using a double enzyme digest, chloroform/isopropanol precipitation (Perisin, 2016, Appendix 6.1.1).

2.2.6   Mutant confirmation

After DNA extraction, each plant sample from the field was tested to confirm it matched the expected genotype using T-DNA insert amplification with the primers listed in Appendix 6.2.1. Only plants that were the expected genotype were included in the downstream analysis. If samples appeared heterozygous for the T-DNA insertion (likely due to well-to-well cross-contamination), they were excluded from the analysis.

2.2.7   Library preparation and sequencing

Amplicon libraries were generated using KAPA HotStart HiFi PCR kits (Roche), with custom Illumina primers with inline barcodes (Appendix 6.2.2). Briefly, in the first amplification round, the V5-V7 region of 16S ribosomal gene (Bodenhausen et al., 2013) or ITS-1 (Horton et al., 2014) were amplified (Appendix 6.3). PCR products were purified with magnetic beads

(Appendix 6.1.2) and indexed with custom Illumina MiSeq indexing primers (Appendix 6.3, Tables 6.13 & 6.12, Appendix 6.2.2, Table 6.4). PCR products were bead purified and quantified with Quant-iT PicoGreen dsDNA kits (Invitrogen) according to manufacturer's instructions (3 μL PCR product in 200 μL total volume per sample). PCR products were pooled based on nucleic acid concentration and concentrated (SpeedVac, ThermoFisher). Concentrated pools were size selected between 200-700 bp on a 1.5% agarose gel to remove primer dimers (BluePippin, Sage Science). Size selected libraries were bead purified and library quality was assessed with a Bioanalyzer (High Sensitivity DNA, Agilent). Final libraries were sequenced on an Illumina MiSeq with a v3 2x 300 kit with $\sim$ 12% PhiX.

2.2.8   Data processing

Raw FASTQs were initially demultiplexed using the MiSeq onboard bcl2fastq2 software. Primer sequences were trimmed using cutadapt (paired 5' primers, e=2.0, minimum length = 100 for both reads) (Martin, 2011). Each MiSeq run was processed separately until chimera removal, after which libraries of the same amplicon were pooled. For 16S libraries, truncation length and maximum expected error for DADA2 were determined using FIGARO on untrimmed reads (Sasada et al., 2020). ITS1 libraries were not trimmed. Reads were filtered, inferred, and merged using DADA2 (merging = minimum 40 bp overlap) (Callahan et al., 2016). Runs within amplicon type were combined and chimeras were removed with DADA2 (method = pooled). Sequences were classified to the genera level with Naive Bayes classifiers custom-built with python scikit-learn in QIIME2 (Bolyen et al., 2019). The 16S classifier was built using the SILVA-138 database (Quast et al., 2013), and the ITS1 classifier was built using the UNITE database (version 8) (Nilsson et al., 2018). Taxonomic trees were generated using MAAFT in QIIME2 (Bolyen et al., 2019).

Spike-in sequences were identified by BLAST alignment in QIIME2. Reads mapping to *E. coli* TOP10 16S sequence were removed from the analysis, as this strain was used to grow

the plasmid carrying the spike sequence. Downstream analysis was performed in R (R Core Team, 2022) using the phyloseq package unless otherwise noted (McMurdie and Holmes, 2013).

2.2.9 Microbial load analysis and scaling for absolute quantitation

For overall load and absolute quantitation, only samples that had 20% - 80% spike reads of the total reads were considered to improve accuracy (Tkacz et al., 2018). Experimental read counts were then scaled by the amount of spike-in sequences recovered using the following equation:

$$Experimental_{scaled} = Experimental_{raw} \times \frac{Spike_{median}}{Spike_{sample}} \tag{2.1}$$

where $Experimental_{raw}$ are the number of experimental (non-spike) reads in the sample, $Spike_{median}$ is the median count of spike reads across the data set and $Spike_{sample}$ is the number of spike reads in the sample.

2.2.10 Quality filtering

For all community composition analyses using 16S and ITS1 data sets, samples with less than 500 reads were discarded. Amplicon sequence variants (ASVs) with less than 10 reads across the entire data set were also discarded. Senescent siliques were excluded from downstream analyses because their low biomass frequently resulted in poor DNA yields and representation in microbiome data set.

2.2.11 α-diversity

Data was repeatedly rarefied to account for read depth variation (Cameron et al., 2021). Sampling depth was determined by analyzing rarefaction curves generated with the vegan package (Oksanen, 2021). Each data set was rarefied by sampling without replacement (sample depth: 16S = 1380, ITS1 = 751) 100 times. Shannon Diversity (Shannon, 1948) and Pielou's Evenness (Pielou, 1966) was calculated after each iteration of raregying for 16S and ITS1 data using the microbiome package in R (Lahti and Shetty, 2017). Faith's Phylogentic Distance corrected for species richness (Faith, 1992) was also calculated for the 16S data set using picante (Kembel et al., 2010). The mean α-diversity of each sample after 100 iterations was used in downstream analysis (Cameron et al., 2021).

Statistical analysis of α-diversity was performed using 3-way permutational ANOVA (Manly, 2007) using the following model where all terms interact:

$$AlphaDiversity = Tissue * Stage * Genotype \qquad (2.2)$$

2.2.12 Defining the core microbiome

As is typical for plant-associated microbiome data from the field, most ASVs present in the data set were very rare (Bodenhausen et al., 2013; Horton et al., 2014; Beilsmith et al., 2021; Brachi et al., 2022). To effectively compare microbial communities to one another, we limited our β-diversity analyses to the core microbiome. We defined the core microbiome in three ways. Core A represents a global plant endophyte core, spanning all plant parts and developmental stages. ASVs with at least 0.5% relative abundance in four or more samples across the data set were retained. Core B represents a core compiled from tissue and stage specific communities, since tissue type and developmental stage affects microbiome composition of *A. thaliana* at our field site (Beilsmith et al., 2021). Samples were separated by tissue type and stage score, and ASVs with $\geq 1\%$ relative abundance in at least 20% of

samples in at least one subset were retained. Finally, the Indicator Core was composed of ASVs enriched in the plant compared to the surrounding soil, determined by the indicspecies package (De Cáceres and Legendre, 2009).

2.2.13 β-diversity analysis

Sample depth variation: rarefying

Filtering levels	Transformation methods	Diversity metrics
Core A	Repeat rarefy	Bray-Curtis
Core B	Repeat rarefy, spike-in scaled	Jaccard
Indicator Core		Weighted Unifrac*

Compositionality: log ratio transformations

Filtering levels	Transformation methods	Diversity metric
Core A	Robust center log ratio	Euclidean (Aitchison)
Core B	Additive log ratio (spike-in scaled)	
Indicator Core		

Table 2.3
Data filtering, transformations, and diversity metrics used in β-diversity analysis. Each factorial combination of core type, data transformation and diversity metric were compared. Core A: Retained ASVs with at least 0.5% relative abundance in four or more samples across the data set. Core B: Retained ASVs with at least 1% relative abundance in at least 20% of samples within one or more tissue by stage subset (i.e. rosettes at the vegetative stage). Indicator Core: Retained ASVs significantly associated with the plant compared with the surrounding soil. *Weighted Unifrac used in 16S analysis only.

β-diversity, or measures of (dis)similarity between communities was assessed to determine the extent that experimental factors (tissue, stage, and genotype) influence community composition. Numerous combinations of core filtering procedures, data transformations, and

β-diversity indices were completed (summarized in Table 2.3).

Two broad classes of transformations methods, rarefying and log ratio transformations, were applied to the data sets. Each transformation method was applied to each core microbiome (as previously defined), which then was analyzed with the appropriate distance metric(s).

Rarefying

Sample depth varies over three orders of magnitude in these data sets. To mitigate the spurious correlations generated by read depth variation, we repeat rarefied the ASV table 100 times (sample depth: 16S = 1380, ITS1 = 751) (Cameron et al., 2021). The mean ASV table from 100 rounds of rarefying was used in downstream analyses. The rarefied table was filtered according to different core definitions described previously. For absolute abundance analyses, ASV counts were scaled using the ratio of spike-in reads to the total sample reads. Bray-Curtis Dissimilarity (Bray and Curtis, 1957), which uses an abundance-weighted presence/absence metric to measure community dissimilarity, and Jaccard Index (Jaccard, 1912), which only uses presence/absence information to compare communities, were calculated on for 16S and ITS1 data sets using vegan (Oksanen, 2021). Weighted UniFrac (Lozupone et al., 2011), which incorporates both the abundance of and phylogenetic distance between each taxa was calculated for 16S data only using QIIME2 (Bolyen et al., 2019). Since UniFrac uses phylogenetic tree branch lengths to determine the phylogenetic relatedness between taxa, it cannot be used on ITS data reliably.

Log ratio transformations

We also used β-diversity analyses appropriate for compositional data sets (Quinn et al., 2019) in parallel with the transformations described above. Transformations included the robust

center log ratio (rCLR) (Martino et al., 2019) and additive log ratio (ALR) (Aitchison, 1986). For rCLR transformations, core microbiomes were scaled to the median read depth before transformation. For ALR calculations, core microbiomes ASV counts were scaled by the number of spike reads within the sample. The Euclidean distances between log-transformed communities were used for downstream cluster analyses (Quinn et al., 2019).

Statistical analysis of β-diversity metrics

The factors influencing microbiome community structure in all resulting distance matrices were evaluated using PERMANOVA (Anderson, 2017) with the *adonis2* function in vegan (Oksanen, 2021), using the equation:

$$Distance \sim MiSeqRun : Plate + Tissue * Stage * Genotype \quad (2.3)$$

where plate nested in MiSeq run is considered a random effect, and tissue, stage, and genotype are fixed effects in a three-way interaction.

2.2.14   Differential abundance

Differential abundance analysis was performed using ANCOM-BC2 (Lin and Peddada, 2020). Untransformed (raw counts) core microbiomes were analyzed in ANCOM-BC2. The effect of genotype was tested with the model:

$$Abundance \sim Tissue + Stage + Genotype \quad (2.4)$$

We also manually tested the interactions between genotype, stage and tissue. To accomplish this, the data were subsetted by tissue, stage, and tissue by stage, and the data was reanalyzed for a genotype effect.

2.2.15   Within genotype microbiome dispersion

To test if microbiome community structure was equally variable within different genotypes, the genotype group dispersion was calculated using PERMDISP2 (Anderson et al., 2006), implemented using the *betadisper* and *permutest* functions in vegan Oksanen (2021). This analysis was applied to distance matrices generated by all microbiome cores, transformation methods, and β-diversity indices generated in previous sections. Additionally, dispersion was evaluated in a minimally filtered data set to capture variability derived from rare community members. Since PERMDISP2 can only be applied to models with a single factor, we evaluated the dispersion of different genotype across all tissues and stages, as well as the genotype within stage, tissue, and tissue within stage to test for an interaction between genotype and other fixed factors.

2.2.16   Microbiome variation within individual plants

We tested if microbiomes derived from different tissues of the same individual plant were more similar to one another in PRR knockout lineages compared to wild type plants. Three different tissue subsets were analyzed: 1) all tissue types (roots, rosettes, stems, cauline leaves, flowers, and siliques) to cover the possible scope of within-plant tissue variation (limited to the final developmental stages) 2) roots and rosettes only to allow all developmental stages to be assessed and 3) all aerial tissues except siliques, because above-ground selective pressures are highly distinct from below-ground pressures. Only individual plants with all relevant tissue types present in the data set were considered in each subset.

After selecting appropriate samples, distance matrices were generated using Bray-Curtis dissimilarity. The *betadisper* function was used to ordinate these data and calculate the distance between the median community of individual plant and each its associated tissues (Oksanen, 2021). The mean of these distances used to quantify tissue similarity within individuals. A permutational ANOVA was used to determine the influence of stage and

genotype on within individual community similarity with the following equation:

$$MeanDistanceToMedian \sim Stage * Genotype$$

2.2.17 Early fitness analysis

Two fitness proxies for vegetative biomass and seed output (Violle et al., 2007) were assessed: rosette dry weight (vegetative biomass) and silique count (seed production). Rosette dry weight and siliques counts were measured during sample processing as described in section 2.2.3. Plants were harvested before all siliques emerged, thus this assay assessed only early fitness. As expected, rosette dry weight typically correlated with total silique count (Figure 2.1).
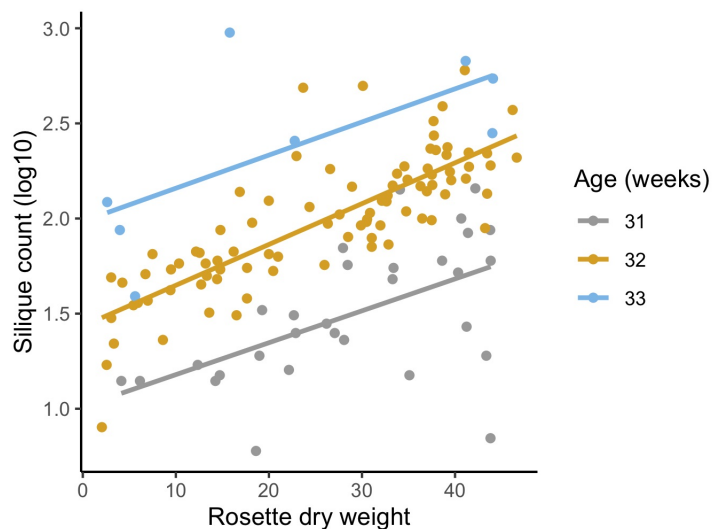
Figure 2.1
Rosette dry weight significantly correlates with silique count in week 31 and week 32. Pearson correlation of rosette dry weight and silique counts by plant age in weeks. Week 31, n=30, R^2=0.55, p=0.002; week 32, n=88, R^2=0.81, p<0.001; week 33, n=8, R^2=0.67, p=0.07.

2.3   Results

2.3.1   A single PRR knockout does not affect endophytic microbiome α-diversity

Endophytic microbiomes appear to actively filter environmental microbes (Bulgarelli et al., 2012; Lundberg et al., 2012; Wippel et al., 2021) As front-line mediators of plant-microbe interactions, MAMP-detecting PRRs may contribute to this effect. We tested if the endosphere microbiomes of PRR mutant plants had increased α-diversity, which could indicate less plant selectivity. We calculated Shannon Diversity (Shannon, 1948) on rarefied 16S and ITS1 data sets and Faith's Phylogenetic Distance scaled for species richness (Faith, 1992) on the rarefied 16S data set. To account for data loss from rarefying, this process was repeated 100 times and the mean diversity score was used in statistical analyses (Cameron et al., 2021). There was no difference between PRR knockouts and wild-type plants in bacterial or fungal Shannon diversity (three-way permutational ANOVA, $p > 0.05$; Figure 2.2, Supplemental Tables 2.4 and 2.5) or the Faith's phylogenetic distance of bacterial communities (three-way permutational ANOVA, $p > 0.05$; Supplemental Figure 2.9, Supplemental Tables 2.4 and 2.5). Tissue type, developmental stage, and the interaction between these factors affected α-diversity (Supplemental Tables 2.4 and 2.5). We also considered the possibility that MAMP-detecting PRRs preferentially filter high-growth, pathogenic microbes. If PRR knockout allows previously excluded pathogens to infiltrate and then dominate the microbiome, community evenness - the distribution of abundances of the species in the community - may be affected. However, we did not find any support for this supposition; Pielou's evenness in bacterial and fungal microbiomes is indistinguishable between PRR knockouts and wild-type plants (three-way permutational ANOVA, $p > 0.05$; Supplemental Figure 2.10, Supplemental Tables (2.4 and 2.5).
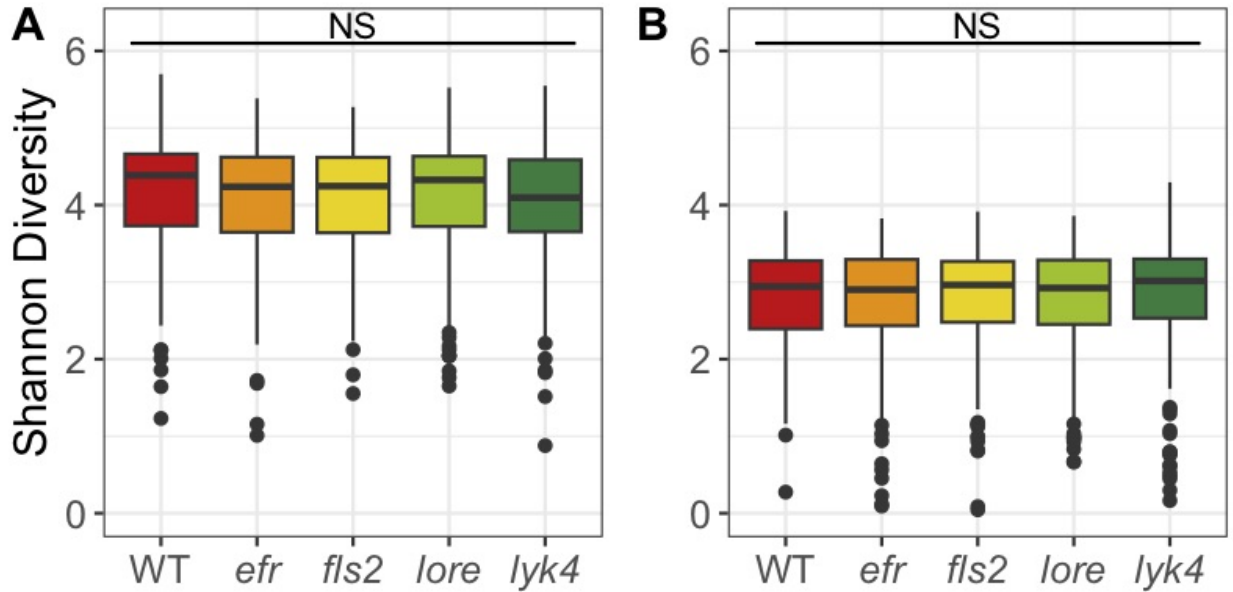
Figure 2.2
No significant effect of PRR knockout on Shannon diversity of bacterial or fungal microbiomes. PRR knockouts *efr, fls2, lore,* and *lyk4* do not have significantly different Shannon diversity than wild-type plants of A) bacterial or B) fungal communities, either as a main effect (permutational ANOVA, $p > 0.05$) or in interactions with tissue and stage (permutational ANOVA, $p > 0.05$; Supplemental Tables 2.4 and 2.5).

2.3.2 A single PRR knockout has a small effect on fungal, but not bacterial, endosphere microbiome composition

We then asked if PRRs affected the β-diversity of endosphere microbiome composition. We evaluated the significance of genotype, tissue type, and developmental stage on core endosphere microbiome structure using several different approaches to target different features of β-diversity (Table 2.3). PRR knockout had a small effect on endophytic fungal communities and interacted with developmental stage (Fig. 2.3, Bray-Curtis, $R^2 = 0.0044$, $p < 0.05$, Supplemental Table 2.8), although this effect was detected in only some β-diversity metrics (Supplemental Tables 2.8 2.9). Post-hoc analyses revealed that genotype affected endosphere fungal communities in the Unripe Siliques and Ripe Siliques stages (PERMANOVA, $p < 0.05$ and $p < 0.05$, respectively). Pairwise comparisons showed that *lore* knockouts had

statistically different fungal communities than wild-type plants in the Ripe Siliques stage (Bray-Curtis, wild-type vs. *lore* pairwise PERMANOVA within the Ripe Siliques developmental stage, $R^2 = 0.015$, $p < 0.05$). This was surprising because *LORE* detects some bacterial lipids (Ranf et al., 2015; Kutschera et al., 2019; Schellenberger et al., 2021), but has no documented effect on fungi. However, it is possible that *LORE* has a yet undocumented interaction with fungal MAMPs - other PRRs detect multiple elicitors and affect plant interactions with both fungi and bacteria (Willmann et al., 2011; Wan et al., 2012). Alternatively, the bacterial microbiome has been shown to strongly influence fungal microbiome structure (Durán et al., 2018); if *LORE* transiently affected the bacterial community, this may have had cascading effects on the fungal microbiome. Other notable but statistically insignificant differences in fungal community composition between wild-type and PRR knockouts include *lore* in the Unripe Siliques stage and *lyk4*, a chitin-responsive PRR, in the Ripe Siliques stage (Bray-Curtis, pairwise PERMANOVA: $R^2 = 0.0081$, $p = 0.069$ and $R^2 = 0.041$, $p = 0.067$, respectively). Finally, genotype effects were only detectable on the ITS1 ASV level (data not shown). In contrast, genotype had no effect on bacterial β-diversity across all core communities, transformation methods and diversity metrics (Figure 2.3, PERMANOVA, $R^2 = 0.005$, $p > 0.05$, Supplemental Table 2.6 and 2.7). Additionally, genotype had no effect on bacterial community composition at higher taxonomic levels (data not shown). Considering all of the β-diversity analyses together, we found that PRRs have little effect on endosphere microbiome β-diversity as effects were limited to a single genotype and developmental stage within the fungal microbiome.

We next evaluated if any bacterial or fungal ASVs were differentially abundant between wild-type and PRR knockout lineages using ANCOM-BC2 (Lin and Peddada, 2020). No bacteria or fungi were differentially abundant when genotype was considered across the entire data set, nor when genotype was tested within tissue, developmental stage, or tissue by stage subsets (ANCOM-BC2, $p > 0.05$).
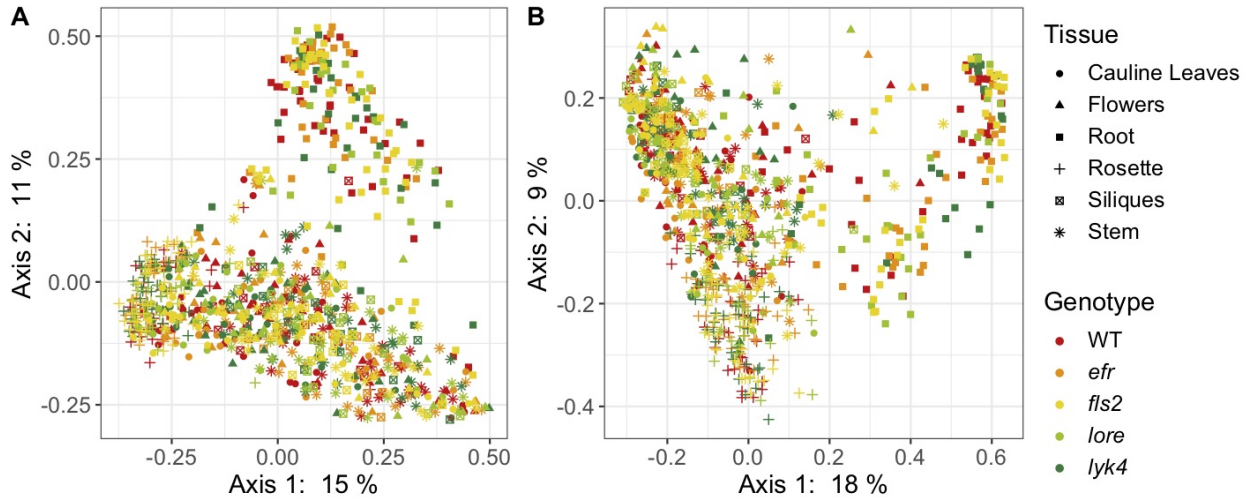
Figure 2.3
PRR knockout has subtle effects on the Bray-Curtis β-diversity of endophytic fungal microbiomes, but not bacterial microbiomes. Principle Coordinate Analysis (PCoA) of Bray-Curtis distances between bacterial (A) or fungal (B) microbiomes. (A) PRR mutations, denoted by color, do not explain community variation in Bray-Curtis distances in endophytic bacterial communities as a main effect or as an interaction with tissue and/or stage (PERMANOVA, $p > 0.05$). (B) PRR genotype had subtle effects on Bray-Curtis distance but this effect is not obvious on primary PCoA axes (PERMANOVA, $R^2 = 0.005$, $p < 0.05$). In accordance with previous work at this field site, tissue type (represented by shape) had the strongest effect on community composition (Beilsmith et al., 2021, PERMANOVA, bacteria: $R^2 = 0.183$, $p < 0.05$; fungi $R^2 = 0.121$, $p < 0.05$).

2.3.3   A single PRR knockout and wild-type plants show no difference in microbiome variability

Plant control of the microbiome can manifest in numerous ways. Host selection is a deterministic force governing microbiome assembly (Bulgarelli et al., 2012; Lundberg et al., 2012; Horton et al., 2014; Tkacz et al., 2020; Wippel et al., 2021; Brachi et al., 2022). If the host plant is unable to effectively select microbes, variability (i.e. dispersion) in microbiome structure between individuals could increase as stochastic processes such as microbial dispersal and drift become more important in community assembly (Arnault et al., 2022). Thus, if PRRs contribute to host control of the microbiome, within-genotype microbiome variability

in PRR mutants may be increased compared to variability between wild-type plants. To test this, we compared β-diversity dispersion of each genotype using the PERMDISP2 procedure (*betadisper* function in vegan (Oksanen, 2021)). Neither bacterial nor fungal communities were more variable within PRR mutants than within wild-type plants, even if the effects of tissue and stage were controlled (Figure 2.4, PERMDISP2 analysis of multivariate homogeneity of group dispersions, $p > 0.05$, Supplemental Table 2.10). This indicates that single PRRs are not required for deterministic selection of environmental microbes.
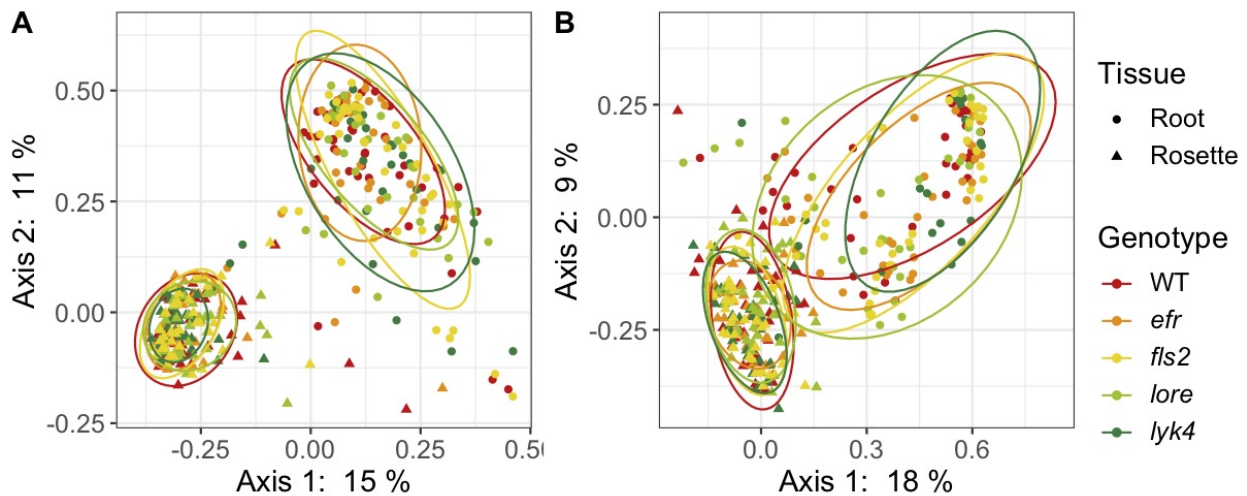
Figure 2.4
PRR mutant microbiomes are not more variable than wild-type microbiomes.
PCoA of Bray-Curtis distance of (A) bacterial and (B) fungal communities. Only roots and rosettes are shown. To visualize group dispersions, ellipses encircle the 80% confidence interval t-distribution of samples in genotype group and are colored according to genotype. Genotype has no statistical effect on within-group microbiome variation (PERMDISP2, $p > 0.05$). Further, there is no effect of genotype on microbiome variability within tissue, stage, and tissue by stage subsets (PERMDISP2, all subsets $p > 0.05$).

2.3.4 The degree of tissue specificity in endophytic microbiome structure is not affected by the loss of individual PRRs, but changes over time.

PRRs and plant immunity may help maintain the distinct microbial communities found in each tissue via two mechanisms. First, the expression patterns of MAMP-detecting PRRs

and the regulation of downstream immune signaling pathways is cell-type specific (Millet et al., 2010; Wan et al., 2012; Beck et al., 2014; Vetter et al., 2016; Rich-Griffin et al., 2020; Emonet et al., 2021; Verbon et al., 2023). Second, PTI may impede the systemic spread of microbes (Yadeta and Thomma, 2013; Beck et al., 2014; de Lamo et al., 2021). Interestingly, there is evidence in humans that within-individual site specificity of microbiomes decline in disease; critically ill patients exhibit reduced body-site specificity (Rogers et al., 2016). We tested if PRRs help maintain tissue specificity within individual plants by calculating Bray-Curtis distances between each tissue within each plant and then calculating the mean distance from the microbiome of each tissue to the median community of the individual plant. A two-way permutational ANOVA with genotype and development stage as fixed effects was used to test statistical significance.

We found that PRR knockout lines had the same degree of tissue-specificity of both fungal and bacterial microbiomes within individual plants (Figure 2.5, Supplemental Table 2.11. Interestingly, we found that both fungal and bacterial microbiomes of aerial tissues, excluding siliques, generally became more similar within individuals as plants matured (Figure 2.6, permutational ANOVA $p < 0.05$ with Wilcoxon post-hoc tests; Supplemental Table 2.11). Thus, although the microbiomes of most aerial tissues become more similar within individuals over time, we found no evidence that PRRs play a direct role in regulating microbiome tissue specificity in *A. thaliana*.
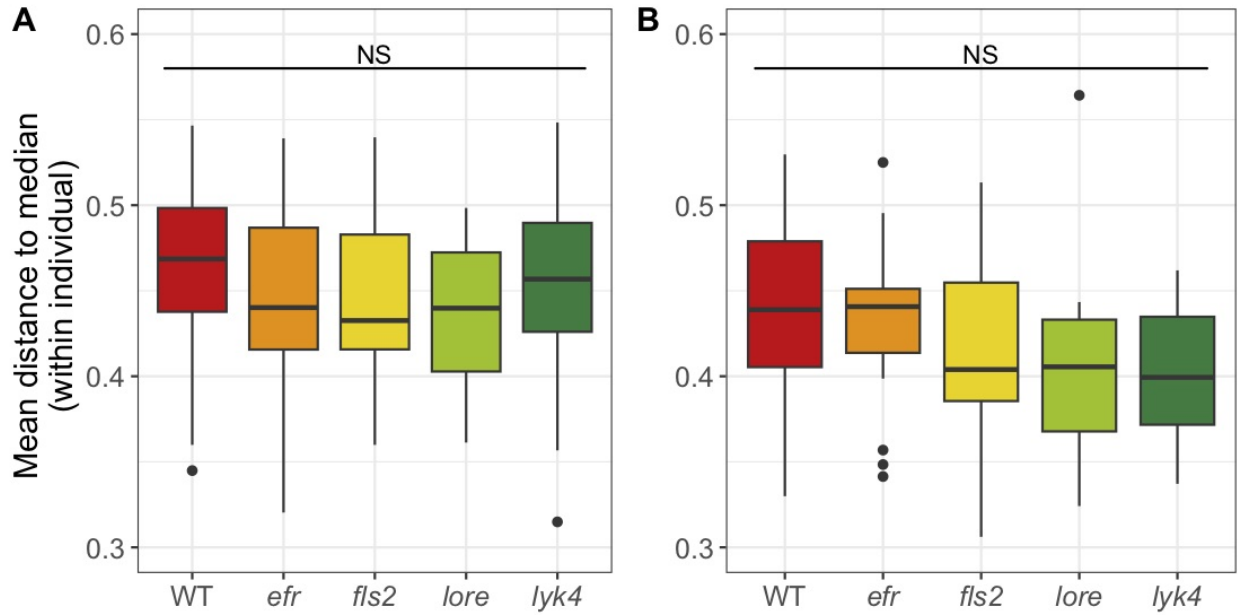
Figure 2.5
Aerial tissues within individual PRR mutants and wild-type plants do not show different levels of site-specific microbiomes. The mean Bray-Curtis distance from the microbial communities of the rosette, stems, cauline leaves, and flowers to the individual median community was calculated to measure within-individual tissue specificity. Within-individual tissue specificity does not vary by genotype in A) bacterial (Kruskal-Wallis, $p > 0.05$) or B) fungal communities (Kruskal-Wallis, $p > 0.05$).
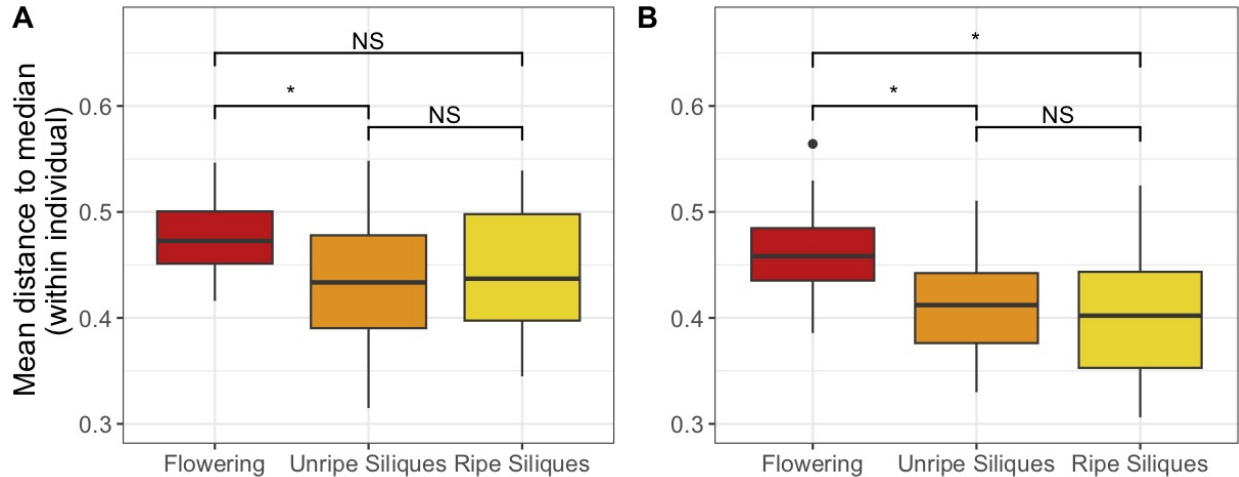
Figure 2.6
Aerial tissues of individual plants generally become more similar as plants age.
In bacterial communities (A), the mean distance of each tissue's microbiome to the plant median community decreased between the Flowering (no siliques present) and Immature Siliques stages, thus tissues became more similar (Kruskal-Wallis, $p < 0.05$, Wilcoxon post-hocs with Benjamini-Hochberg correction for multiple testing). However, this trend did not hold in the Mature Siliques stage (Wilcoxon post-hoc, $p > 0.05$ after p-value adjustment.) In fungal communities (B), site specificity was significantly higher in Flowering plants than both the Immature Siliques and Mature Siliques stages, indicating that, like bacterial communities, fungal communities associated with different tissues became more similar over time (Kruskal-Wallis, $p < 0.05$, with Wilcoxon post-hocs with Benjamini-Hochberg correction for multiple testing).

2.3.5   No evidence of increased microbial load or reduced fitness in single PRR knockouts

In binary laboratory infections, a single PRR knockout can increase microbial load (Zipfel et al., 2004; Wan et al., 2008; Nekrasov et al., 2009; Willmann et al., 2011; Wan et al., 2012; Ranf et al., 2015). It is critical that plants regulate the total microbial load, as high microbial loads are associated with reduced fitness in the field (Traw et al., 2007). We thus asked if PRRs regulate total microbial load and if PRR mutants affected early fitness indicators. To estimate microbial load, a known amount of synthetic spike-in DNA that co-amplified with 16S or ITS1 was added to the initial PCR reaction. This allowed us to estimate total

microbial load by scaling total read counts by the number of spike sequences (Tkacz et al., 2018). We detected no change in either bacterial or fungal load in PRR knockouts compared to wild-type plants (Figure 2.7A, Bacterial load: ANOVA, $p > 0.05$, Figure 2.7B, Fungal load: ANOVA, $p > 0.05$, and Supplemental Table 2.12). We also failed to find evidence that loss of MAMP-detecting PRRs impacted early silique counts (Figure 2.8A: Kruskal-Wallis, $p > 0.05$) or rosette dry weight (Figure 2.8B: Kruskal-Wallis, $p > 0.05$). Thus, we found no evidence that individual MAMP-detecting PRRs control total microbial load in the field, nor that PRRs impact early plant fitness.
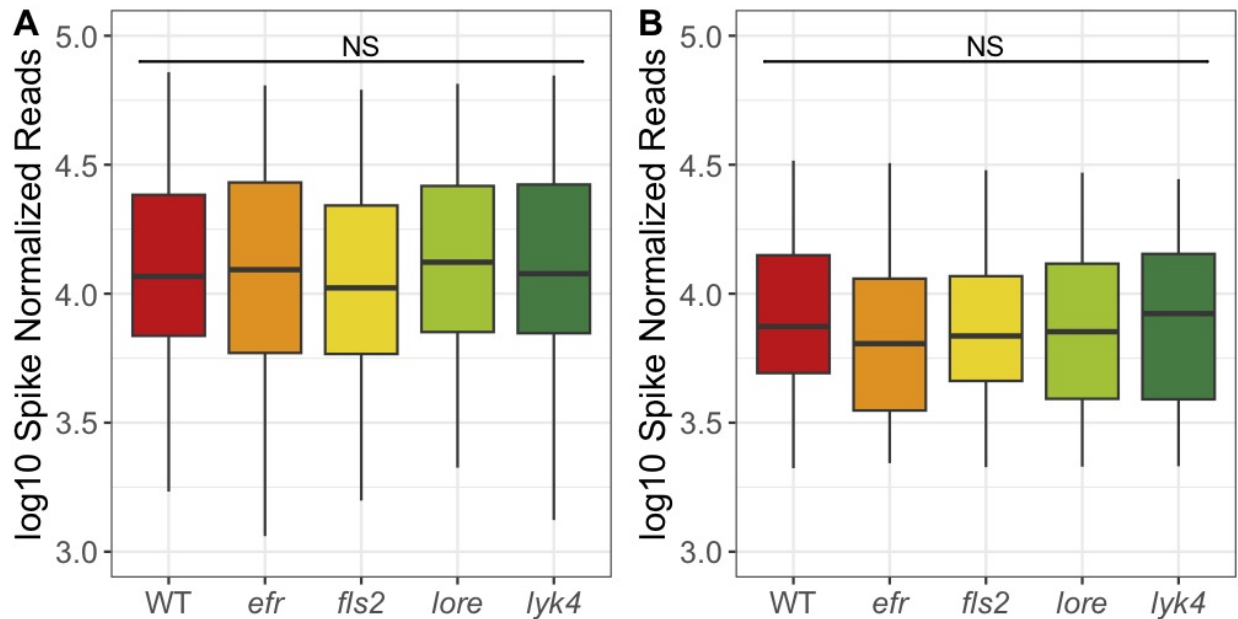
Figure 2.7
PRR knockout does not affect bacterial or fungal load. Microbial load was calculated by adjusting to microbial reads to synthetic spike-in read counts. Wild type and PRR knockout plants do not have significantly different microbial loads of bacteria (A) or fungi (B) (ANOVA, $p > 0.05$)
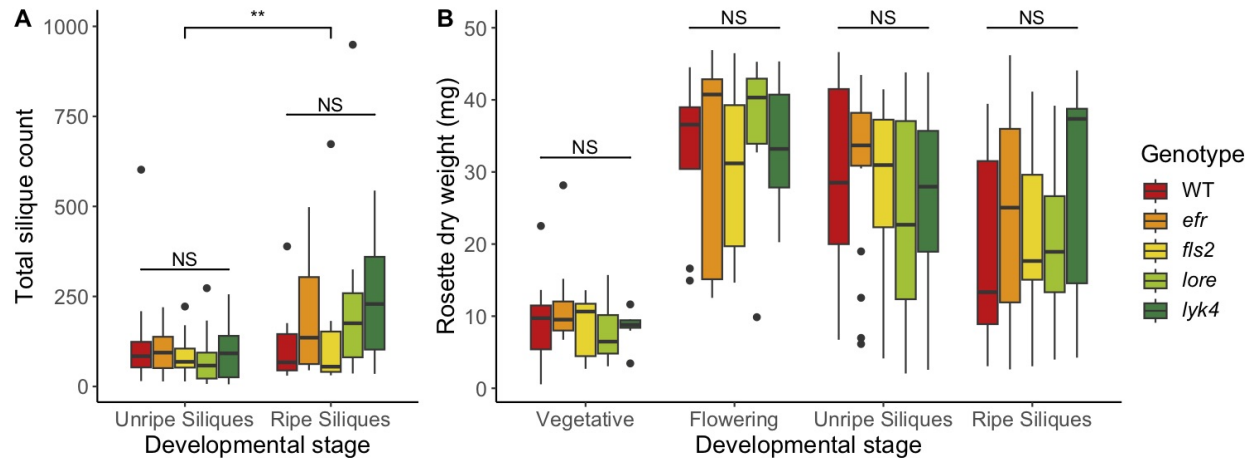
Figure 2.8
No significant effect of PRR knockout on early plant fitness in the field. (A)
Silique counts and (B) rosette dry weight were measured as early fitness indicators. PRR
knockouts *efr, fls2, lore*, and *lyk4* do not have significantly different silique counts
(Kruskal-Wallis within stage, $p > 0.05$) or rosette dry weight (Kruskal-Wallis within stage,
$p > 0.05$) than wild-type plants when grown under field conditions. Sample size per
genotype within stage: Vegetative: n = 7-8, Flowering: n = 7-8, Immature Siliques: n =
17-19, Mature Siliques: n = 7-8.

2.4   Discussion

Complex microbial communities assemble on and within plant tissues, influencing plant
phenotype. A key aim of many research programs is to effectively engineer these plant-
associated microbiomes to achieve agricultural objectives, such as increased yield or resilience
to abiotic and biotic stress. Elucidation of microbial community assembly rules has the
potential to improve the efficiency and reproducibility of these efforts.

Plant-associated microbiomes are comprised of only a subset of the microbes present
in the environment, suggesting that plants filter and/or select associated microbes. Plant
immunity, which includes pattern recognition receptors that detect microbial MAMPs, is
thought to impact the structure of microbial communities (Kniskern et al., 2007; Traw et al.,
2007; Carvalhais et al., 2015; Lebeis et al., 2015; Hacquard et al., 2017; Kudjordjie et al.,
2021; Colaianni et al., 2021; Parys et al., 2021; Fonseca et al., 2022). Indeed, in binary

plant-microbe interactions, single MAMP-detecting PRRs affect the colonization and *in planta* growth of particular bacteria or fungi (Zipfel et al., 2004; Nekrasov et al., 2009; Vetter et al., 2012; Wan et al., 2012; Ranf et al., 2015; Colaianni et al., 2021; Parys et al., 2021). However, the impact of PRRs on the assembly of complex endophytic microbial communities in the field is unknown. We characterized both bacterial and fungal endophytic microbiomes of wild-type *A. thaliana* and MAMP-detecting PRR knockout lines grown in the field, across several developmental stages and plant parts. This unprecedented scope allowed us to determine if, when, and where individual MAMP-detecting PRRs shape the endophytic microbiome in the field.

We found little evidence that individual MAMP-detecting PRRs impact endophytic microbiome structure despite measuring several α-diversity and β-diversity metrics, the variability in microbiome composition, the degree of tissue differentiation within individual plants, and the estimated total microbial load. We also failed to find an impact of PRRs on early plant fitness indicators. Indeed, we found no effect of PRR knockouts on the composition of bacterial communities and, for fungal communities, only Bray-Curtis and Jaccard diversity were altered in PRR knockout lineages (both $R^2 = 0.005$, $p = 0.03$; Supplemental Table 2.8). Post-hoc analyses revealed that *lore* mutants hosted slightly modified fungal communities compared to wild-type plants, potentially revealing a role for *LORE* in plant-fungal interactions. Field data suggests that fungal communities can be affected by host factors that do not impact the bacteria community (Horton et al., 2014; Bergelson et al., 2019; Brachi et al., 2022) and that fungal communities are more strongly affected by host genotype than bacterial communities (Bergelson et al., 2019). A restricted impact of PRRs on fungi is furthermore consistent with analyses of co-occurrence networks suggesting that most microbe-microbe effects in wild *A. thaliana* occur within kingdom (Agler et al., 2016; Bergelson et al., 2019; Brachi et al., 2022).

There are several possible explanations for the general lack of effect of PRRs on micro-

biome community structure. First, redundancy in the plant immune system may maintain robust plant immune responses despite the loss of a single PRR. Members of microbial consortia produce diverse MAMPs that induce PTI to varying degrees (Garrido-Oter et al., 2018; Colaianni et al., 2021; Parys et al., 2021). Although loss of an individual PRR allows increased microbial proliferation in single microbe inoculations (Zipfel et al., 2004; Wan et al., 2008; Nekrasov et al., 2009; Willmann et al., 2011; Wan et al., 2012; Ranf et al., 2015), in complex microbial consortia, there may be some microbes that elicit PTI via other intact PRRs which could counteract this phenomenon. In nature, the plant respond to a complex input of MAMPs, DAMPs, effectors and other signals. Compellingly, Zhou *et al.* (2020) demonstrated that MAMP signaling must coincide with cellular damage to generate substantial PTI. Thus, depending on the combination of signals produced by the microbiome, commensals may largely avoid activating PTI.

Some plant-associated microbes have the ability to suppress plant immune responses, a process that facilitates the colonization of PTI-triggering microbes (Ma et al., 2021; Teixeira et al., 2019). Three independent surveys (Yu et al., 2019; Ma et al., 2021; Teixeira et al., 2021) found that 31%-42% of plant-associated bacteria suppress PTI. This trait spans broad taxonomic categories and, importantly, the impact of suppressive strains dominates that of nonsuppressive strains in mixed bacterial communities (Ma et al., 2021; Teixeira et al., 2019). Considering the frequency, taxonomic diversity, and dominance of this trait, immunosuppressive microbes almost certainly affected community assembly in our natural microbiomes. If the anti-microbial response generated by stimulating PRRs is dampened by the endophytic microbiome, loss of a PRR would have little effect on subsequent microbiome assembly, as observed in our experiment. In this case, other aspects of plant-microbe associations such as plant structural components, bacterial metabolism, and microbe-microbe interactions (Horton et al., 2014; Bai et al., 2015; Levy et al., 2018; Salas-González et al., 2021; Velásquez et al., 2022) would have relatively more influence on commensal microbiome

structure.

This study provokes two related questions. First, if PRRs are effectively redundant, why does selection maintain multiple PRRs? Second, if pattern-triggered immunity is broadly suppressed, why maintain PRRs at all? One hypothesis (Hacquard et al., 2017) is that rather than filtering microbes from the environment, PRRs help regulate the total microbial load of the commensal microbiome to prevent damaging overgrowth. We found no evidence that single MAMP-detecting PRR knockouts supported higher microbial loads in the field (Figure 2.7 and Supplemental Table 2.12). Related experiments using PRR and PRR coreceptor multi-mutants report conflicting impacts of these genes on microbial load, both within and between experiments (Xin et al., 2016; Wolinska et al., 2021). This inconsistency suggests that PRRs regulate the microbial load of some communities, but that this is not a general effect.

An alternative hypothesis is that individual MAMP-detecting PRRs are maintained by selection from virulent pathogens or mutualists, rather than from interactions with commensals. Aggressive pathogen growth is typically accompanied by other signals such as DAMPs and effectors, which may allow the plant to overcome background PTI suppression. These pathogens are often controlled by powerful effector-triggered immunity which requires sustained PTI signaling to adequately function (Ngou et al., 2021; Yuan et al., 2021). Thus, pathogens may exert selective pressure on the specific subset of PRRs they activate, and, since different pathogens activate overlapping PRRs (Zipfel et al., 2006; Wan et al., 2012; Ranf et al., 2015; Colaianni et al., 2021; Parys et al., 2021), each receptor could be maintained through interactions with numerous pathogens, even if encounters with a particular pathogen species are infrequent. Another possibility is that mutualisms exert selective pressure on specific PRRs. For example, orthologs of the PRR *CERK1* are required for both defense against pathogenic fungi and establishing mutualisms with arbuscular mycorrhizal fungi (AMF) in several distantly related plant species (Miyata et al., 2014; Bozsoki et al.,

2017; Feng et al., 2019; Gibelin-Viala et al., 2019; Zhang et al., 2019). Because the effect of PRRs on microbiome composition would only be detectable in the presence of virulent pathogens or important mutualists in these scenarios, results between different microbiomes could be inconsistent, as has been observed in this study and others (Bodenhausen et al., 2014; Chen et al., 2020; Wippel et al., 2021; Wolinska et al., 2021; Fonseca et al., 2022). Finally, specific PRRs may be maintained due to pleiotropic effects. For example, *CERK1* appears to have a conserved role in promoting lateral root formation in numerous plants, including *A. thaliana*, independently of accommodating an AMF mutualism (Chiu et al., 2022). It is feasible that other PRRs may have developed additional functions, especially since MAMP-detecting PRRs are already integrated into growth-defense signaling pathways (Huot et al., 2014).

Finally, other biological and technical factors could explain why we detected few effects of PRRs on microbiome structure in the field. Myriad environmental conditions including temperature, humidity, soil salinity, phosphorus availability and drought are known to modulate the strength of plant immunity and affect microbiome composition (Cheng et al., 2013; Castrillo et al., 2017; Naylor et al., 2017; Santos-Medellín et al., 2017; Berens et al., 2019; Chen et al., 2020). Although the field conditions in our experiment were representative of Midwestern USA, an area in which *A. thaliana* is common (Platt et al., 2010; Exposito-Alonso et al., 2018; Shirsekar et al., 2021), it is possible that PRR signaling was rendered unimportant by environmental conditions. Nevertheless, two lines of evidence suggest that our results may be generalizable. First, we characterized endophytic microbiomes over several time points, which would mitigate the chance of mischaracterizing the effects of plant immunity due to short-term environmental fluctuations. Second, genome-wide association analyses on field-grown *A. thaliana* across years and locations occasionally identify known PRRs as candidate genomic features that affect microbiome composition, but these effects are limited to one or two specific microbes rather than overall community composition and

are often ephemeral (Horton et al., 2014; Brachi et al., 2022; Roux et al., 2023). We also cannot rule out the possibility that our lack of signal is a result of technical limitations. For example, the immunogenicity of flagellin is broadly linked to taxonomy (Colaianni et al., 2021; Parys et al., 2021), but the substantial within-genera and within-species variation of flagellin epitopes and their capacity to trigger PTI is unlikely to be resolved by 16S marker-gene sequencing (Vetter et al., 2016; Colaianni et al., 2021; Parys et al., 2021). In addition, PRRs may impact microbial subcommunities within tissues due to their localized, cell-type specific responses (Millet et al., 2010; Rich-Griffin et al., 2020; Emonet et al., 2021; Verbon et al., 2023); assessing microbiome structure of whole plant parts as we did in this experiment may mask these effects. Finally, we did not test every MAMP-detecting PRR identified in *A. thaliana*. However, even if other PRRs actively shape the commensal microbiome, why selection maintains the PRRs assessed in this experiment remains an important question.

In conclusion, we demonstrate that individual PRRs have little effect on the overall endophytic bacterial and fungal microbiome in *A. thaliana* in the field, as measured at the level of 16S and ITS1 characterization. Although initially surprising, these results offer valuable insight into the function of MAMP-detecting PRRs in the field and help target the search for plant genetic factors that play an important role in sculpting commensal microbiomes. Further investigation of hypotheses concerning the role of plant immunity in structuring the microbiome will broaden our understanding of plant-microbe interactions in a complex setting, leading to more effective plant microbiome engineering.

2.5 Supplemental Material

Diversity Metric	Factor	df	*pseudo*-F	*p*
Shannon Diversity	Tissue	5	21.066	<0.001 *
	Stage	3	4.294	0.007 *
	Genotype	4	0.749	0.565
	Tissue x Stage	10	3.122	<0.001 *
	Tissue x Genotype	20	0.763	0.742
	Stage x Genotype	12	0.517	0.891
	Tissue x Stage x Genotype	40	0.858	0.708
Faith's Phylogenetic	Tissue	5	23.732	<0.001 *
Distance (adjusted)	Stage	3	0.755	0.523
	Genotype	4	0.516	0.749
	Tissue x Stage	10	2.422	0.009 *
	Tissue x Genotype	20	1.067	0.377
	Stage x Genotype	12	0.971	0.458
	Tissue x Stage x Genotype	40	0.71	0.91
Pielou's evenness	Tissue	5	11.522	<0.001 *
	Stage	3	3.962	0.009 *
	Genotype	4	0.464	0.756
	Tissue x Stage	10	3.127	<0.001 *
	Tissue x Genotype	20	0.633	0.889
	Stage x Genotype	12	0.351	0.969
	Tissue x Stage x Genotype	40	1.204	0.185

Table 2.4
Genotype does not explain α-diversity variation in repeat rarefied bacterial microbiomes. Permutational ANOVA analyses on Shannon diversity, Faith's Phylogenetic Distance adjusted for species richness, and Pielou's Evenness. Variation in endophytic microbiome α-diversity is not explained by genotype as a main effect nor an interaction between genotype and other factors ($p > 0.05$). Tissue, developmental stage and their interaction affect α-diversity ($p < 0.05$).

Diversity Metric	Factor	df	*pseudo*-F	p
Shannon Diversity	Tissue	5	41.031	<0.001 *
	Stage	3	10.841	<0.001 *
	Genotype	4	0.603	0.685
	Tissue x Stage	10	3.446	<0.001 *
	Tissue x Genotype	20	0.928	0.551
	Stage x Genotype	12	0.882	0.548
	Tissue x Stage x Genotype	40	1.011	0.445
Pielou's evenness	Tissue	5	46.298	<0.001 *
	Stage	3	2.9	0.038 *
	Genotype	4	1.826	0.104
	Tissue x Stage	10	2.88	0.002 *
	Tissue x Genotype	20	0.769	0.736
	Stage x Genotype	12	0.83	0.613
	Tissue x Stage x Genotype	40	0.948	0.566

Table 2.5

Genotype does not explain α-diversity variation in repeat rarefied fungal microbiomes. Permutational ANOVA analyses on Shannon diversity and Pielou's Evenness. Variation in endophytic ITS1 microbiome α-diversity is not explained by genotype as a main effect nor an interaction between genotype and other factors ($p > 0.05$). Tissue, developmental stage and their interaction affect α-diversity ($p < 0.05$).
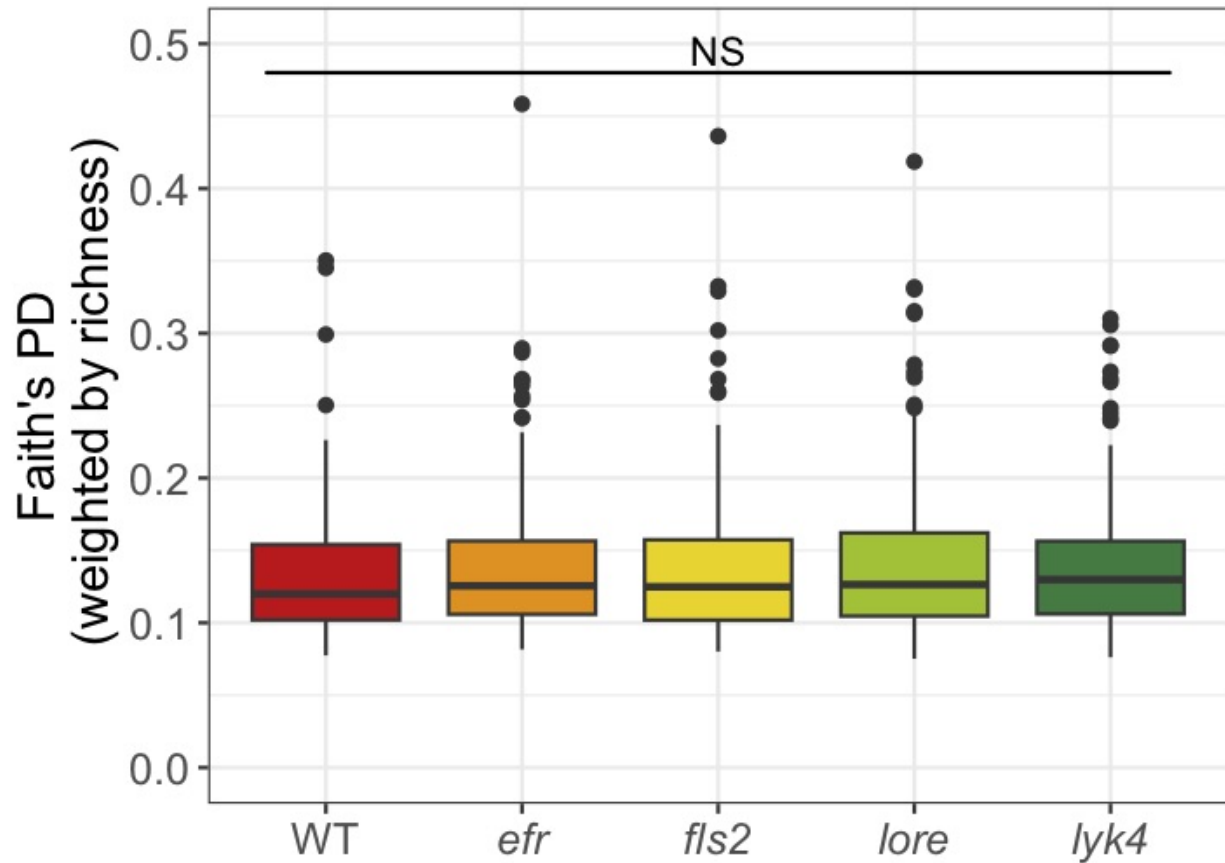
Figure 2.9
No significant effect of PRR knockout on Faith's Phylogenetic Distance (corrected for species richness) in bacterial microbiomes. Endophytic bacterial communities in PRR knockouts *efr, fls2, lore,* and *lyk4* do not differ in Faith's Phylogenetic Distance compared to wild-type plants (3-way ANOVA, $p > 0.05$).
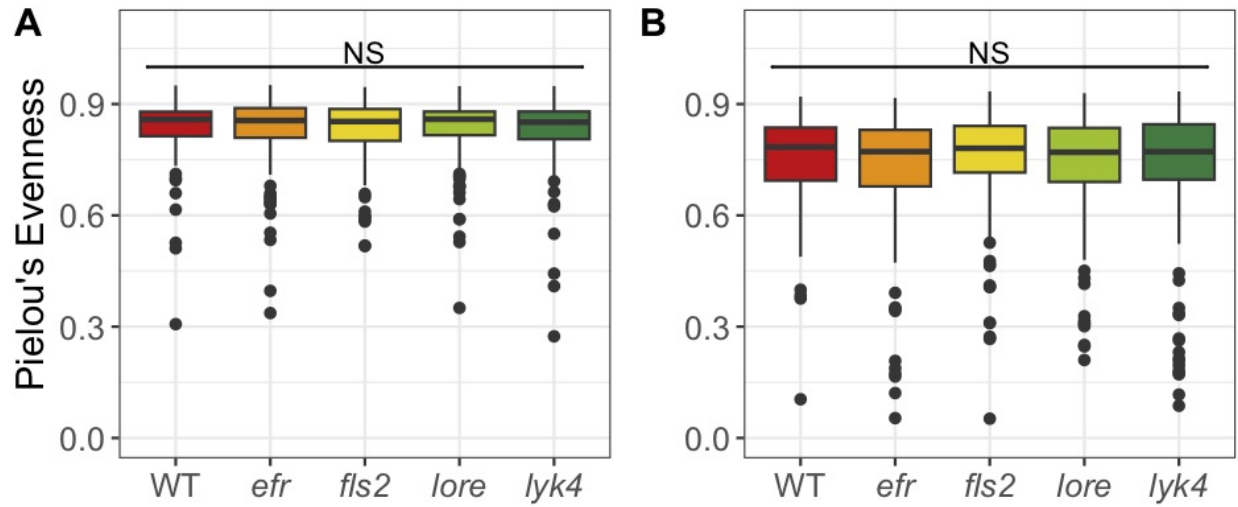
Figure 2.10
No significant effect of PRR knockout on Pielou's evenness in bacterial or fungal microbiomes. Bacterial or fungal microbiomes in PRR knockouts *efr, fls2, lore,* and *lyk4* do not differ in Pielou's evenness compared to the microbiome associated with wild-type plants (3-way ANOVA, $p > 0.05$).

Diversity Metric	Factor	df	R^2	$pseudo$-F	p
Bray-Curtis	MiSeq Run	5	0.016	3.674	0.001 *
	Tissue	5	0.183	43.159	0.001 *
	Stage	3	0.031	12.122	0.001 *
	Genotype	4	0.003	1.003	0.458
	MiSeq Run:Plate	9	0.019	2.451	0.001 *
	Tissue x Stage	10	0.031	3.596	0.001 *
	Tissue x Genotype	20	0.016	0.954	0.736
	Stage x Genotype	12	0.010	0.934	0.783
	Tissue x Stage x Genotype	40	0.031	0.915	0.972
Jaccard	MiSeq Run	5	0.013	2.694	0.001 *
	Tissue	5	0.119	25.229	0.001 *
	Stage	3	0.023	8.041	0.001 *
	Genotype	4	0.004	1.015	0.414
	MiSeq Run:Plate	9	0.017	1.973	0.001 *
	Tissue x Stage	10	0.028	3.011	0.001 *
	Tissue x Genotype	20	0.018	0.974	0.734
	Stage x Genotype	12	0.011	0.947	0.839
	Tissue x Stage x Genotype	40	0.036	0.947	0.97
Weighted UniFrac	MiSeq Run	5	0.026	6.110	0.001 *
	Tissue	5	0.327	77.960	0.001 *
	Stage	3	0.071	28.423	0.001 *
	Genotype	4	0.003	0.771	0.714
	MiSeq Run:Plate	9	0.018	2.446	0.001 *
	Tissue x Stage	10	0.028	3.382	0.001 *
	Tissue x Genotype	20	0.012	0.702	0.981
	Stage x Genotype	12	0.009	0.889	0.696
	Tissue x Stage x Genotype	40	0.030	0.885	0.824

Table 2.6
Genotype does not explain β-diversity variation in rarefied 16S core communities. PERMANOVA analyses on beta-diveristy distance matrices generated with Bray-Curtis, Jaccard and Weighted Unifrac β-diversity meterics on rarefied data sets. ASVs were included in this analysis if present at 1% relative abundance in 20% of samples in at least one tissue by stage subset (Core B). Genotype does not explain 16S core community β-diversity variation as a main effect nor interact with other factors. Statistically significant factors are denoted by asterisks and include tissue, developmental stage and their interaction (fixed effects), MiSeq run and PCR plate nested within MiSeq run (random effects).

Diversity Metric	Factor	df	R^2	$pseudo$-F	p
Robust CLR	MiSeq Run	5	0.012	2.600	0.001 *
	Tissue	5	0.121	26.385	0.001 *
	Stage	3	0.017	6.301	0.001 *
	Genotype	4	0.004	1.049	0.266
	MiSeq Run:Plate	9	0.012	1.429	0.001 *
	Tissue x Stage	10	0.027	2.952	0.001 *
	Tissue x Genotype	20	0.018	0.958	0.801
	Stage x Genotype	12	0.012	1.081	0.101
	Tissue x Stage x Genotype	40	0.036	0.989	0.58
ALR	MiSeq Run	5	0.014	2.477	0.001 *
	Tissue	5	0.176	31.046	0.001 *
	Stage	3	0.026	7.592	0.001 *
	Genotype	4	0.005	1.095	0.204
	MiSeq Run:Plate	9	0.017	1.657	0.001 *
	Tissue x Stage	10	0.033	2.904	0.001 *
	Tissue x Genotype	20	0.022	0.955	0.761
	Stage x Genotype	12	0.015	1.086	0.166
	Tissue x Stage x Genotype	40	0.043	0.955	0.834

Table 2.7
Genotype does not explain β-diversity variation in log-transformed 16S core communities. PERMANOVA analyses on Euclidean distances between robust CLR or ALR transformed core communities. ASVs were included in this analysis if present at 1% relative abundance in 20% of samples of at least one tissue by stage subset (Core B). Genotype does not explain 16S core community β-diversity variation as a main effect nor does genotype interact with other factors. Statistically significant factors are denoted by asterisks and include tissue, developmental stage and their interaction (fixed effects), MiSeq run and PCR plate nested within MiSeq run (random effects).

Diversity Metric	Factor	df	R^2	pseudo-F	p
Bray-Curtis	MiSeq Run	2	0.012	6.309	0.001 *
	Tissue	5	0.195	42.710	0.001 *
	Stage	3	0.027	9.947	0.001 *
	Genotype	4	0.005	1.349	0.031 *
	MiSeq Run:Plate	11	0.020	1.972	0.001 *
	Tissue x Stage	10	0.033	3.670	0.001 *
	Tissue x Genotype	20	0.017	0.915	0.862
	Stage x Genotype	12	0.013	1.182	0.047 *
	Tissue x Stage x Genotype	40	0.033	0.912	0.947
Jaccard	MiSeq Run	2	0.008	4.124	0.001 *
	Tissue	5	0.130	25.489	0.001 *
	Stage	3	0.020	6.461	0.001 *
	Genotype	4	0.005	1.218	0.034 *
	MiSeq Run:Plate	11	0.018	1.619	0.001 *
	Tissue x Stage	10	0.029	2.819	0.001 *
	Tissue x Genotype	20	0.019	0.954	0.803
	Stage x Genotype	12	0.014	1.114	0.052
	Tissue x Stage x Genotype	40	0.038	0.932	0.982

Table 2.8
Genotype explains a small fraction of β-diversity variation of rarefied ITS1 core communities. PERMANOVA analyses on β-diversity distance matrices generated by Bray-Curtis and Jaccard distances on rarefied data sets ASVs were included in this analysis if present at 1% relative abundance in 20% of samples of at least one tissue and stage subset (Core B). Genotype explains a small fraction (0.5%) of ITS1 core community variation as a main effect and significantly interacts with developmental stage in Bray-Curtis community variation. The genotype-stage interaction is marginal using the Jaccard Index. Statistically significant factors and/or interactions are denoted by asterisks.

Diversity Metric	Factor	df	R^2	pseudo-F	p
Robust CLR	MiSeq Run	2	0.006	3.328	0.001 *
	Tissue	5	0.117	24.008	0.001 *
	Stage	3	0.024	8.120	0.001 *
	Genotype	4	0.005	1.187	0.077
	MiSeq Run:Plate	11	0.015	1.434	0.001 *
	Tissue x Stage	10	0.037	3.842	0.001 *
	Tissue x Genotype	20	0.018	0.947	0.833
	Stage x Genotype	12	0.013	1.121	0.057
	Tissue x Stage x Genotype	40	0.036	0.937	0.962
ALR	MiSeq Run	2	0.012	3.939	0.001 *
	Tissue	5	0.150	19.750	0.001 *
	Stage	3	0.031	6.895	0.001 *
	Genotype	4	0.007	1.118	0.175
	MiSeq Run:Plate	11	0.022	1.328	0.001 *
	Tissue x Stage	10	0.034	2.227	0.001 *
	Tissue x Genotype	20	0.027	0.896	0.961
	Stage x Genotype	12	0.017	0.932	0.82
	Tissue x Stage x Genotype	36	0.047	0.870	1

Table 2.9
Genotype does not explain β-diversity variation of log-transformed ITS1 core communities. PERMANOVA analyses on the Euclidean distance between robust-CLR or ALR transformed communities. ASVs were included in this analysis if present at 1% relative abundance in 20% of samples of at least one tissue and stage subset (Core B). Genotype is not statistically significant after robust CLR transformation or ALR transformation (PERMANOVA, p ¿ 0.05). Statistically significant factors and/or interactions are denoted by asterisks.

Marker	Subset type	Subset name	df	pseudo-F	p
16S	Overall (none)	Overall (none)	4	0.873	0.469
	Within tissues	Roots	4	0.827	0.508
		Rosettes	4	1.410	0.251
		Stems	4	0.470	0.755
		Cauline leaves	4	0.305	0.872
		Siliques	4	0.328	0.849
		Flowers	4	0.639	0.631
	Within stage	Vegetative	4	1.174	0.322
		Flowering	4	0.205	0.931
		Unripe siliques	4	1.497	0.184
		Ripe siliques	4	0.730	0.553
ITS	Overall (none)	Overall (none)	4	0.649	0.616
	Within tissues	Roots	4	1.470	0.229
		Rosettes	4	1.538	0.193
		Stems	4	0.298	0.874
		Cauline leaves	4	0.448	0.791
		Siliques	4	0.080	0.986
		Flowers	4	0.551	0.695
	Within stage	Vegetative	4	0.330	0.85
		Flowering	4	0.197	0.941
		Unripe siliques	4	0.395	0.805
		Ripe siliques	4	0.635	0.636

Table 2.10
Microbiome β-diversity dispersions are not different in PRR knockout genotypes compared to wild-type plants. Multivariate homogeneity of group dispersions (PERMDISP2) on Bray-Curtis distances of core 16S and ITS1 microbiomes (Core B) reveals that wild-type and mutant genotypes do not have significantly different variability. The effect of genotype on group dispersions was tested in the overall data set and within tissue, developmental stage, and tissue by stage subsets. This effect was additionally tested using the Jaccard distance, other cores, and with a minimally filtered ASV set (non-core). Similar results were obtained in all analyses (data not shown).

Marker	Factor	df	$pseudo$-F	p
16S	Stage	2	6.969	0.001 *
	Genotype	4	0.609	0.666
	Stage x Genotype	8	0.824	0.590
ITS	Stage	2	7.969	< 0.001 *
	Genotype	4	1.249	0.299
	Stage x Genotype	8	1.127	0.357

Table 2.11
Within-individual tissue specificity of bacterial and fungal microbiomes is affected by developmental stage but not PRR knockout. The results of permutational ANOVAs testing the effect of developmental stage and genotype on mean Bray-Curtis distance of aerial tissues to the individual plant median, a measure of tissue specificity. Asterisks denote significant results. Only samples from plants with all tissues retained were considered for analysis. Sample size for Stage x Genotype subsets: Bacteria: n=2-13, Fungi: n=2-12.

Marker	Factor	df	pseudo-F	p
16S	Tissue	5	59.885	<0.001 *
	Stage	3	2.084	0.101
	Genotype	4	1.234	0.295
	Tissue x Stage	10	3.166	0.001 *
	Tissue x Genotype	20	1.388	0.121
	Stage x Genotype	12	1.374	0.174
	Tissue x Stage x Genotype	40	1.027	0.428
ITS	Tissue	5	17.012	<0.001 *
	Stage	3	5.428	0.001 *
	Genotype	4	0.996	0.409
	Tissue x Stage	10	1.795	0.059 .
	Tissue x Genotype	20	0.906	0.580
	Stage x Genotype	12	0.597	0.845
	Tissue x Stage x Genotype	36	0.835	0.741

Table 2.12
Single PRR knockout does not affect microbial load. ANOVA table showing factors tested for their effects on microbial load variation. Relative microbial load was determined by comparing the ratio of spike-in copy number to marker gene copy number, and $\log_{10}$ transformed for analysis. Tissue and developmental stage affect microbial load, but PRR knockout genotype does not.

CHAPTER 3

INVESTIGATING TRANSGENERATIONAL INHERITANCE OF RESISTANCE PHENOTYPES IN *A. THALIANA* TO TWO NATURAL PATHOGENS, *PSEUDOMONAS VIRIDIFLAVA* AND *PSEUDOMONAS SYRINGAE*

3.1 Introduction

The dynamics of plant-microbe interactions are influenced by numerous external factors, including abiotic conditions (Saijo and Loo, 2020) and the presence of other organisms (Tollenaere et al., 2016; Hassani et al., 2018). Interestingly, these factors can impact the trajectory of a microbial infection even if they do not occur at the same time as the infection. Historic conditions, previously experienced within the lifetime of the host plant or by its parents, can impact future plant-microbe interactions (Mauch-Mani et al., 2017).

Consider the phenomenon of plant priming, for example. When plants encounter a pathogen, a complex, multifaceted response is triggered that causes a broad range of physiological changes (Dodds and Rathjen, 2010) that can persist across the lifetime of the plant and, in some cases, be transmitted to the next generation (Mauch-Mani et al., 2017). Retained epigenetic modifications promote a faster and/or stronger defense response if the pathogen is encountered again (Conrath et al., 2006), resulting in less severe disease phenotypes and higher fitness relative to unprimed plants (Van Hulten et al., 2006; Traw et al., 2007). The fitness cost of maintaining a primed state is not well-studied, but, in the absence of the stressor, costs appear to be low to undetectable (Van Hulten et al., 2006; Walters et al., 2008). On the other hand, priming for a particular pathogen can interfere with the defense response to other pathogens (De Vos et al., 2005; Abdullah et al., 2017). This trade-off is particularly likely when plants encounter pathogens, which grow on live host cells,

and necrotrophic pathogens, which consume dead host cells. Biotrophs typically activate the salicylic acid defense pathway, whereas necrotrophs activate the jasmonic acid/ethlyene pathway (Glazebrook, 2005). These two major plant defense signaling pathways are mutually antagonistic (Pieterse et al., 2009). The activation of salicylic acid defense pathways can increase susceptibility to pathogens that stimulate jasmonic acid defense pathways, and vice versa (Spoel et al., 2007).

A handful of studies have demonstrated that under intense disease pressure in laboratory conditions, *A. thaliana* can transmit a primed phenotype to the next generation (Luna et al., 2012; Slaughter et al., 2012; López Sánchez et al., 2021). This phenomena, transgenerational induced resistance, is associated with offspring epigenetic states (e.g. chromatin structure and DNA methylation patterns) that reflect the disease experience of their parents (Hannan Parker et al., 2022). Plants that experience severe infection from *Pseudomonas syringae* pv. *tomato* DC3000 (*Pst* DC3000), a hemi-biotrophic bacteria, produce offspring that exhibit fewer disease symptoms and lower bacterial loads when infected with the same isolate, compared to offspring of mock infected plants (Luna et al., 2012; Slaughter et al., 2012; López Sánchez et al., 2021). However, progeny of *Pst* DC3000-infected plants are more susceptible than offspring from mock-treated plants to the necrotrophic fungus *Alternaria brassicicola* (Luna et al., 2012). These trade-offs illustrate that any benefit derived from transgenerational induced resistance is highly dependent upon the ecological context of both parent and offspring. Thus, it is unsurprising that the epigenetic transmission of stress resistance to the next generation is not a general response to stress (Pecinka et al., 2009; Uller et al., 2013).

Most stress-induced epigenetic marks are reset either within the lifetime of the stressed plant or between generations (Iwasaki, 2015). This processes uses the considerable cellular machinery that exists to reset the epigenetic state after the stress is alleviated (Pecinka and Mittelsten Scheid, 2012). The exact conditions and stressors that trigger transgener-

ational induced resistance are poorly understood, though it is known that responses are variable, even when the same plant lines and stressors are assayed (for example, compare salt tolerance in Boyko *et al.* 2010 and Lopez-Sanchez *et al.* 2021). Furthermore, plants experience numerous, concurrent stressors in nature, whereas lab experiments typically test a single stressor in isolation. Due to a dearth of investigations that evaluate stress-induced transgenerational resistance in conditions that mimic the experience of plants in the field, the ecological and evolutionary significance of this phenomenon remains an open and contentious question (Uller et al., 2013; Crisp et al., 2016; López Sánchez et al., 2021; Hannan Parker et al., 2022).

Existing studies that demonstrate transgenerational induced resistance in *A. thaliana* - bacteria pathosystems (Luna et al., 2012; Slaughter et al., 2012; López Sánchez et al., 2021) poorly represent wild *A. thaliana*-bacterial interactions for several reasons. First, they use *Pst* DC3000, a highly aggressive pathogen isolated from tomato, as the representative bacterial strain. *Pst* DC3000 consistently grows in excess of 10^6 CFU/cm^2 in leaf tissues, whereas strains of *Pseudomonas syringae* isolated from wild *A. thaliana* consistently grow to population sizes in the range of 10^3 - 10^5 CFU/cm^2 when tested in standardized conditions (Kniskern et al., 2011; Karasov et al., 2019). In the field, pathogen densities in naturally infected *A. thaliana* leaves rarely exceed 10^5 CFU/cm^2 (Dunning, 2008). Second, the inducing infections in the parental generations were uncharacteristically intense. In Luna *et al.* (2012) and Lopez-Sanchez *et al.* (2021), plants were sprayed 2-5 times with 10^7 to 10^9 colony forming units (CFU) per mL of virulent *Pst* DC3000; this is a high intensity infection even in the context of laboratory assays (Katagiri et al., 2002). Slaughter *et al.* (2012) syringe inoculated 10^8 CFU/mL of avirulent *Pst* DC3000 *avrRpt2*. This infection condition rapidly and visibly induces hypersensitive response, i.e programmed cell death (Katagiri et al., 2002). Third, these studies evaluate a single pathogen strain at a time. Co-infections are common in many pathosystems (Abdullah et al., 2017) and can play a major role in

epidemiological and evolutionary processes (Tollenaere et al., 2016). In wild *A. thaliana*, multispecies co-infections are more common than expected given the prevalence of single species infections (Dunning, 2008). Furthermore, within a bacterial species, infection with multiple pathogenic strains of *P. syringae* is common (Karasov et al., 2018). In summary, while these initial studies offer a proof of concept, their relevance in ecologically realistic conditions remains unclear.

To address this gap in knowledge, we tested if bacterial pathogens induced transgenerational resistance in *A. thaliana* using a experimental design that more closely reflects infection parameters in nature. Jacob Herman developed *A. thaliana* infection lineages with two naturally occurring bacterial strains that were isolated from, and cause disease on, *A. thaliana*: *Pseudomonas viridiflava* RMX3.1b (*Pv* RMX3.1b), and *P. syringae* NP29.1a (*Ps* NP29.1a*) (Jakob et al., 2002). Genetically identical *A. thaliana* were spray inoculated once with 10^7 - 10^8 CFU/mL of *Pv* RMX3.1b alone, *Ps* NP29.1a alone, a mixture of both bacteria (co-infection), or sterile 10mM $MgSO_4$ (mock) to create four foundational lineages (P generation, Figure 3.1). These infection lineages were extended another generation in a full factorial design: the progeny of each of these parental plants were spray inoculated with one of these four treatments, resulting in 16 different infection lineages (S1, Figure 3.1).

In these infection conditions, the average growth of both *Pv* RMX3.1b and *Ps* NP29.1a typically peaks below 10^6 CFU in wild-type plants (Fig. 3.6), which more closely replicates characteristics of strong infections observed in the field (Karasov et al., 2019). The co-infection treatment was designed to investigate how transgenerational induced resistance is affected when mutually antagonistic components of the plant immune system are activated. *Ps* NP29.1a more strongly activates the salicylic acid defense pathway, whereas representative strains of *P. virdiflava* more strongly activate the jasmonic acid defense pathway (Jakob et al., 2007). Importantly, despite the prevalence of multispecies co-infections in nature, to our knowledge there has been no investigation of transgenerational induced resistance in this

context. These infection lineages offer an excellent opportunity to investigate transgenerational induced resistance in an ecologically realistic context.

Experimental design and previous work

The effect of bacterial infections on genomic methylation and the transcriptome were measured in the parental and S1 generations, respectively. Using bisulfite sequencing, Jacob Herman found that the pathogen treatments affected the overall genomic methylation patterns in the parental generation (Supplemental Figure 3.10). Each inoculation type, *Pv* RMX3.1b, *Ps* NP29.1a, co-infection, or sterile $MgSO_4$, resulted in many distinct differentially methylated regions (DMRs) that had minimal overlap with each other (Supplemental Figure 3.11). Plants thus had different epigenetic responses to each pathogen and to the co-infection treatment. Interestingly, there was evidence of transgenerational effects in the S1 generation. The transcriptomes of 7/16 lineages (Fig. 3.1) revealed a number of differentially regulated genes as a function of inoculation type in both generations, including several pathogenesis-related genes (Beilsmith, 2020).
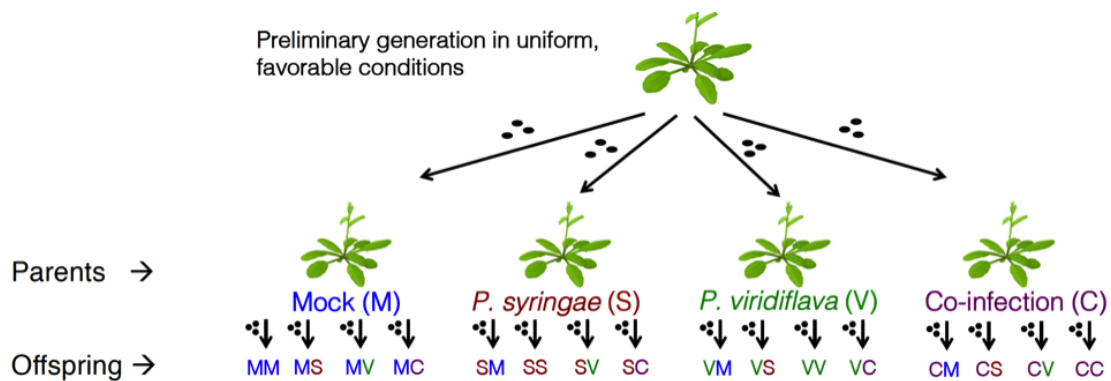
Figure 3.1
Generation of infection lineages. Two-letter abbreviations at the bottom of the figure indicate the parental (P) (first letter) and S1 (second letter) treatments. Resistance phenotypes were evaluated in the S2 generation. Asterisks denote the lineages selected for phenotyping.

Current work

While differences in genomic methylation patterns and transcription suggest transgenerational effects are occurring, whether these effects are strong enough to impact subsequent levels of resistance is unknown. Confirming that selectable phenotypes are generated is key to understanding the ecological and evolutionary importance of transgenerational induced resistance. Here, I test if two generations of exposure to *Pv* RMX3.1b, *Ps* NP29.1a, or a co-infection treatment affects the bacterial growth and symptom severity in their progeny (S2 in Fig. 3.1). Plants with parents and grandparents exposed to the same infection regime were used in this experiment due to the expectation that they would have the strongest and most straightforward phenotypes out of the 16 infections lineages.

Based on preliminary results and previous publications, we generated two main hypotheses: 1) Pathogen exposure in two previous generations will produce progeny with increased resistance to the same pathogen. We expected that the offspring of plants in the *Ps* NP29.1a infection lineage would show decreased bacterial growth and/or decreased symptoms compared to plants with a mock treatment lineage when inoculated with *Ps* NP29.1a. We expected the same would be true for *Pv* RMX3.1b infections in *Pv* RMX3.1b infection lineages. 2) Pathogen exposure in two previous generations would increase offspring susceptibility to a pathogen with an alternative infection strategy. We thus expected that exposure to *Ps* NP29.1a in previous generations would result in increased bacterial growth and/or increased symptoms following a *Pv* RMX3.1b infection and vice versa.

The effect of historic co-infections, on the other hand, was difficult to anticipate. If the two microbes trigger mutually antagonistic plant defense pathways, the protective priming could be cancelled out, resulting in no difference in phenotype when compared to the mock treatment. Alternatively, if one pathogen is competitively dominant to the other, we might expect the dominant microbe to induce resistance patterns akin to a single infection treatment. Finally, a co-infection could lead to increased resistance or susceptibility to both single

57

infection challenges. Although there is no research on transgenerational induced resistance in the face of multiple, simultaneous biotic stressors, plastic resistance phenotypes are often erased in the next generation when plants are challenged with multiple abiotic stressors (Lampei, 2019).

Here, I evaluate these hypotheses using two infection procedures and two measures of disease severity. The infection lineages were initially generated via spray infection. I measured resistance phenotypes using both spray inoculation assays and syringe (pressure) inoculation assays. Syringe inoculations force bacteria directly into the leaf apoplast leading to more consistent infections between biological replicates (Katagiri et al., 2002). However, some early plant defenses are bypassed. Spray inoculation deposits microbes on the surface of the plant leaves and requires that bacteria migrate into the plant tissues for an internal infection to progress (Katagiri et al., 2002). This often results in more variability between biological replicates, but more faithfully imitates field infections and exposes pathogens to more components of plant defense. Disease severity was characterized by quantifying microbial growth as well as by measuring symptomatic leaf area. Each experiment was completed twice for each inoculation type and pathogen to confirm observed trends.

3.2 Materials & Methods

3.2.1 Overview of experiment

Inoculation Method	Syringe				Spray			
Round	Round 1		Round 2		Round 1		Round 2	
Pathogen challenge	*P. syringae*	*P. viridiflava*	*P. syringae*	*P. viridiflava*	*P. syringae*	*P. viridiflava*	*P. syringae*	*P. viridiflava*
Normalization	wet weight	wet weight	area (1.1 cm²)	area (1.1 cm²)	area (1.1 cm²)	area (1.1 cm²)	area (1.1 cm²)	area (1.1 cm²)
Leaf processing	4 leaves, pooled	4 leaves, pooled	4 punches, processed separately	4 punches, processed separately	4 punches, pooled	4 punches, pooled	4 punches, processed separately	4 punches, processed separately
Microbial quantification method	CFU	CFU	CFU and luminescence	CFU and luminescence	CFU	CFU	luminescence	luminescence
Symptoms	N/A	N/A	Day 7	Day 7	Day 5	Day 5	Day 5	Day 5

Figure 3.2
Experiments to quantify transgenerational induced resistance phenotypes.
Resistance to single infections of *Ps* NP29.1a or *Pv* RMX3.1b was measured in plants with
different infection lineages. Although infection lineages were originally generated using
spray infections, resistance was evaluated in the S2 generation using both syringe and
spray inoculation. Each combination of bacteria and inoculation type was tested twice,
with minor variations.

The broad overview of the experimental layout is detailed above (Figure 3.2). There were two
iterations (Round 1 and Round 2) of each inoculation method (spray and syringe). Within
each iteration, plants were challenged with single infections of either bioluminescent *lux*-
tagged *Ps* NP29.1a or *lux*-tagged *Pv* RMX3.1b. Bacterial load was quantified by counting
CFUs or measuring bacterial luminescence. Symptoms were assessed in most iterations of
the experiment. There were minor procedural adjustments between each infection round, as
noted in Figure 3.2.

3.2.2 Plant materials and growth conditions

Resistance phenotypes were tested using plants grown from seeds produced by the second
generation of four different infection lineages: 1) two previous generations of *Pv* RMX3.1b
infection (V-V, lineage 3-8), 2) two previous generations of *Ps* NP29.1a infection (S-S, lineage

2-7), 3) two generations of a co-infection treatment (C-C, lineage 2-12) and 4) two generations of mock treatment (M-M, lineage 1-5). All lineages were in the Columbia-0 (Col-0) genetic background, and historic infection regimes of one spray inoculation of $10^7 - 10^8$ CFU/mL of bacteria or mock treatment per generation. Seeds were surfaced sterilized via exposure to chlorine gas for two hours. Sterilized seeds were then stratified in sterile, deionized water for three days at 4 °C. Stratified seeds were planted using a pipette in a pseudo-random layout in 36-cell flats in a peat based potting mix (50:50 Berger BM-1 and BM-2), avoiding the four corner cells (32 plants). Ultimately there were 8 plants per infection lineage in each flat. Flats were grown in growth chambers at 22°C, 80% RH, 60% white light and rotated through the chamber every 2-3 days. Plants were infected 4.5 weeks after planting.

3.2.3   Development of Pv RMX3.1b and Ps NP29.1a bioluminescent reporter system

I sought to develop a bioluminescent reporter system for *Pv* RMX3.1b and *Ps* NP29.1a to efficiently measure bacterial growth and circumvent the laborious and time-intensive procedures of serial dilution, plating, and colony counting. Previous work reported measuring microbial titers from luminescent signal intensity of *lux*-tagged bacteria (Fan et al., 2008). Developing a similar system would eliminate the need for colony counting, thus enabling a higher sample size and the evaluation of more infection lineage and pathogen combinations.

3.2.4   Generation of electrocompetent Pv RMX3.1b and Ps NP29.1a for transformation with lux reporter

Labelled microbial strains were generated from *Pv* RMX3.1b and *Ps* NP29.1a colonies streaked from J. Herman's stocks, both of which are natural pathogens isolated from wild *A. thaliana* in the field (Jakob et al., 2002). Electrocompetent cells were generated according

to protocols described in Perisin (2016). Single colonies were picked and grown in 5 mL King's Broth media (KB) overnight at 28 °C, 200 RPM. The following morning, cultures were diluted and grown to mid-log phase: 5 mL of the overnight cultures were added to 100 mL fresh KB and incubated for 4-5 hours at 28°C, 150 RPM. 50 mL of the cultures were transferred to conical tubes. Cells were pelleted at ~6500 x g for 10 minutes, the supernatant was removed, and cells were resuspended in 50 mL sterile 300 mM sucrose. Cells were washed a total of three times. After the final wash, the supernatant was completely removed, and cells were resuspended in 1 mL 300 mM sucrose. 100 μL of this final suspension was aliquoted and stored at -80 °C until electroporation.

3.2.5 *Generation of transgenic Pv RMX3.1b and Ps NP29.1a expressing the bioluminescent lux reporter*

The bioluminescent *lux* reporter gene was integrated into *Pv* RMX3.1b and *Ps* NP29.1a, using the mini-Tn7 system developed by Choi and Schweizer (2006) and protocols developed specifically for these strains by Perisin (2016). The plasmid carrying the transposase (pTNS3) and the mini-Tn7 plasmid (hereafter pLux) carrying the bacterial lux gene and gentamicin resistance (Choi et al., 2005) were isolated using the Qiagen MiniPrep kit and eluted in water. 100μL of electrocompetent bacteria, 170 ng pLux and 200 ng pTNS3 (10 μL of DNA total) were combined in a 2 mm gap cuvette and mixed by gentle stirring. The bacterial-DNA mix was electroporated with a BioRad MiniPulser using the Eco2 settings (1 pulse, 2.5 kV). 1 mL of KB was immediately added to electoporated cells. Cells were transferred to a cell culture tube and an additional 4 mL of KB was added. Cultures were incubated at 28 °C at 225 RPM for 6 hours. Cells were then pelleted (10 minutes at 6500 x g) and all but ~100 μL of the supernatant was removed. The entire 100 μL of cells were plated on selective KB agar plates with 5 μg/μL gentamicin. Plates were allowed to grow for 2-3 days at 28°C. Antibiotic resistant colonies were checked for luminescence using a CCD

camera. Several *lux*-positive, antibiotic resistant colonies were picked and grown in liquid KB overnight, at 28 °C, 200 RPM. An equal volume of 40% glycerol was added to each stock stored at -20 °C.

3.2.6 Evaluating luminescent signal as representative of colony forming units

The relationship between *lux* signal and CFUs of *Pv* RMX3.1b and *Ps* NP29.1a was evaluated. For these measurements, 100 μL of the undiluted leaf homogenate from infected plants was pipetted into opaque, white 96 well plates. These plates were read on a luminescence plate reader (Tecan SparkControl) using a 30s exposure per well and a 60s exposure time for *Ps* NP29.1a; these differences were necessary because NP29.1a had a much dimmer signal than the *Pv* RMX3.1b strain. The luminescence signal decayed over the course of reading the samples. This is expected because the total light generated in each sample is the combined output of light from the external environment and light produced by the *lux* protein within the sample. Various tactics were used to minimize external light exposure, but some environmental light was unavoidable. A luminescence decay curve was created by sampling blank buffer over the course of the luminescence reading process. The resulting decay curve was used to normalize the luminescence counts from each sample. Decay curves were generated for each plate.

Below 10^4 CFUs per 28 mm^2 leaf area, bacterial luminescence could not be distinguished from environmental noise (Figure 3.3). Below this threshold, some true negatives, confirmed by plating, had positive luminescence values after signal normalization. Additionally, below this threshold, true positives sometimes had negative or zero luminescence values after signal normalization with negative controls (Fig. 3.3).

The brightness of signal and CFUs were moderately well-correlated (*Pv* RMX3.1b: $R^2 = 0.73$, 95% CI [0.48, 0.82], $p < 0.001$; *Ps* NP29.1a: $R^2 = 0.54$, 95% CI [0.41, 0.63], $p < 0.001$),
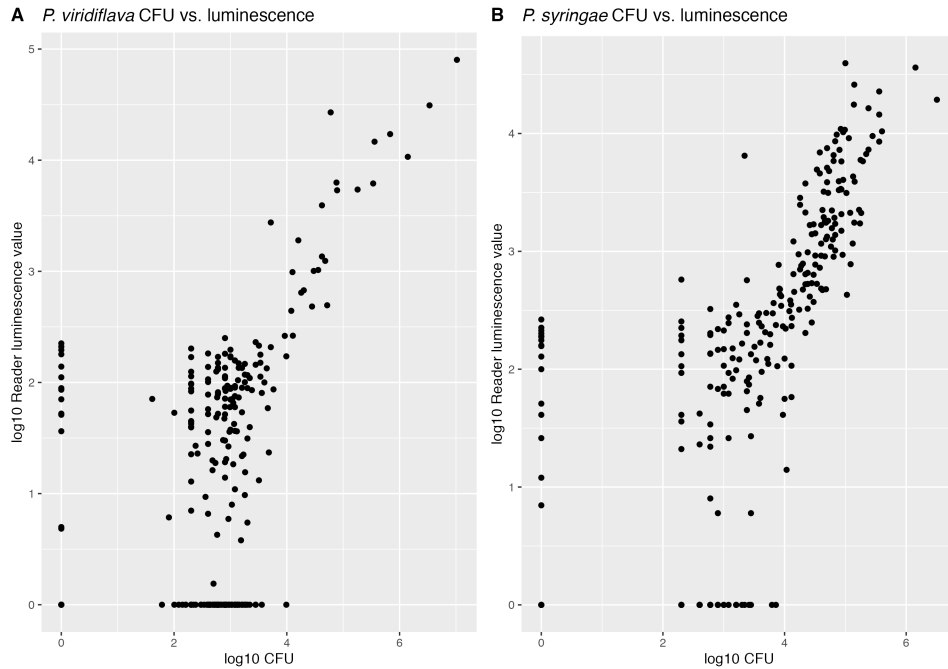
Figure 3.3
Relationship of bacterial CFU to *lux* output, including samples below detection limits.

Figure 3.4. Nevertheless, this model exhibited two important limitations associated with the use of luminescence to infer bacterial titers. First, residual analysis could not confirm accuracy for bacterial titers above 10^5 CFUs per 28 mm^2 leaf tissue due to a paucity of data at high-infection titers. Second, variation around the CFU-luminescence model is substantial, reducing the resolution (Fig. 3.4). As we expected growth patterns to be fairly variable between replicates, it is unlikely that our bioluminescence assay alone would be sensitive enough to detect transgenerational induced resistance. Because of these limitations, bacterial growth in our experiments was primarily measured by traditional serial dilution and colony counting. Luminescence alone was used only in the second iteration of spray infections (Fig. 3.1, Spray - Round 2). In this round, we attempted to find an infection "breakaway" point in infections by analyzing each leaf punch individually, which quadrupled the number of samples in which we measured bacterial titers. No breakaway point was found, so this component of the analysis is not shown.

A *P. viridiflava* CFU vs. luminescence, in Reader range

$y = -0.164 + 0.733 \, x \quad R^2 = 0.73$

B *P. syringae* CFU vs. luminescence, in Reader range

$y = -0.727 + 0.851 \, x \quad R^2 = 0.54$
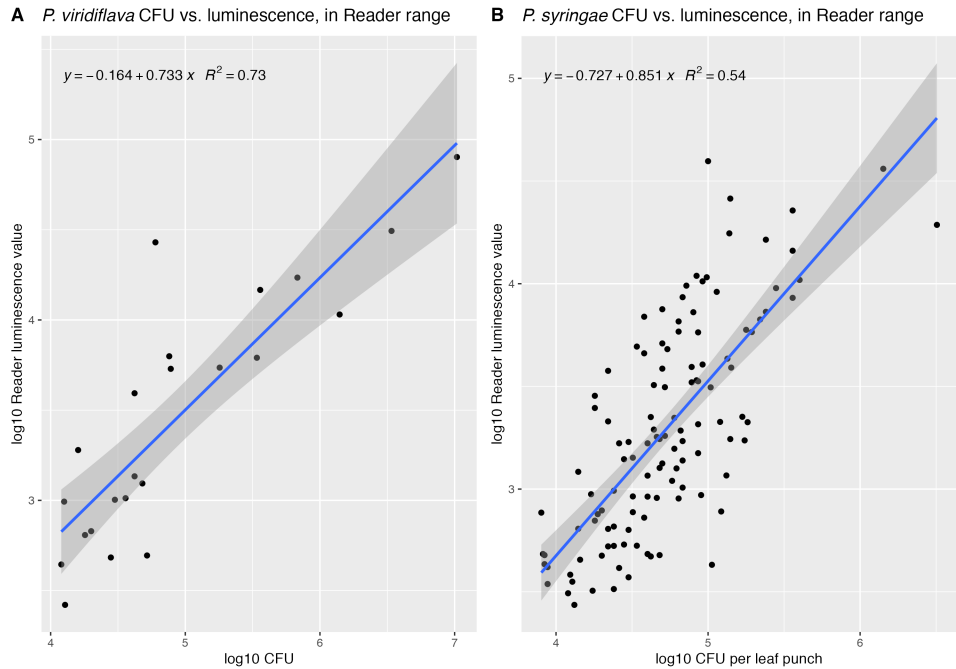
Figure 3.4
Relationship of bacterial CFU to *lux* output within detection limits. *Pv*
RMX3.1b 95% CI [0.48, 0.82], $p < 0.001$, *Ps* NP29.1a: 95% CI [0.41, 0.63], $p < 0.001$

3.2.7   Bacterial growth and infection procedures

Colonies of *Pv* RMX3.1b and *Ps* NP29.1a transformed with the luminescent *lux* reporter
were plated on KB with agar and grown for two days at 28°C. A single colony was picked
and grown in liquid KB for 24 hours, at 28°C and 225 RPM. For spray inoculations, 1 mL
of the 24h culture was used to inoculate 100 mL KB flask and allowed to grow overnight.

Syringe infiltration: Bacteria were diluted to 1.5 x 10^6 colony forming units (CFU) per
mL in sterile 10mM $MgSO_4$. In each round, each strain was inoculated into 96 plants:
24 individual plants of the 4 infection lineages. In addition, 8 plants per infection lineage
were mock inoculated. True leaves 3, 4, 5, and 6 were selected for inoculation and their
petioles were marked with a permanent marker for accurate resampling. Bacteria were gently
infiltrated into leaves with a blunt-end syringe until the entire leaf appeared water soaked.
Plants receiving a mock treatment were infiltrated with sterile 10mM $MgSO_4$. Plants were
allowed to dry for ~1.5 hours, or until water soaking symptoms had disappeared. The plants

were then placed in humidity domes, which remained for the duration of the experiment, and returned to the growth chamber. This process was performed twice with *Ps* NP29.1a and twice with *Pv* RMX3.1b (Fig. 3.1, Syringe inoculations).

Spray inoculations: Bacterial concentrations were adjusted to 5 x 10^8 CFU/mL in sterile DI water with 0.04% Silwet L-77, a surfactant that facilitates entry into the leaf. In total, each strain was inoculated into 96 plants: 8 individual plants of each of the four infection lineages at two sampling time points plus one replicate set that was reserved for symptom scoring. Eight plants per infection lineage were mock inoculated. Bacteria were immediately sprayed onto plants using a sterilized airbrush applicator, until all leaves were visibly covered with the microbial solution, approximately 25 mL per flat. Mock treated plants were sprayed with sterile DI water with 0.04% Silwet L-77. Leaves were allowed to dry for 1.5 hours, and then placed in humidity domes, which remained for the duration of the experiment, and returned to the growth chamber. This process was performed twice with *Ps* NP29.1a and twice with *Pv* RMX3.1b (Fig. 3.1, Spray inoculations).

3.2.8 Measuring bacterial growth

For syringe inoculated plants, leaf samples were harvested at three time points, 4 hours post-infection to measure the initial density of microbes in plant tissues, and 24 and 48 hours post-infection to assay microbial growth. Two methods were used to account for variation in leaf sizes. In Round 1, four leaves per plant were clipped at the base and weighed. The wet weight was used to standardize the CFU counts. In Round 2, one 28 mm^2 punch per leaf was harvested from four leaves per plant. Whole leaves or leaf punches were dipped in freshly prepared 70% ethanol for 15 seconds to remove surface microbes, rinsed in sterile DI water and blotted on paper towels. Sterilized punches were then placed in a 96-well DeepWell plate (Nunc 2mL) with 2-3 2.3 mm steel beads per well. In Round 1, the four punches from the same plant were pooled into a single well. In Round 2, each leaf punch was processed

individually (Fig. 3.2). Samples were then homogenized by bead beating on a Spex 2010 Geno/Grinder for 2 cycles of 15 seconds at 1750 RPM. 200 μL of 10mM $MgSO_4$ was added to each well and homogenized for 2 cycles of 20 seconds at 1750 RPM.

Spray inoculated plants were collected at only two time points, 24 hours and 48 hours post-infection; plants were not harvested immediately after infection because time for the bacteria to enter the leaf tissues is required. In order to assess the basal levels of microbes in the leaves, untreated plants were harvested the same day that spray infections took place. In both Round 1 and Round 2, one 28 mm^2 punch per leaf was harvested from four leaves per plant. Leaf punches were then dipped in freshly prepared 70% ethanol for 15 seconds to remove surface microbes, rinsed in sterile DI water and blotted on paper towels. Punches were subsequently transferred to a 96-well DeepWell plate (Nunc 2mL) with 2-3 2.3 mm steel beads per well. In Round 1, the four punches from the same plant were pooled into a single well. In Round 2, each leaf punch was processed individually (Fig. 3.2). Samples were then homogenized by bead beating on a Spex 2010 Geno/Grinder for 2 cycles of 15 seconds at 1750 RPM. 200 μL of 10mM $MgSO_4$ was added to each well and homogenized for 2 cycles of 20 seconds at 1750 RPM.

In both rounds of syringe inoculations and Round 1 of spray inoculations, CFUs were quantified by serial dilution and plating. Leaf homogenates were serially diluted in 10mM $MgSO_4$. 10μL of each dilution was plated on KB plates and incubated at 28°C. After colonies appeared, between 24-36 hours, colonies were counted by hand. Since both *Pv* RMX3.1b and *Ps* NP29.1a were *lux* transformed, plates were photographed using a CCD camera to confirm that they were *lux* positive. The vast majority of colonies were luminescent. In cases where contaminating microbes were observed, both the luminescent titer (target bacteria) and the non-luminesent titer (contamination) were recorded. In Round 2 of the syringe inoculations, luminescence was measured on the plate reader in addition to colony counting. In Round 2 of the spray infections, only luminescence on the plate reader was recorded. The methods for

this direct measurement of luminescence is detailed above. Given the previously discussed limitations associated with luminescence reads, results from this round of the experiment are reported only as support for the CFU counts.

3.2.9   Symptom analysis

In order to score symptoms, plants were photographed daily for several days post-infection after one iteration of syringe infections (Round 2) and both iterations of spray infections. Syringe infections were compared at 7 days post-infection and spray infections were compared 5 days post-infection. This discrepancy is due to incomplete data: the symptom analysis was added while the experiment was already in progress; 7 days post-infection as the only day that both *Ps* NP29.1a and *Pv* RMX3.1b syringe infections were photographed, whereas spray infections were photographed 5 days post-infection. Symptoms were scored by eye on a scale of 0-3. 0: no visible symptoms, 1: 1-33% of leaf symptomatic, 2: 34-66% of leaf symptomatic, 3: 67-100% of leaf symptomatic (Roux et al., 2010). Symptoms included water soaking, leaf yellowing, and leaf necrosis. The scores from 4 leaves per plant were summed to get a Sum Symptom Score. This total score was used to test if infection lineage affected overall plant symptom severity. In addition, the relationship between infection lineage and the distribution of symptom severity was evaluated by comparing the proportion of leaves receiving each score (0-3) within each infection lineage.

3.2.10   Statistical analysis

All statistical analyses were performed in R, using the stats, ggsignif and ggpmisc packages.

CFU - luminescence regression analysis: After removal of all values below detection limits, the remaining data was fit to a linear model using *stat_poly_eq* function in R. Other polynomial fits were explored, but none had improved fits over a linear model.

Bacterial load assays: CFU titers (all syringe assays and spray inoculations, Round 1) or

normalized luminescence scores (spray inoculations, Round 2) were $\log_{10}$ transformed before analysis. If leaf punches were measured separately (Fig. 3.1, Syringe Round 2 and Spray Round 2), the mean of the CFU count or luminescence score per plant was used in the statistical analysis. All microbial titers were compared using the Kruskal-Wallis rank sum test.

Symptom analysis: In the overall symptom analysis, Kruskal-Wallis rank sum tests were used to compare the Sum Symptom Score of total plant symptoms. Fisher's Exact Test was used to determine of the proportion of leaves receiving each score (0-3), varied by infection lineage. In this analysis, each leaf was considered individually.

3.3   Results

3.3.1   *Exposure to pathogens in previous generations does not impact growth of Pv RMX3.1b or Ps NP29.1a in A. thaliana leaves after syringe inoculation*

Infection lineage had no effect on the growth of *Pv* RMX3.1b nor *Ps* NP29.1a after syringe inoculation (Figure 3.5). *Pv* RMX3.1b grew to the same titers in plants descended from mock, *Ps* NP29.1a, *Pv* RMX3.1b, and co-infection lineages at both 24 hours post-infection (Kruskal-Wallis rank sum test, $p > 0.05$) and 48 hours post-infection, when growth had typically plateaued (Kruskal-Wallis rank sum test, $p > 0.05$). However, this conclusion is based on experimental Round 1 (3.5A), because *Pv* RMX3.1b failed to vigorously grow in Round 2 (3.5B). Similarly, infection lineage had no effect on growth of *Ps* NP29.1a after a syringe inoculations (Figure 3.5, C and D). Note that during the harvest at T0 in Round 1 of the *Ps* NP29.1a infection, technical errors required the removal of several replicates.
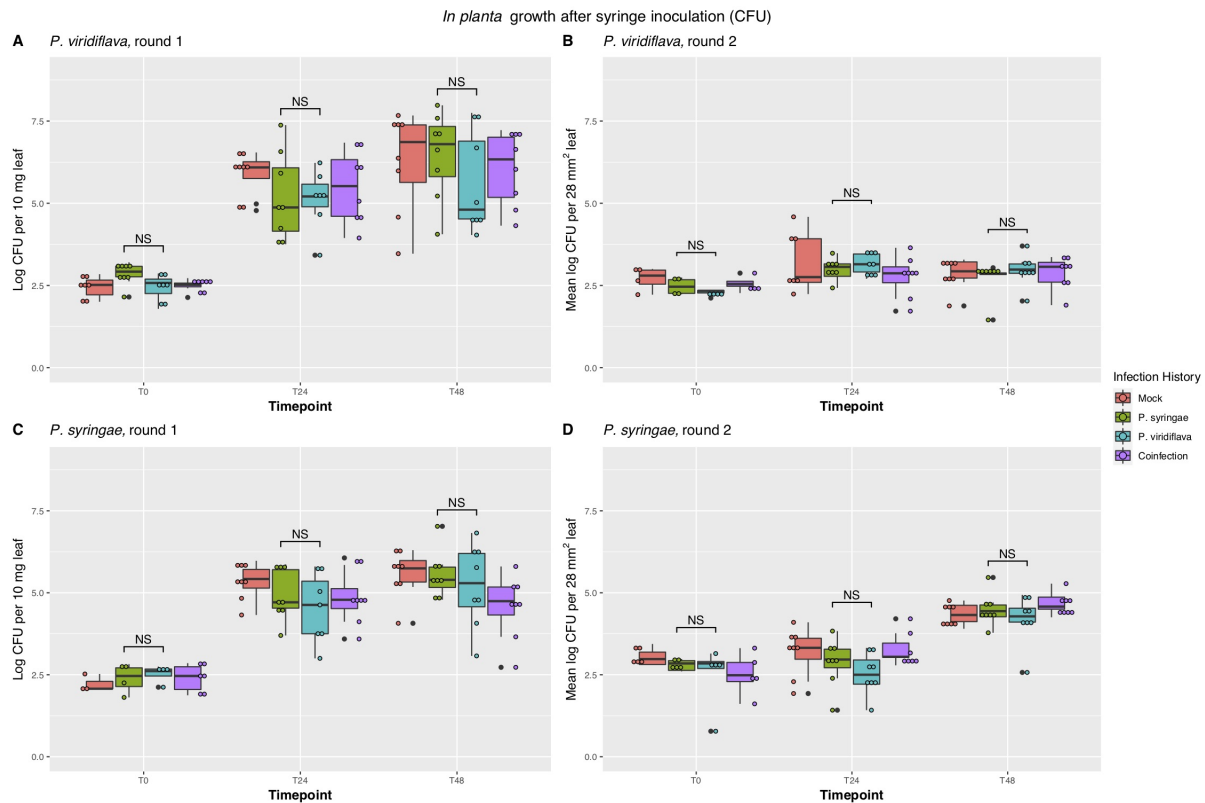
Figure 3.5
Growth of bacterial (CFUs) in *A. thaliana* leaves after syringe inoculation. *A. thaliana* with distinct infection lineages (n = 8), were infected with either *Pv* RMX3.1b (A, B) or *Ps* NP29.1a (C, D). In experiment 1 (A, C), total CFUs from four pooled leaves per plant were quantified and standardized by wet weight. In experiment 2 (B, D), the per plant mean of CFUs per leaf punch from four leaves is presented.

3.3.2 Exposure to pathogens in previous generations does not impact growth of Pv RMX3.1b or Ps NP29.1a in A. thaliana leaves after spray inoculation

In agreement with the syringe infection assays, there was no evidence of transgenerational induced resistance on bacterial growth after spray infection. In Round 1, *Pv* RMX3.1b grew to the same titers in all four plant lineages (historic mock, *Ps* NP29.1a, *Pv* RMX3.1b, or co-infection) at both 24 hours post-infection or 48 hours post-infection (Figure 3.6 A, Kruskal-Wallis rank sum test, p > 0.05). Spray infections of *Ps* NP29.1a resulted in the

same pattern - bacterial growth was not impacted by infection lineage (Fig. 3.6, B). This finding was supported in the second round of spray infections, where strength of luminescent signal was used to measure bacterial load (Figure 3.6, C and D, Kruskal-Wallis rank sum test, p > 0.05).
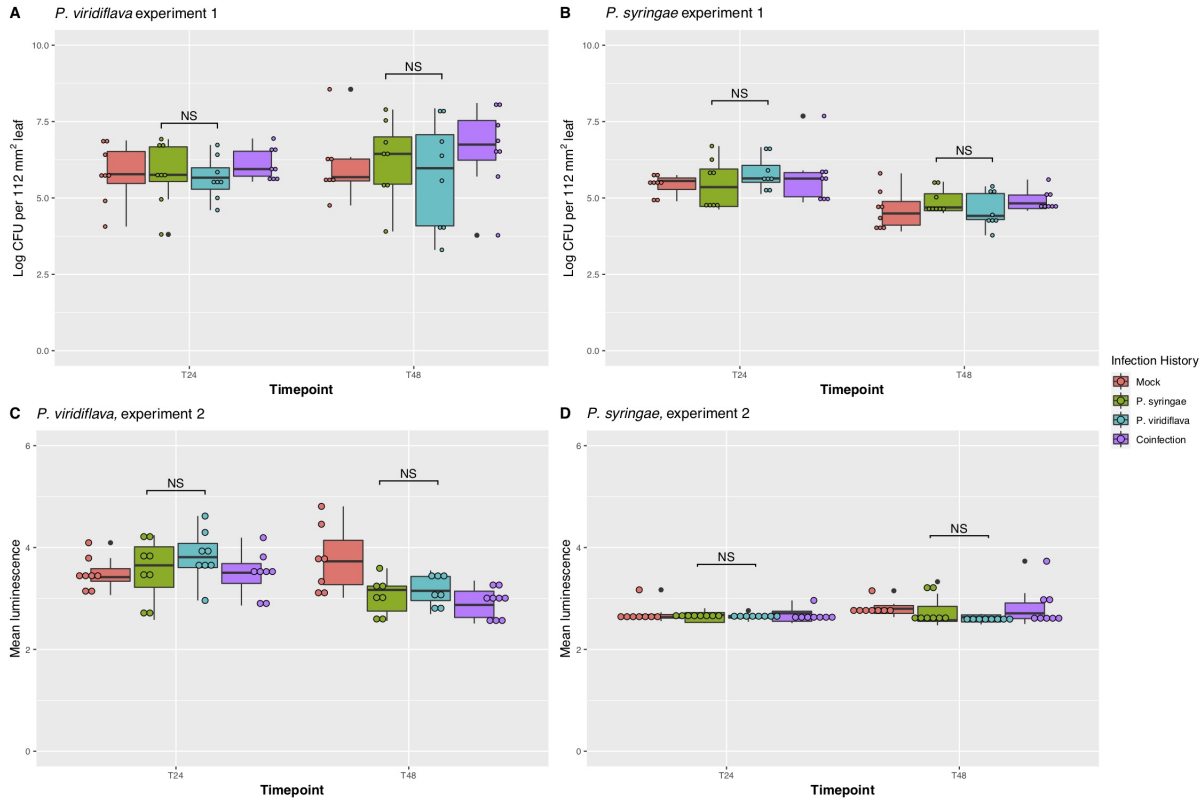
Figure 3.6
Growth of bacterial (CFUs) in *A. thaliana* leaves after spray inoculation. *A. thaliana* with distinct infection lineages (n = 8), were spray infected with either *Pv* RMX3.1b (A, C) or *Ps* NP29.1a (B, D). In A and B, points represent total CFUs from four pooled leaf punches per plant. In C and D, each point represents the mean luminescence from each individual plant, calculated as the mean of 4 leaf punches.

3.3.3   Infection lineage does not impact disease symptom severity in syringe or spray infections

Plants derived from *Ps* NP29.1a, *Pv* RMX3.1b, or co-infection infection lineages had the same overall symptom severity as plants derived from mock lineages and each other when

challenged with either *Ps* NP29.1a or *Pv* RMX3.1b. In each plant, symptom scores of four leaves were added together to obtain the sum symptom score. There was no difference in the sum symptom score 7 days after syringe (Fig. 3.7) or 5 days after spray infections (Fig. 3.8) with either microbe (Kruskal-Wallis, p>0.05). for Following syringe infections, symptoms were evaluated in Round 2 only. Symptoms were evaluated in both Round 1 and Round 2 of spray infections.
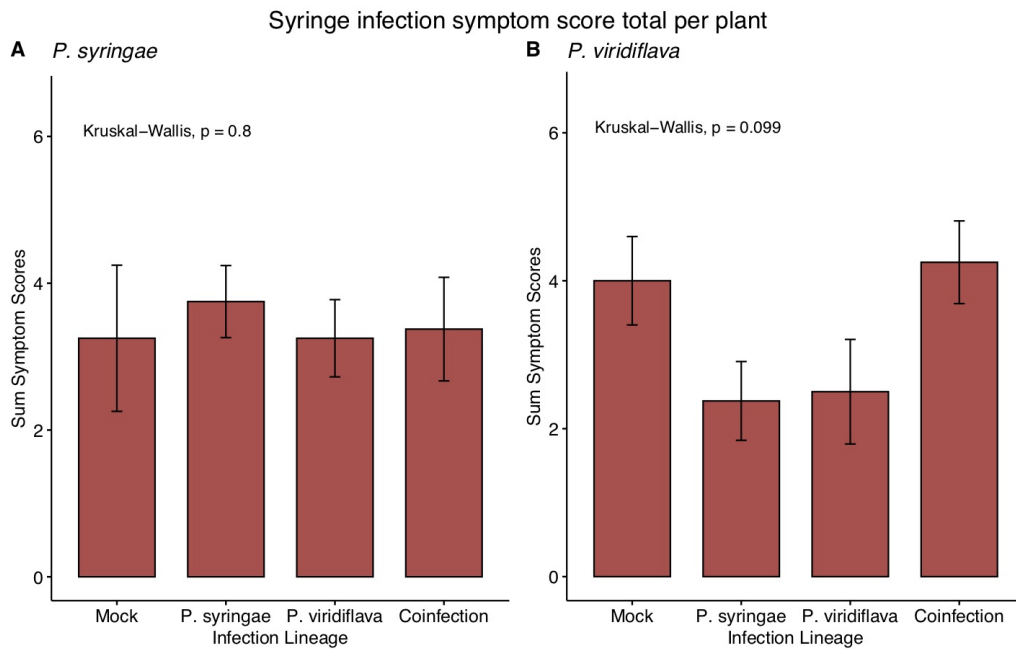
Figure 3.7
Symptom severity in *A. thaliana* leaves 7 days after syringe inoculation. *A. thaliana* of four distinct infection lineages (n = 7-8), were inoculated with either *Ps* NP29.1a (A) or *Pv* RMX3.1b (B). Four leaves per plant (n = 7-8) were scored for symptoms. Scale: 0 = no symptoms, 1 < 33% symptomatic leaf area, 2 = 34-67% symptomatic leaf area, 3 > 67% symptomatic leaf area. The scores of the 4 leaves were added together to obtain the sum symptom score. The mean and standard error of the sum symptom score are plotted.
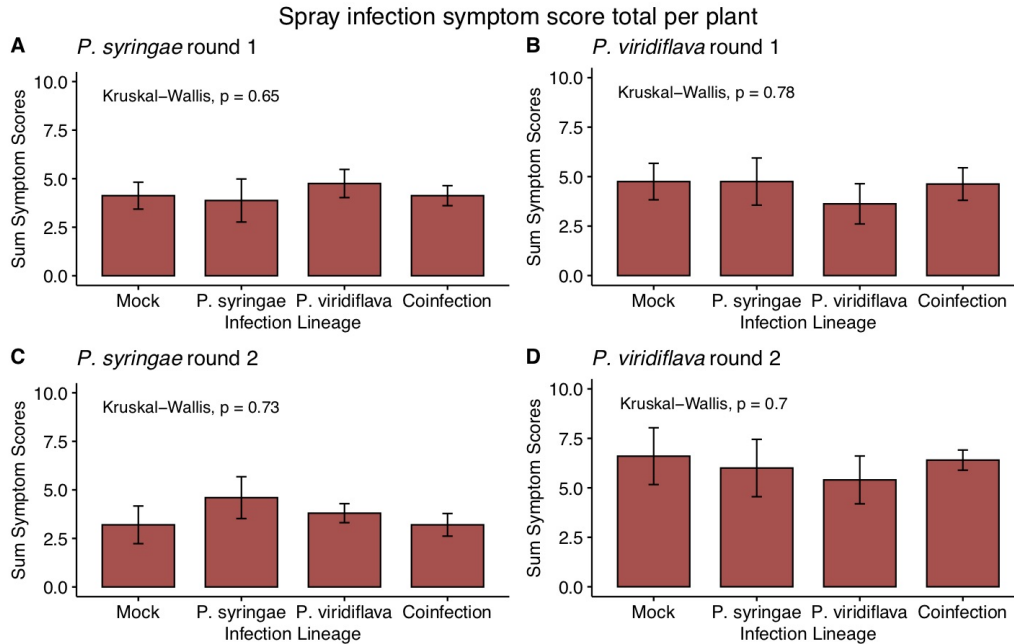
Figure 3.8
Symptom severity in *A. thaliana* leaves 5 days after spray inoculation. *A. thaliana* with distinct infection lineages (n = 7-8), were infected with either *Ps* NP29.1a (A, C) or *Pv* RMX3.1b (B, D). Four leaves per plant (n = 7-8) were scored for symptoms. Scale: 0 = no symptoms, 1 < 33% symptomatic leaf area, 2 = 34-67% symptomatic leaf area, 3 > 67% symptomatic leaf area. The scores of the 4 leaves were added together to obtain the sum symptom score. The mean and standard error of the sum symptom score are plotted.

In addition to analyzing overall plant symptom severity, we attempted to increase the resolution of our symptom analysis by determining the distribution of the symptom scores of individual leaves was compared between plant lineages. For example, a bimodal symptom pattern (with some leaves developing severe symptoms and some leaves remaining asymptomatic, i.e. leaf scores 3, 3, 0, 0) could result in the same overall score as a more uniform symptom pattern (all leaves developing moderate symptoms, i.e. leaf scores 2, 2, 1, 1). Plant lineage had no effect on the distribution of disease symptom severity of individual leaves in any infection condition (Fisher's exact test, $p > 0.05$). Symptoms were measured after Round 2 *Ps* NP29.1a and *Pv* RMX3.1b syringe infections (figure not shown) and after both rounds of *Ps* NP29.1a and *Pv* RMX3.1b spray infections (Figure 3.9).
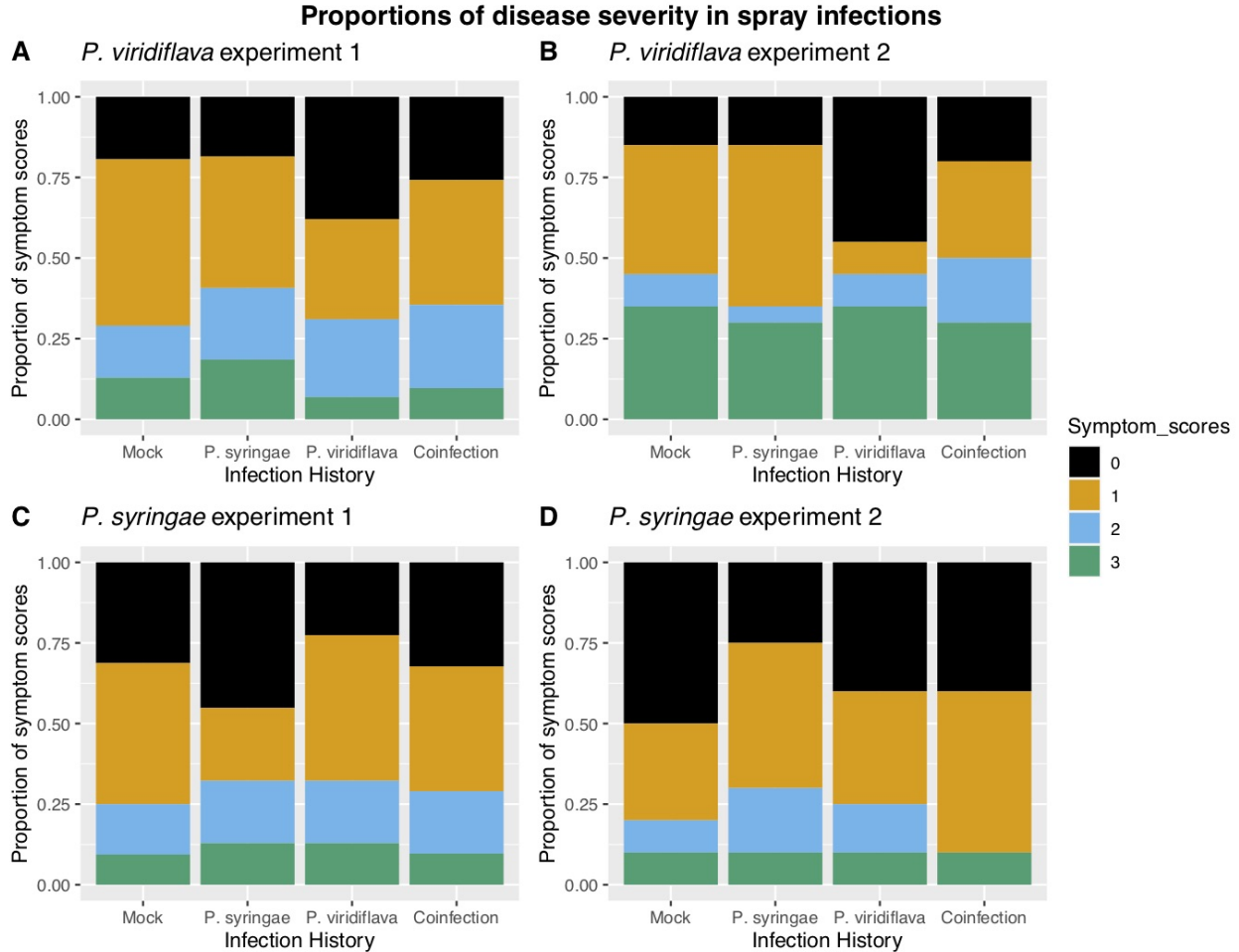
Figure 3.9
Proportions of symptom severity in leaves after spray infection, by infection lineage. Four leaves per plant (n = 7-8) were scored for symptoms following *Pv* RMX3.1b (A, B) or *Ps* NP29.1a (C, D) spray infection. Scale: 0 = no symptoms, 1 < 33% symptomatic leaf area, 2 = 34-67% symptomatic leaf area, 3 > 67% symptomatic leaf area. The number of leaves in each bin was counted by infection lineage.

3.4   Discussion

Current and historic abiotic and biotic conditions impact the pathogenesis of bacterial infections (Tollenaere et al., 2016; Hassani et al., 2018; Saijo and Loo, 2020). High-intensity infections with an aggressive bacterial pathogen, *Pst* DC3000, can even affect pathogenesis in future generations, as infected plants produce offspring that are more resistant to *Pst*

DC3000 infections but exhibit increased susceptibility to necrotrophic pathogens (Luna et al., 2012; Slaughter et al., 2012; López Sánchez et al., 2021). However, the infection conditions in these experiments are highly atypical in the field, thus, the importance of transgenerational induced resistance in nature is unclear. We addressed this question by better emulating key parameters of field infections in *A. thaliana* for two generations and then evaluating the progeny for transgenerational induced resistance phenotypes. We found no evidence that exposure to resident, naturally occurring bacterial strains at realistic titers triggers transgenerational induced resistance phenotypes, despite transgenerational epigenetic changes at the molecular level (Beilsmith, 2020).

Field surveys indicate that our experiments are representative of strong bacterial infections in nature (Dunning, 2008; Karasov et al., 2019), but that wild *A. thaliana* rarely, if ever, experience infections akin to the high-intensity *Pst* DC3000 infections assayed in previous work. *In planta* growth of *Ps* NP29.1a and *Pv* RMX3.1b is comparable to the growth of numerous *P. syringae* and *P. viridiflava* strains that have been isolated from wild *A. thaliana* (Jakob et al., 2002, 2007; Kniskern et al., 2011). *Pst* DC3000, on the other hand, consistently grows to titers at least an order of magnitude higher (Jakob et al., 2007; Kniskern et al., 2011). In addition to phenotypic differences among strains, we used relatively moderate infection conditions compared to previous studies, with lower bacterial loads and/or fewer within-generation exposures (Luna et al., 2012; Slaughter et al., 2012; López Sánchez et al., 2021). Our initial conditions produce infections that peak on the high end of leaf microbial titers observed in nature (Dunning, 2008; Karasov et al., 2019); more intense initial conditions produce infections that are more extreme than natural infections. The strength of the stress can determine the strength of resistance phenotypes in the next generation (Hannan Parker et al., 2022), thus, typical field infections may simply be too weak to trigger transgenerational induced resistance. Since there is no evidence of transgenerational induced resistance in these ecologically relevant conditions, the ecological and

evolutionary significance of this phenomena in *A. thaliana* - bacterial interactions is called into question.

How likely is it that bacterial infections often trigger transgenerational induced resistance, yet we failed to detect it? Although our sample size was modest (n = 7-8), we found no consistent trends or marginally significant results ($p < 0.1$), except for symptoms after syringe infection of *Pv* RMX3.1b (p = 0.099, see Fig. 3.7). Thus, there is no clear indication that increasing the sample size would reveal transgenerational induced resistance phenotypes. Another possible limitation is that each infection lineage is represented by the progeny of a single plant. Bacterial infections are variable between biological replicates; using a single lineage risks randomly selecting a line with an unusually strong (or weak) inducing infection, which could impact the strength of resistance phenotypes in the next generation (Hannan Parker et al., 2022). The fact that we used lines that had two generations of the same stress treatment, however, likely mitigated variability between plant lines from potential uneven infection conditions in one generation. Third, the seeds used in our experiment were approximately two years old. Lang-Mladek *et al.* (2010) found that stress-induced genomic instability decays rapidly as seeds age; plants derived from stressed parents are indistinguishable from control plants in as little as 2-4 months of seed aging. It is therefore possible that our experimental conditions initially triggered transgenerational induced resistance, but resistance phenotypes were reset before the offspring were challenged with the pathogens. That said, the time between generations of wild *A. thaliana* is ∼6 months (Shindo et al., 2007): in the field, inherited resistance from previous generations may be reset prior to germination if these phenotypes decay quickly. Further research examining the stability of transgenerational induced resistance is critical to understanding its relevance in an ecological context.

The challenges of observing transgenerational induced resistance would likely be greater in field conditions. In nature, plants are subject to a slew of abiotic and biotic stressors over

the course of a lifetime. Simultaneous exposure to multiple abiotic stressors generally impedes transmission of plastic resistance phenotypes to the next generation (Lampei, 2019). Similarly, we found that plants subjected to multispecies co-infections produced offspring with the same resistance phenotypes as the offspring of mock treated plants; co-infection lineages did not exhibit increased resistance or susceptibility to *Pv* RMX3.1b nor *Ps* NP29.1b. Furthermore, any plastic resistance phenotypes that are successfully transmitted to the next generation are often overwhelmed and quickly reset by within-generation stress (Uller et al., 2013; Ballhorn et al., 2016). Thus, field conditions are less likely to generate and maintain measurable transgenerational induced resistance than high-intensity, single-stress exposures assayed in the lab.

The disparity between our study and previous work in transgenerational induced resistance in *A. thaliana*-bacterial pathosystems highlights the need for experiments utilizing conditions that more closely replicate field conditions, or better yet, true field studies. It is clear that transgenerationally transmitted plastic phenotypes *can* be generated in many scenarios in the lab, but unusually intense, single-stress assays in the laboratory do not always translate well to ecologically relevant conditions.

In conclusion, we argue that in nature, typical pathogenic bacterial infections of *A. thaliana* are unlikely to cause transgenerational induced resistance that impacts the evolution of *A. thaliana*-bacterial pathosystems. We found no evidence that pathogenic bacterial infections result in transgenerational induced resistance in *A. thaliana* when basic infection parameters mimic natural infections. Indeed, this makes sense in light of observations that wild *A. thaliana* interacts diffusely with its bacterial pathogens (Karasov et al., 2014); thus it is unlikely that parental disease pressure accurately predicts disease pressure in offspring. Selection is not predicted to favor transgenerational induced resistance unless the ecological context of parental plants strongly predicts the ecological context of their offspring (Kuijper et al., 2014). Thus, it is unlikely that transgenerational induced resistance is an important

factor in *A. thaliana* - bacterial interactions in nature.

3.5 Supplemental Figures
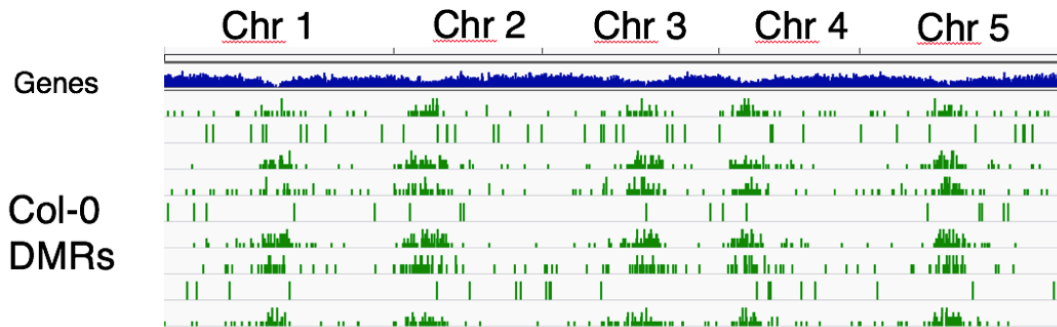
Figure 3.10
**Inoculation-induced differentially methylated regions (DMRs) in the parental
generation**. Each green tick denotes a genomic region where the methylation level
changed more than 20% in response infection, as compared to the methylation level of the
same region in the mock-treated sample. There are 9 methylation profiles, 3 comparisons x
3 sequence contexts: the first three rows are mock vs. *Ps* NP29.1a CG methylation, CHG
methylation, and CHH methylation; the next three rows are mock vs. *Pv* RMX3.1b CG,
CHG, and CHH; and last three rows are mock vs. co-infection CG, CHG, and CHH. Image
credit, J. Herman
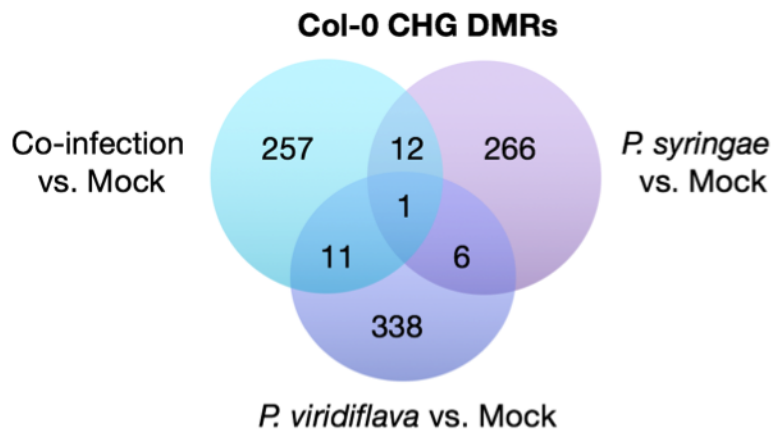
Figure 3.11
Col-0 CHG DMRs in different infection contexts. co-infection induced distinct
changes compared to single-species inoculations. Results for the CG and CHH sequence
contexts are similar (data not shown). Figure credit: J. Herman.

CHAPTER 4

NATURAL VARIATION IN BACTERIAL THROUGH-SOIL DISPERSAL RATES GENERATES CASCADING PRIORITY EFFECTS IN PLANTS AND SOIL WITH ENDURING EFFECTS ON MICROBIOME STRUCTURE

4.0.1   Abstract

Despite the importance of dispersal in community assembly (Vellend, 2010) little is known about its impact on plant and soil microbiome assembly. Here I show that dispersal rate variation across bacterial isolates substantially affects community assembly processes with long-term consequences for plant and soil microbiome structure. Using a moderate-complexity synthetic bacterial community in a closed, peat-based microcosm, I show that remarkable variation in through-soil colonization rates across bacterial isolates rapidly generates restrictive microbial communities within centimeters of soil. These "biological barriers" interfere with subsequent bacterial dispersal, which, in conjunction with plant-specific priority effects, has enduring consequences for plant microbiome structure. Furthermore, when dispersal is required to colonize distant soil sites in this experimental system, the impact of priority effects on soil community structure increases with the distance to the microbial inoculation site, likely from greater spacing between arrival times. These processes occur at spatial and temporal scales that are highly relevant to plants in the field and underlie the maintenance of divergent communities in a continuous soil environment. Given the growing efforts to manipulate microbial communities for agricultural, health, and industrial purposes, microbial dispersal - a key driver of community assembly - deserves increased attention.

4.0.2 Introduction

Dispersal, or the movement of species through space, is widely accepted as a major factor in macroscopic community assembly (Vellend, 2010) and is likely to play a key role in free-living and host-associated microbiome assembly (Baltrus, 2020; Custer et al., 2022). In addition to determining the ability of an organism to reach a target community, relative dispersal ability affects the order and timing of species' arrival to a community. This is important because arrival order and timing can change how community members interact with one another, leading to significant alterations in community membership and composition (Chase, 2003). For example, when similar species compete for the same niche space, species that arrive early in community assembly may gain an advantage over later arrivals by preempting niche space. Additionally, early arrivals may modify the environment to the detriment, or benefit, of later arrivals (Fukami, 2015). This phenomenon, known as priority effects, can have long-term effects on community structure and function and has been documented in many ecological systems (Fukami, 2015). In plants, experiments manipulating the arrival order and timing of microbes to plant tissues show that priority effects can have lasting effects on microbiome structure (Toju et al., 2018; Carlström et al., 2019; Debray et al., 2022). However, it remains uncertain if natural variation in microbial dispersal rates is likely to generate priority effects.

Dispersal rate variation is well-documented across macroscopic taxa. Dispersal rate variation among microbial taxa, on the other hand, is poorly elucidated (Barbour et al., 2023). A wide range of microbial dispersal rates in terrestrial environments is certainly possible. Microbes employ diverse cellular machinery to move through space (Wadhwa and Berg, 2022) and vary in their movement speeds across agar and other surfaces (Henrichsen, 1972; Krüger et al., 2018). Nevertheless, data on the variation of active, through-soil microbial dispersal rates is almost nonexistent; to my knowledge only one study with a short temporal scope exists (Wolf et al., 2015). Understanding through-soil bacterial dispersal patterns is key to understanding plant microbiome assembly because the soil surrounding the plants is

a major source of bacteria that populate the plant microbiome (Bodenhausen et al., 2013; Tkacz et al., 2020). Critically, if microbial through-soil dispersal rate variation generates priority effects with meaningful, long-term impacts on plant microbiome structure, priority effects likely play a role in plant microbiome assembly in nature.
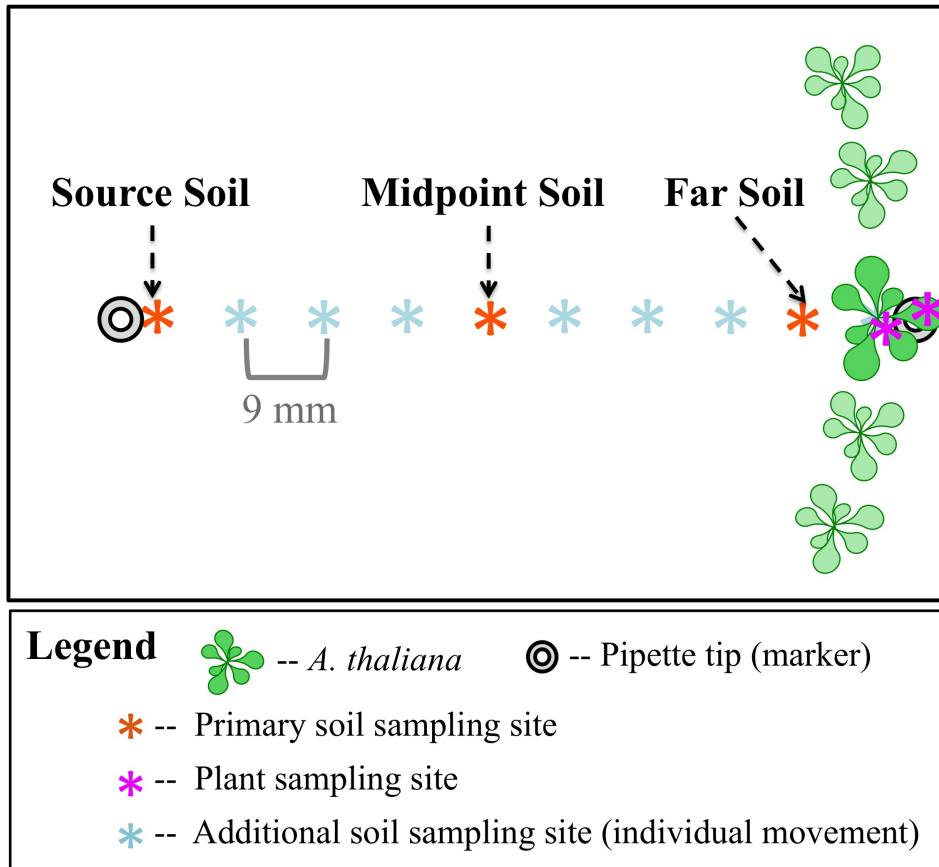
Figure 4.1
Sampling procedure with soil microcosm. Before inoculation, 10 μL pipette tips were placed 90 mm apart in microcosms to ensure equivalent testing locations across replicates. Soil cores were extracted at three points, Source Soil, Midpoint Soil, and Far Soil, as indicated by the orange asterisks. Plant tissues were harvested at each time point (pink asterisks) with entire cotelydons and young seedlings harvested as a single sample. After Day 14, roots and rosettes were processed separately. All plants within a microcosm were combined into a single sample. In Localized Start microcosms, Source Soil was the inoculation point for the SynCom. In Mixed Start Boxes, the SynCom was evenly distributed throughout the entire microcosm, including onto host plants. Blue asterisks denote the additional sampling points for individual movement assays, in which each SynCom member was inoculated alone at the Source Soil location.

To address these open questions, I curated a bacterial Synthetic Community (SynCom) composed of 83 isolates, representing 42 species, from field-grown *Arabidopsis thaliana* rhi-

zospheres (Supplementary Table 4.1). Isolates were selected to maximize phylogenetic diversity of the synthetic community rather than by functional characterizations. In closed, peat-based microcosms (loosely based on Kremer et al. (2021)), I inoculated the SynCom using two methods that altered the amount of through-soil dispersal required to reach the host plant and compared the resulting plant microbiome structure. In the first treatment, designated "Mixed Start", the SynCom was evenly distributed throughout the microcosm, including direct inoculation onto plants; thus, there was limited opportunity for dispersal variation to impact microbiome assembly. In the second treatment, designated "Localized Start", the SynCom was inoculated at a single location (Source Soil), requiring bacteria to disperse through approximately 6 centimeters of soil to colonize plants. Microbiome structure was characterized for five weeks by marker gene sequencing. Plant tissues and soil cores from three locations (Source, Midpoint, and Far) were destructively harvested at two days post-inoculation and weekly from Day 7 - Day 35 (Figure 4.1, n = 7 with plants, per inoculation method per time point). Thus, I tested if microbial dispersal through several centimeters of soil altered plant and soil microbiome structure over time frames relevant to the lifespan of *A. thaliana*.
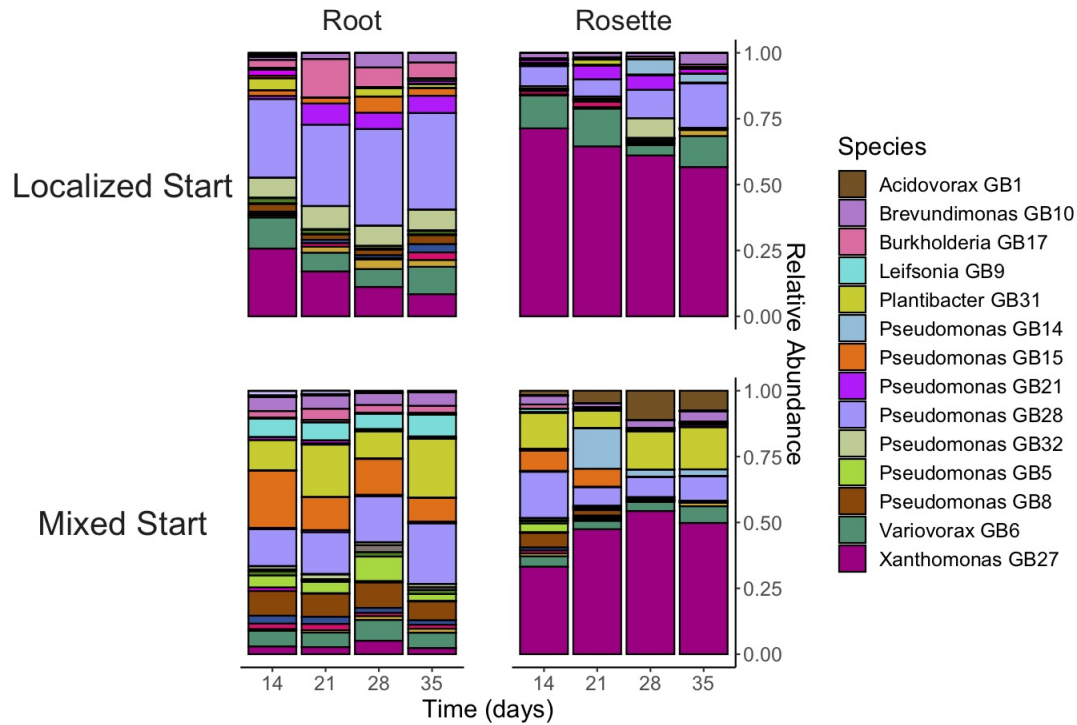
Figure 4.2
Plant community structure varies between dispersal treatments and tissue types. Each stacked bar represents the mean community composition of biological replicates at one time point. Each color represents a distinct species; only species that reached at least 5% relative abundance or greater are included on the legend. Top row: Localized Start (colonized) plant tissues. Bottom row: Mixed Start (directly inoculated) plant tissues.
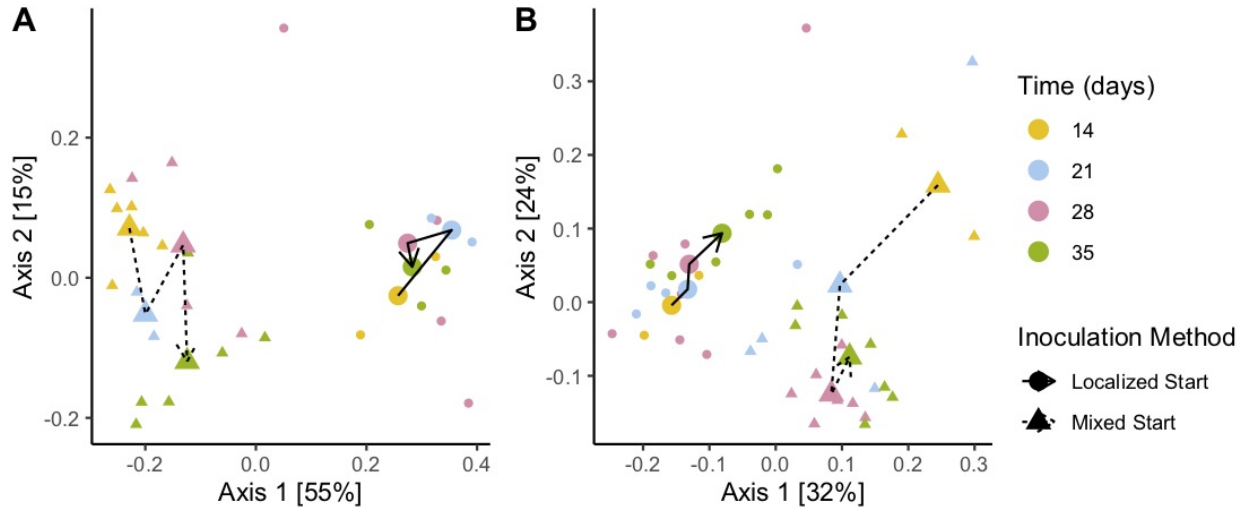
Figure 4.3
Root and rosette associated microbiomes in different dispersal treatments do not converge. Principal coordinate analysis of Bray-Curtis dissimilarity. A) Root and B) Rosette community structure over time. Circles denote Localized Start communities while triangles denote Mixed Start communities. The color of the point denotes time as indicated in the legend. The enlarged points represent the group median of each dispersal treatment and time point combination. Solid arrows follow Localized Start communities over time, while dashed arrows follow Mixed Start communities over time.

Initial dispersal limitation had long-lasting and substantial effects on plant microbiome structure. Considering all plant tissues over the course of the experiment, dispersal treatment accounted for 17% of the variation in community structure (Bray-Curtis dissimilarity, PERMANOVA, df = 1, F = 52.9, $p < 0.01$). In addition to dispersal treatment, tissue type, time, and the interaction between these three factors also explained significant portions of community structure (Supplemental Table 4.2), as expected from previous work Fitzpatrick et al. (2020). These effects remained consistent across data transformation procedures and community composition metrics (Supplemental Table 4.2).

Localized Start rosettes and roots remained distinct from their Mixed Start counterparts over several weeks (Figures 4.2 & 4.3). Post-hoc analyses within tissues revealed that dispersal treatment explained large portions of variation in community structure (Bray-Curtis dissimilarity, within roots: df = 1, $R^2 = 0.49$, F = 28.8, $p < 0.01$; within rosettes: df = 1,

84

$R^2 = 0.25$, F = 15.6, $p < 0.01$). Additionally, effect of dispersal remained significant when comparing Localized Start tissues with their Mixed Start counterparts at Day 35 ($p < 0.01$). Not only did the two dispersal treatments remain distinct, they did not appear to be on a trajectory moving towards convergence over time on major principal coordinate axes, thus these differences were likely to extend beyond the five weeks of the experiment (Fig. 4.3).
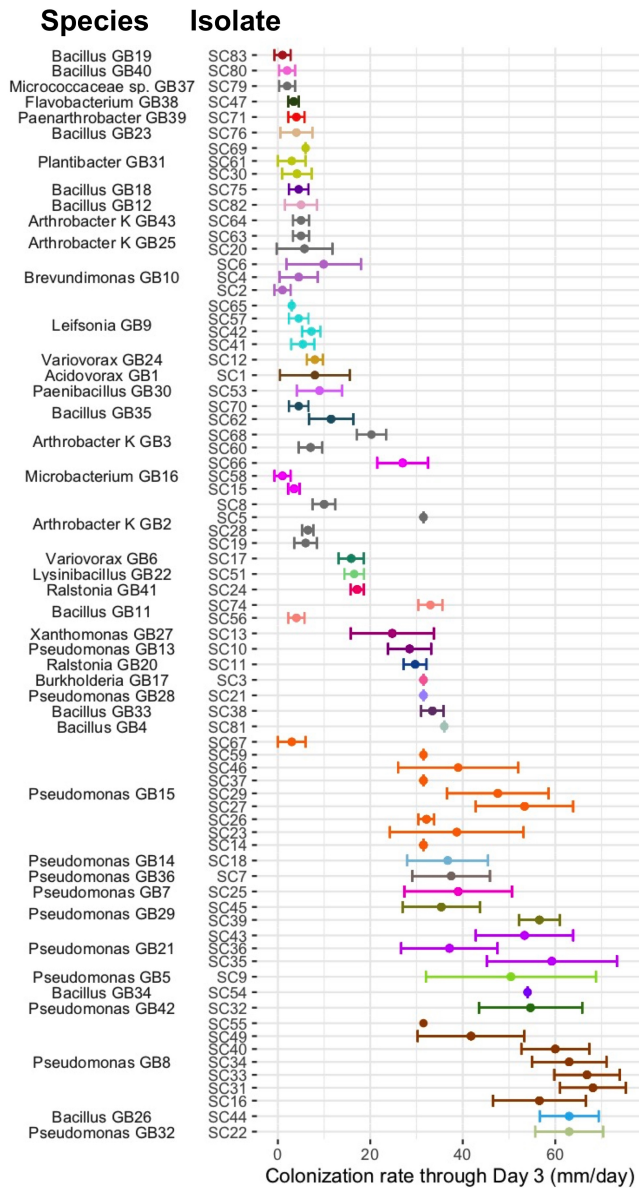
Figure 4.4
SynCom isolates colonize the soil microcosm at variable rates. Each horizontal line represents an isolate. The point represents the mean colonization rate of the isolate, and error bars represent one standard deviation. Isolates within a species complex (defined as containing a unique fragment of DNA *gyrase β*) are the same color and proximal to each other on the graph. The graph is ordered by the mean colonization rate of the species complex. Colonization rates were calculated by averaging the daily movement rates for three days. In instances where isolates moved across the box in less than 3 days, rates were calculated from daily movement rates of the first 1-2 days.

86
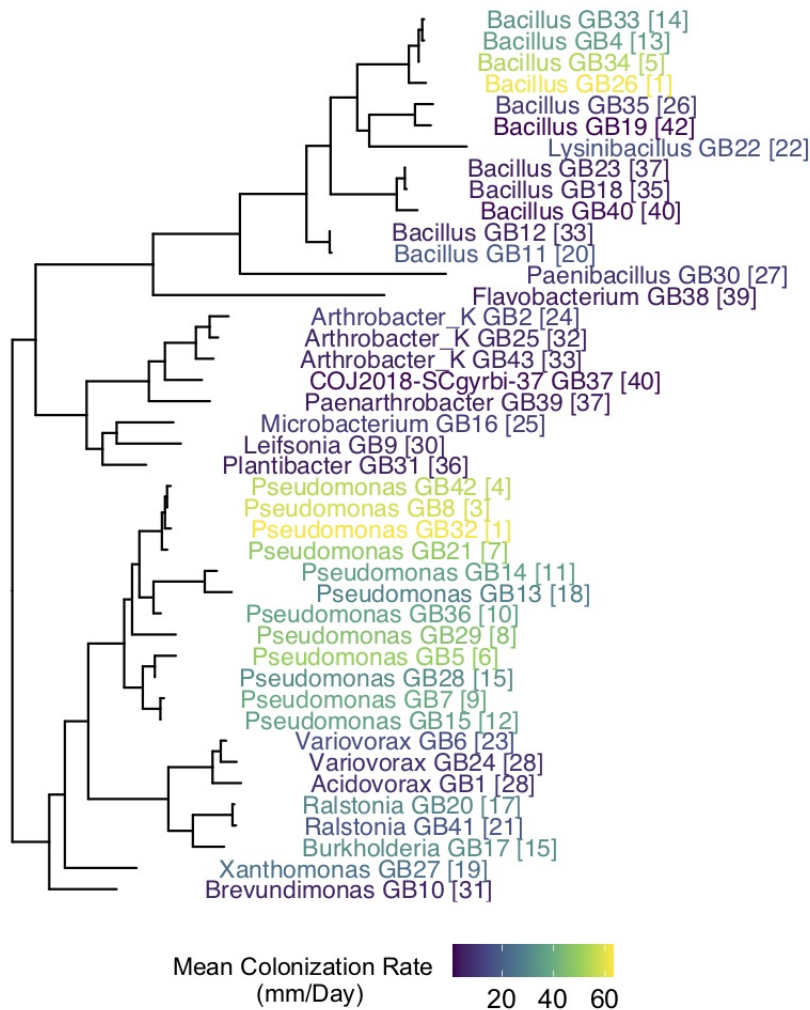
Figure 4.5
Closely related species disperse through and colonize the soil at similar rates.
Phylogeny was based on genomic *gyrB* sequences using MAFFT to align sequences and
FastTree to construct the phylogenetic tree. SynCom species are colored by mean dispersal
rate as indicated on the legend. The ranked dispersal rate out of 42 SynCom species is
listed in brackets by each species' name, with 1 being the fastest.

If variation in motility is sufficient to explain the differences in microbiome structure
across dispersal treatments, I predicted that immobile or low-motility species would be ab-
sent from Localized Start plant tissues but present in Mixed Start plant tissues. To explore
this hypothesis, I first determined the individual through-soil dispersal rates of each Syn-
Com member when released alone in the soil microcosm by recording the locations of colony

87

forming units in 10 evenly spaced sites across the soil (modified from Bashan (1986), Supplemental Figure 4.19). Microcosms were repeatedly sampled immediately post-inoculation and every 24 hours thereafter to obtain a per day dispersal rate. There was impressive variation in species' colonization rates, ranging from ~0.3 mm per day to >63 mm per day (Figure 4.4). Isolates colonized the soil at approximately linear rates (Supplemental Figure 4.11). All SynCom species, with the exception of two *Bacillus* species, colonized the entire soil sampling region well within the experimental time frame (Supplemental Figure 4.11). However, the absence of these two Bacilli did not explain differences between the complex communities that formed in the two dispersal treatments. Instead, I found that these two largely immobile Bacilli species were immediately excluded from all soil and plant associated communities, regardless of dispersal requirements. Thus, innate motility limitation did not prevent SynCom members from reaching the plants (Supplemental Figure 4.14, *Bacillus* GB19 and GB40).

I additionally found that through-soil dispersal rate was linked to phylogeny. In general, isolates within a species complex, defined here as sharing identical copies of a fragment of DNA *gyrase* β-subunit (*gyrB*), dispersed at comparable rates (but note several clear instances of intraspecific variation, Fig. 4.4). Closely related species likewise exhibited similar movement rates; several non-random clusters of movement rates were observed across the tree (Fig. 4.5, Local Indicator of Phylogenetic Association, $p < 0.05$). Thus, two important patterns emerged; first, species arrived asynchronously to distant sites (including plant tissues) and second, related species were often predicted to arrive at the plant at similar times.
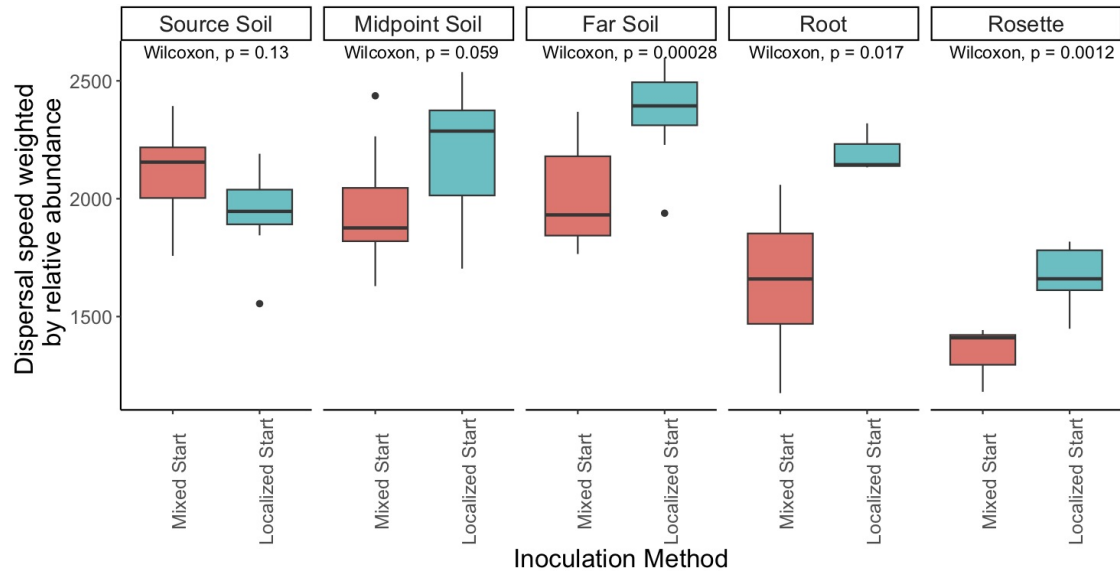
Figure 4.6
Microbiomes in Localized Start plant tissue and Far Soil are enriched for fast-moving microbes compared to Mixed Start microbiomes. The relative abundance of each species was multiplied by its mean colonization speed to obtain mean community level colonization speed. At Day 35, the overall community speed of roots, rosettes, and Far Soil was faster when substantial through-soil dispersal was required (Localized Start) compared to directly inoculated counterparts (Mixed Start). Kruskal-Wallis ($p < 0.05$), using within sample type Wilcoxon post-hocs ($p < 0.05$).

Although immobility was insufficient to explain the differences between plant microbiomes in Localized and Mixed Start inoculations, microbial dispersal rate could still affect community composition if priority effects altered community interactions. Because priority effects typically benefit early arrivals in related systems (Carlström et al., 2019), I asked if fast dispersers were over-represented in microbiomes assembled after Localized Start inoculation. To test this, I calculated the community-level dispersal rate of final microbiomes by multiplying the relative abundance of each species by its mean individual colonization speed and compared community level dispersal rates between dispersal treatments. Total community dispersal rates were significantly higher in Localized Start plant tissues and Far Soil sites relative to Mixed Start plant and soil sites (Fig. 4.6). This suggests that priority effects, with an early arrival advantage, may be contributing to the structure of soil and

plant microbiomes.
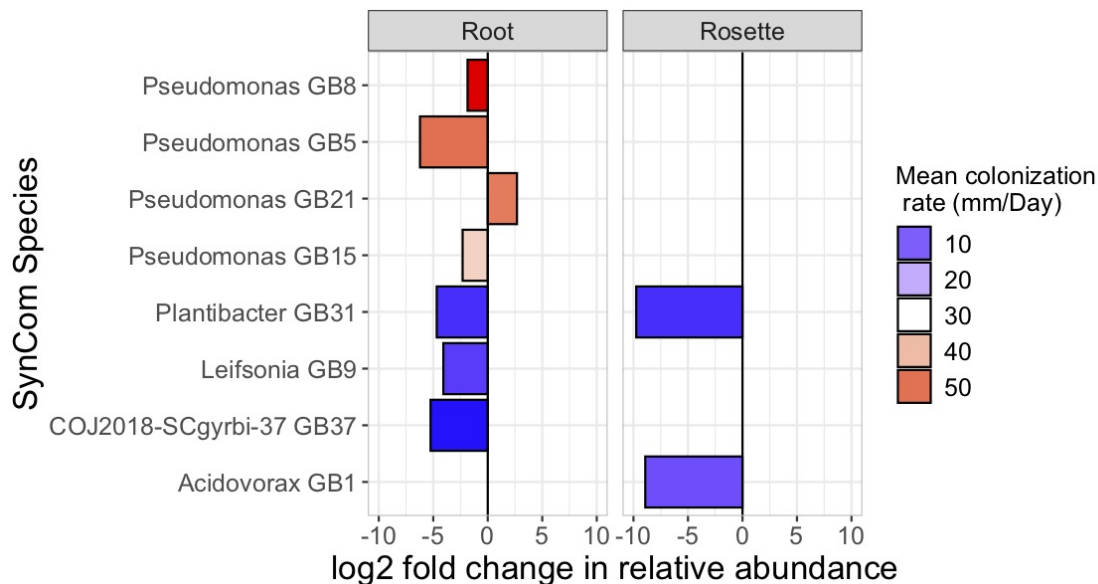
Figure 4.7
Differentially abundant SynCom species in roots and rosettes. Bars show the
log2-fold enrichment or depletion of SynCom species in Localized Start plant tissues
compared to their Mixed Start counterparts on Day 35 (DESeq2, p < 0.01). Bars are
colored on a gradient scale by the species' mean colonization rate.

To further investigate whether priority effects acted through a modification of species
interactions, I explored the simplistic hypothesis that dispersal rate would correlate pos-
itively with membership or final relative abundance of individual taxa in Localized Start
communities. I found that dispersal rate did not predict membership in Localized Start
communities (Supplemental Figure 4.12, Kruskal-Wallis, p > 0.05) and did not correlate
with relative abundance of species within microbiomes (4.13, linear regression, $R^2 < 0.01$).
I then asked which species were affected by dispersal treatment, and if this had any relation
to dispersal rate. Of the 8/42 SynCom species that were differentially abundant in Localized
Start plant tissues compared to Mixed Start plant tissues, both relatively fast- and slow-
moving taxa were affected (Figure 4.7, DESeq2, p < 0.01). Generally, species were depleted
in Localized Start plant microbiomes compared to Mixed Start microbiomes, but depleted
taxa exhibited a range of dispersal rates. Thus, while dispersal rate variation affected overall

community structure, the impact of dispersal rate on individual species was more complex, likely reflecting the interplay between dispersal, selection by the environment and species interactions.

Priority effects appear to drive at least some of these changes in relative abundance across dispersal treatments. One particularly compelling example is *Plantibacter* GB31, which was highly successful in Mixed Start rosettes, reaching ∼15% relative abundance by Day 35, but was absent from Localized Start rosettes (Fig. 4.2, Supplemental Figure 4.14). This absence is not explained by motility limitation because *Plantibacter* GB31 established populations in roots and the surrounding Far Soil in Localized Start microcosms, albeit at lower prevalence and abundance (Fig. 4.7 and Supplemental Figure 4.14). This suggests *Plantibacter* GB31 was excluded from rosette communities via rosette-specific priority effects. Indeed, of the 8 differentially abundant taxa between dispersal treatments, 6 species successfully established in plant tissues or the immediately surrounding soil. This suggests that plant-based priority effects altered the final representation of these species in the community.

Intriguingly, priority effects in soil communities appeared to prevent some species from reaching the plant at all. Like *Plantibacter* GB31, *Acidovorax* GB1 was well-represented in Mixed Start rosettes and colonized the soil matrix in approximately one week in isolation. However, *Acidovorax* GB1 failed to colonize Localized Start rosettes (Fig. 4.2 & 4.7, Supplemental Figure 4.11). The absence of this relatively slow-dispersing species was mirrored in the roots and in the Far Soil surrounding the plant (Supplemental Figure 4.14). Unexpectedly, *Acidovorax* GB1 coexisted for 5 weeks within the SynCom at the inoculation site (Source Soil), suggesting that its exclusion from other soil communities was a result of its late arrival. This suggests that restrictive bacterial communities quickly established within soil, effectively creating "biological barriers" that impaired otherwise mobile species from reaching favorable environments like plant tissues. Such barriers could theoretically be established through numerous mechanisms, for example, early arrivals may have consumed the

resources required to support active motility (Martínez-García et al., 2014), secreted toxic compounds (Lewis, 1929), or established physical structures (e.g. biofilms) that inhibit colonization (Nadell et al., 2015). Strikingly, biological barriers appeared over short time scales and distances. Considering the individual colonization rates of these bacteria, restrictive communities must have assembled within days and over centimeters of soil.
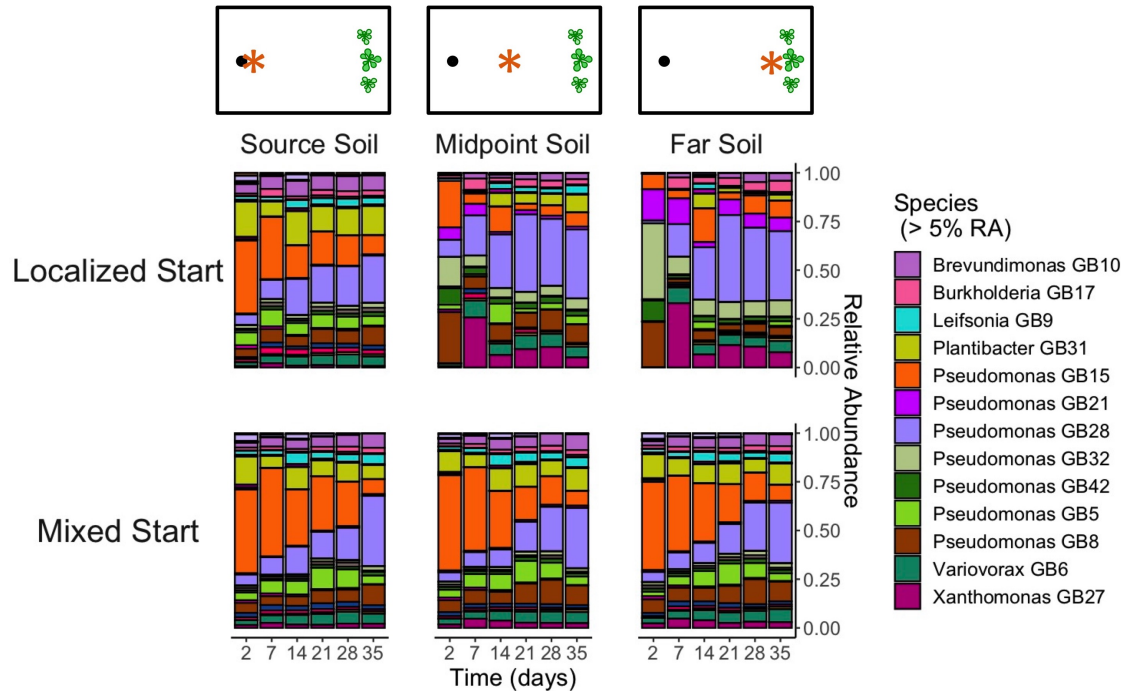
Figure 4.8
Distinct communities in different soil locations are maintained after Localized Start inoculations. Each stacked bar represents the mean community composition of biological replicates at one time point. Each color represents a species; only species that reached at least 5% relative abundance or greater are included on the legend. Columns displays communities from different soil location; the schematic above the column label shows the sampling location (orange asterisk) in relation to the plants (green symbols). Top row: Localized Start - the SynCom was inoculated into Source Soil, other soil locations are colonized by movement from this pool. Bottom row: Mixed Start - all locations were directly inoculated with the same initial community.
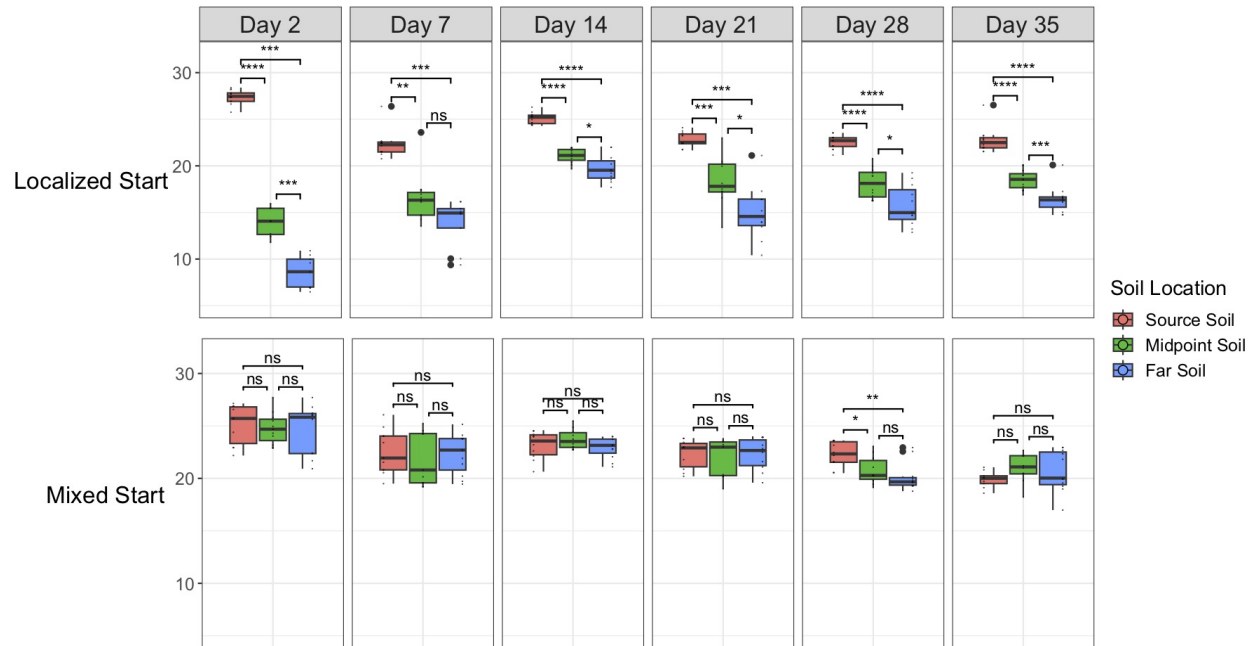
Figure 4.9
Species richness in the soil decreases as distance to inoculation site increases.
Top row: Richness of soil communities at three sites after a Localized Start inoculation.
Bottom row: Richness of soil communities after a Mixed Start inoculation. Each panel
denotes a different time point and the color of the box plot represents the soil site, as
indicated by the legend. In Localized Start microcosms, Far and Midpoint Soil (blue and
green) never attain the species richness maintained in the inoculation site (Source Soil,
red). Midpoint Soil maintains greater diversity than Far Soil. In Mixed Start microcosms,
all sites were directly inoculated and maintain the same number of species as one another
except at Day 28. Asterisks denote statistically significant differences ($p < 0.05$) in
Wilcoxon post-hoc tests with Benjamini-Hochberg correction for multiple testing. "ns" =
not significant.
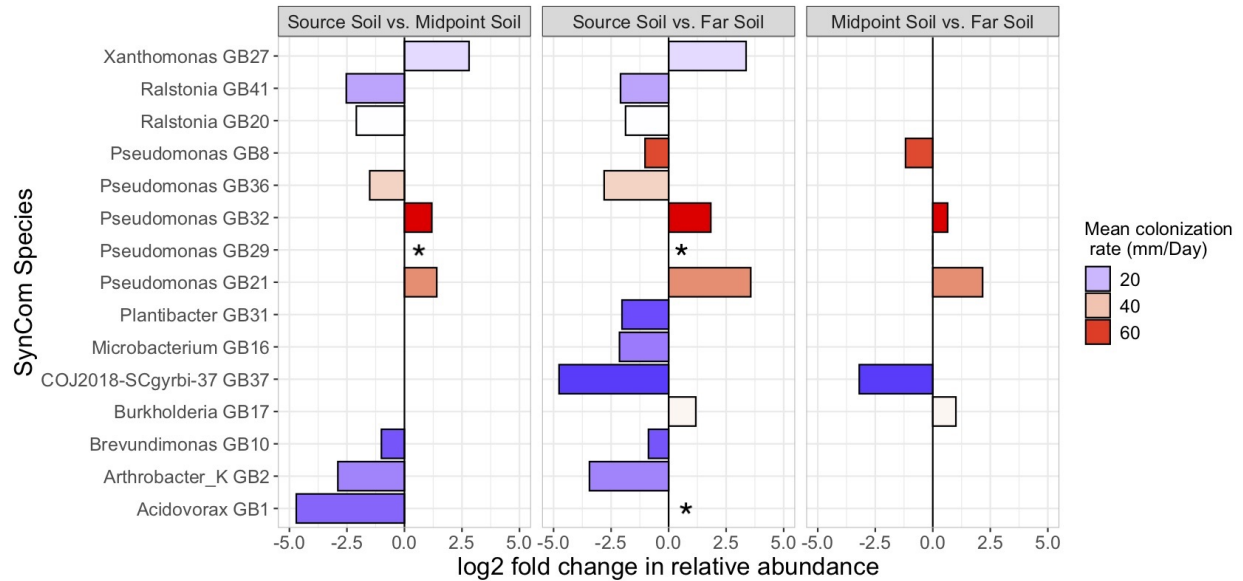
Figure 4.10
More species are affected by priority effects in soil as distance to inoculation site increases. Differentially abundant species at different soil sites within Localized Start microcosms. Bars show $\log_2$ fold enrichment or depletion of species between soil sites (DESeq2, $p < 0.05$ and ANCOM). Asterisks denote significance using ANCOM including structural zeros, i.e. species were present in Source Soil but absent from distant soil sites. More species are differentially abundant in Source Soil vs. Far Soil than in Source Soil vs. Midpoint Soil. Increased distance from the inoculation site augments the advantage for *Pseudomonas* GB21 and *Pseudomonas* GB32 in Localized Start microcosms.

To further investigate the ecological significance of priority effects on the structure of soil communities, I compared community composition of the three sampled soil locations. Across all soil samples, dispersal treatment, soil site, time and the interactions between these factors explained significant components of community variation (PERMANOVA, Bray-Curtis dissimilarity, p < 0.01). Consistent with the importance of priority effects in plants, Midpoint and Far Soil sites remained distinct and on separate successional trajectories from the Source Soil within Localized Start treatments over the course of the experiment (PERMANOVA site effect within each time point: p < 0.01), whereas soil sites within Mixed Start treatments were indistinguishable from one another (PERMANOVA site effect within each time point: p > 0.01) (Figure 4.8, Supplemental Figure 4.15). The dissimilarity between soil

94

communities in Localized Start dispersal treatments increased as physical distance from the Source Soil increased (effect of site in pairwise PERMANOVAs on Bray-Curtis dissimilarilty at Day 35, Source versus Midpoint: $R^2 = 0.24$, F = 20.0, p < 0.01; Source versus Far: $R^2 = 0.49$, F = 7.30, p < 0.01), which was likely due to the extended intervals between species' arrivals enhancing priority effects (Svoboda et al., 2018). Species richness of soil communities reflected the presence of biological barriers; fewer species successfully established in Far Soil than in Midpoint Soil, which in turn had lower richness than Source Soil (Figure 4.9, Kruskal-Wallis (p < 0.05), Wilcoxon posthoc with Benjamini-Hochberg adjustment, p < 0.05). Overall, the dispersal treatment affected the representation of more than a third of the SynCom (15/42 species) in soil communities (Figure 4.10). Thus, priority effects appeared to have a widespread influence on soil communities, generating and maintaining distinct microbial communities within a continuous environment. This suggests that variation in bacterial dispersal rates will generate localized distributions of soil microbes and support the maintenance of well-documented heterogeneity in local soil communities (O'Brien et al., 2016).

Finally, I considered the possibility that the presence of *A. thaliana* altered nearby Far Soil communities, contributing to this difference in community structure between Far Soil and Source Soil. The presence of *A. thaliana* explained a small but statistically significant portion of community variation in Far Soil but was vastly overshadowed by the impact of inoculation method (PERMANOVA, Inoculation Method: $R^2 = 0.29$, Plant presence: $R^2 = 0.01$, p > 0.01, Supplemental Table 4.3). Interestingly, post-hoc analyses within inoculation method revealed that Far Soil microbiomes were affected by plant presence only in Localized Start inoculations (PERMANOVA, p < 0.05), but small effects in Mixed Start inoculations may have been undetected due to a relatively smaller sample size.

4.0.4   Conclusion

This experiment demonstrates that natural variation in through-soil bacterial dispersal rates, over small physical and temporal scales, generates priority effects with lasting effects on plant microbiome structure. Dispersal through centimeters of soil, with arrival intervals between hours to days, alter plant microbiomes for upwards of five weeks. This is, in part, due to priority effects within plant microbiomes, a phenomenon that has been experimentally demonstrated by manipulating the arrival sequence of individual taxa or groups of species (Toju et al., 2018; Carlström et al., 2019; Debray et al., 2022). Here, I extend this result to consider arrival order that results from natural variation in dispersal rates. In addition, I show that the rapid establishment of locally restrictive microbial communities in the soil affects subsequent microbial dispersal, contributing to the maintenance of distinct soil communities within a well-connected and initially identical abiotic environment. This has significant implications for plant microbiome assembly in nature because a significant portion of the plant microbiome is derived from the soil (Bodenhausen et al., 2013; Tkacz et al., 2020), and these biological barriers can interfere with dispersal to the host. My results thus reveal the importance of biotic structure for understanding microbial dispersal patterns in soil, with significant implications for plant microbiome assembly. How these observations will translate to natural settings, where there are more avenues of dispersal and more potential for priority effects, is an exciting question.

These results provoke additional questions regarding observed patterns in plant microbiome structure in nature. Within plant populations in the field, a significant proportion of inter-individual variation in microbiome structure remains unexplained by deterministic factors such as environment (Beilsmith et al., 2021). Do highly localized soil microbial communities and/or priority effects contribute to this variability? Considering the variation in movement rates across microbial taxa, a natural question that arises is whether the predominance of Pseudomonads in wild *A. thaliana* microbiomes (Bodenhausen et al., 2013; Bartoli

et al., 2018; Karasov et al., 2018) is driven in part by their relatively high dispersal rates and priority effects? Addressing these questions will help define plant microbiome assembly rules in the field and enhance our understanding of ecological processes that drive the evolution of plants. A deeper understanding of microbial dispersal patterns and their link to priority effects and other community assembly processes will improve predictability in microbiome assembly, a major stumbling block in microbiome engineering.

Phylum	Genus	Number of Species	Species Name, Isolates within Species
Actinobacteria	Leifsonia	1	GB9 - Isolates (4): SC41, SC42, SC50, SC57, SC65
Actinobacteria	Arthrobacter_K	3*	GB25 - Isolates (2): SC20, SC63 GB2* - Isolates (8): SC19, SC28, SC5, SC60, SC68, SC73, SC78, SC8, GB43 - Isolates (2): SC64, SC72
Actinobacteria	Microbacterium	1	GB16 - Isolates (4): SC15, SC52, SC58, SC66
Actinobacteria	Paenarthrobacter	1	GB39 - Isolates (1): SC71
Actinobacteria	Plantibacter	1	GB31 - Isolates (3): SC30, SC61, SC69
Actinobacteria	Unclassified-COJ2018_SCgyrB-37	1	GB37 - Isolates (1): SC79
Bacteroidota	Flavobacterium	1	GB38 - Isolates (2): SC47, SC48
Firmicutes	Bacillus	11	GB11 - Isolates (2): SC56, SC74 GB12 - Isolates (1): SC82 GB18 - Isolates (1): SC75 GB19 - Isolates (1): SC83 GB23 - Isolates (2): SC76, SC77 GB26 - Isolates (1): SC44 GB33 - Isolates (1): SC38 GB34 - Isolates (1): SC54 GB35 - Isolates (2): SC62, SC70 GB4 - Isolates (1): SC81 GB40 - Isolates (1): SC80
Firmicutes	Lysinibacillus	1	GB22 - Isolates (1): SC51
Firmicutes	Paenibacillus	1	GB30 - Isolates (1): SC53
Proteobacteria	Acidovorax	1	GB1 - Isolates (1): SC1
Proteobacteria	Brevundimonas	1	GB10 - Isolates (3): SC2, SC4, SC6
Proteobacteria	Burkholderia	1	GB17 - Isolates (1): SC3
Proteobacteria	Pseudomonas	12	GB13 - Isolates (1): SC10 GB14 - Isolates (1): SC18 GB15 - Isolates (9): SC14, SC23, SC26, SC27, SC29, SC37, SC46, SC59, SC67 GB21 - Isolates (3): SC35, SC36, SC43 GB28 - Isolates (1): SC21 GB29 - Isolates (2): SC39, SC45 GB32 - Isolates (1): SC22 GB36 - Isolates (1): SC7 GB42 - Isolates (1): SC32 GB5 - Isolates (1): SC9 GB7 - Isolates (1): SC25 GB8 - Isolates (8): SC15, SC16, SC31, SC33, SC34, SC40, SC49, SC55
Proteobacteria	Ralstonia	2	GB20 - Isolates (1): SC11 GB41 - Isolates (1): SC24
Proteobacteria	Variovorax	2	GB24 - Isolates (1): SC12 GB6 - Isolates (1): SC17
Proteobacteria	Xanthomonas	1	GB27 - Isolates (1): SC13

Table 4.1
Synthetic Community members. The SynCom is composed of 83 isolates that fall into 42 species groups. Species are defined as containing a unique *gyrase B* fragment and are listed here with names beginning with "GB". The number of isolates within each species complex is listed in parentheses after the species name. Isolate names are listed after the semicolon, with names beginning with "SC".

	Bray-Curtis		Jaccard		Unifrac	
Factor	R^2	p value	R^2	p value	R^2	p value
Tissue	0.46602	0.001	0.35506	0.001	0.10066	0.001
Inoc. Method	0.1747	0.001	0.13894	0.001	0.23292	0.001
Time	0.05233	0.001	0.05862	0.001	0.08014	0.001
Tissue x Inoc. Method	0.03712	0.001	0.0636	0.001	0.0358	0.009
Tissue x Time	0.01481	0.151	0.02391	0.047	0.06638	0.001
Time x Inoc. Method	0.02245	0.021	0.02663	0.018	0.04444	0.01
Tissue x Time x Inoc. Method	0.01475	0.148	0.02306	0.061	0.03196	0.079

PERMANOVA results

Table 4.2
The effect of dispersal treatment is robust across β-diversity metrics. Sample type (roots or rosettes), time, inoculation method, and all interactions explain variation in community structure across many metrics. Significance was tested performing PERMANOVA on the model $Tissue \times InoculationMethod \times Timepoint$ (999 permutations).
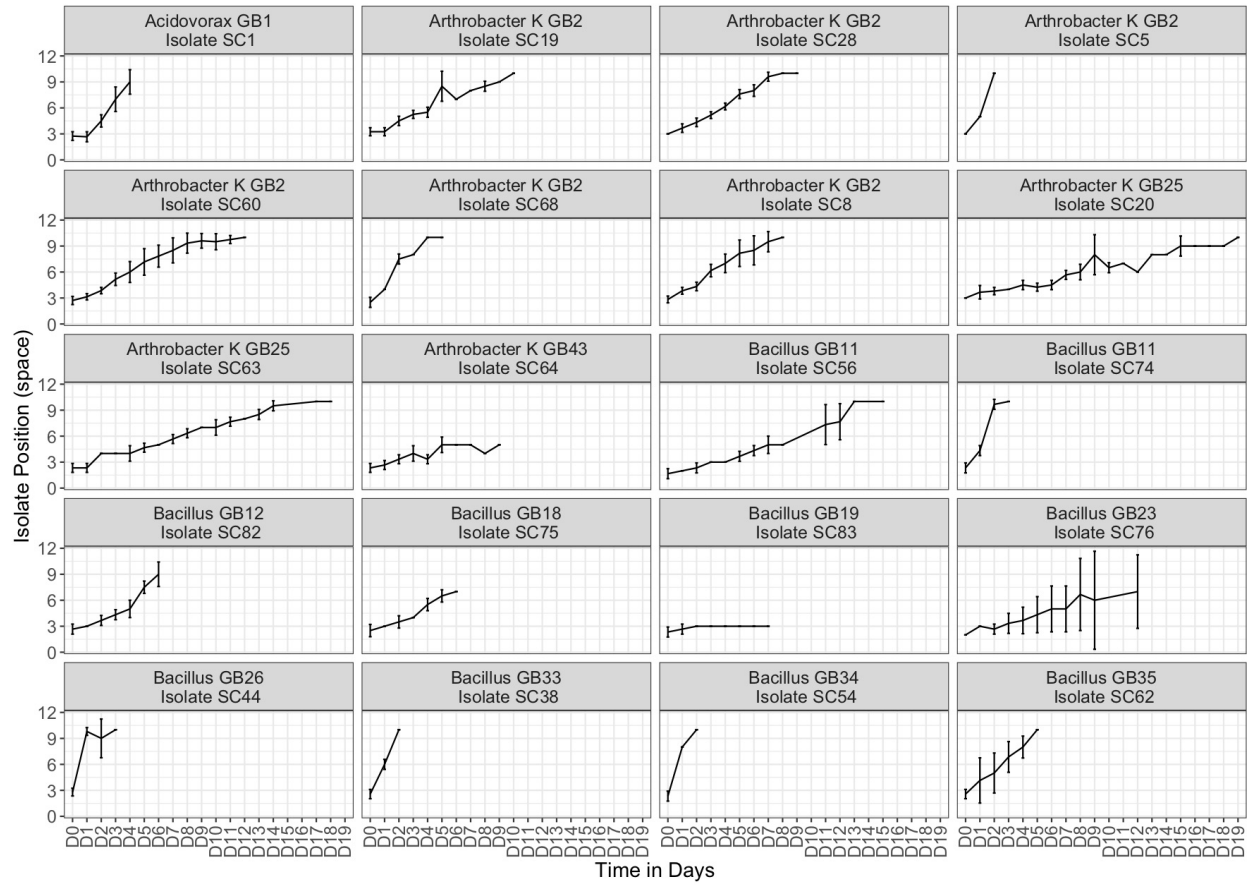
(a) Soil colonization over time for individual isolates, set 1.
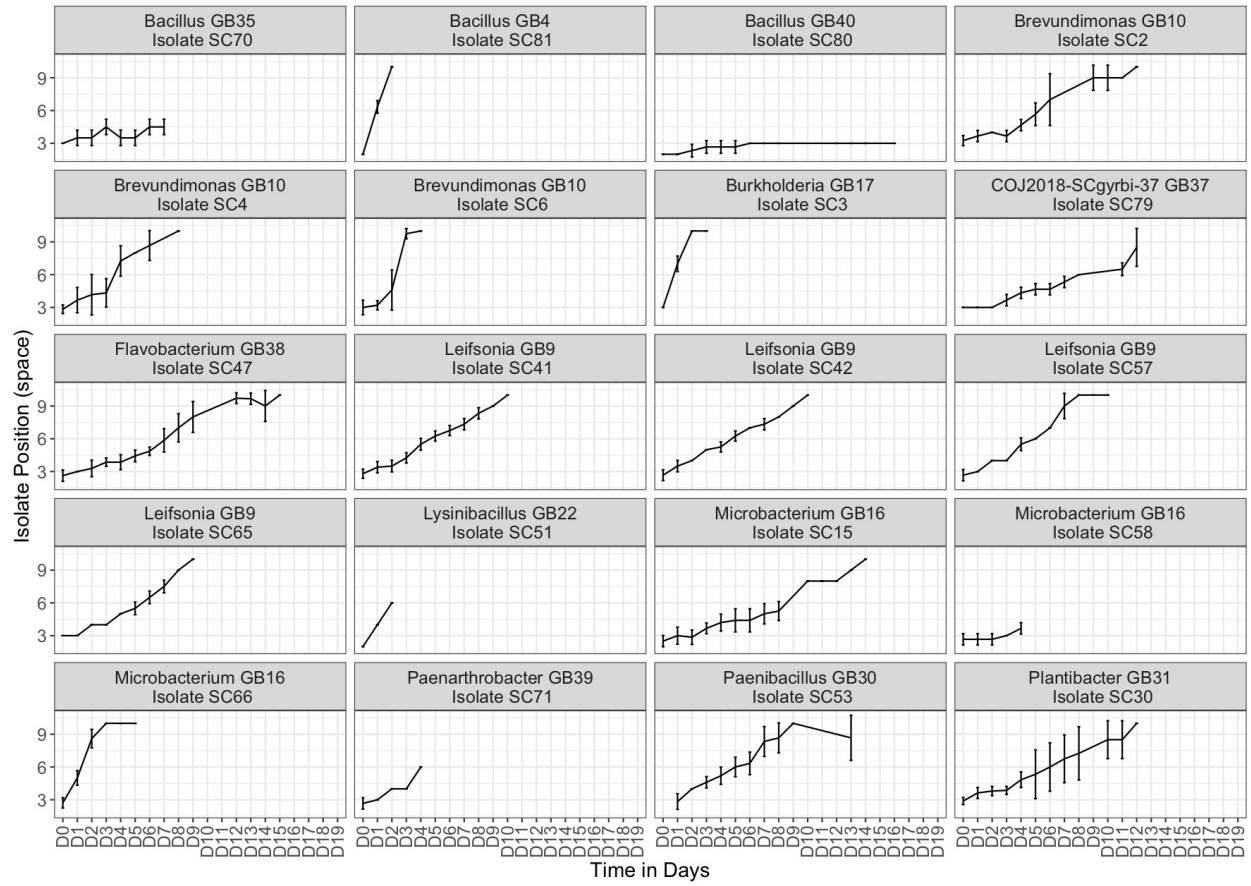
(b) Soil colonization over time for individual isolates, set 2.
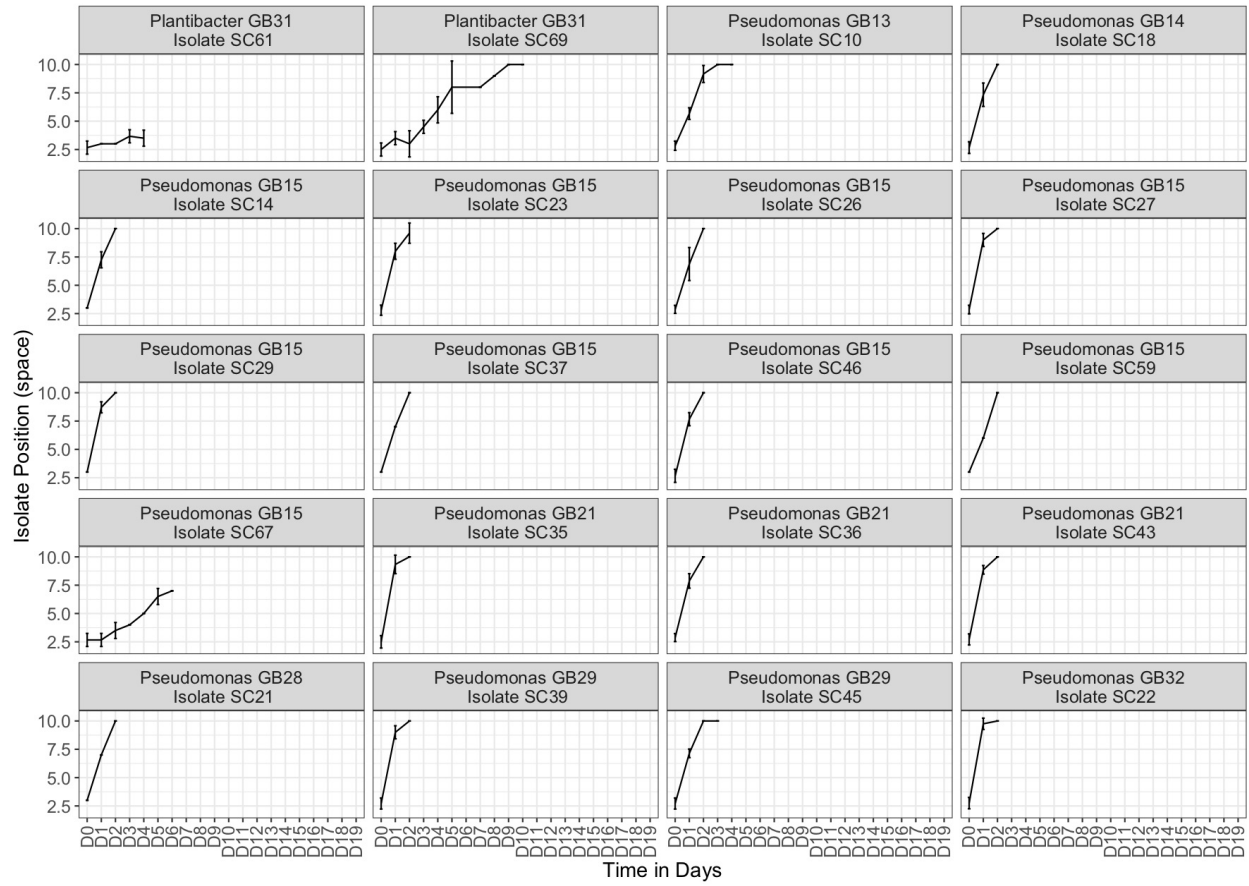
(c) Soil colonization over time for individual isolates, set 3.
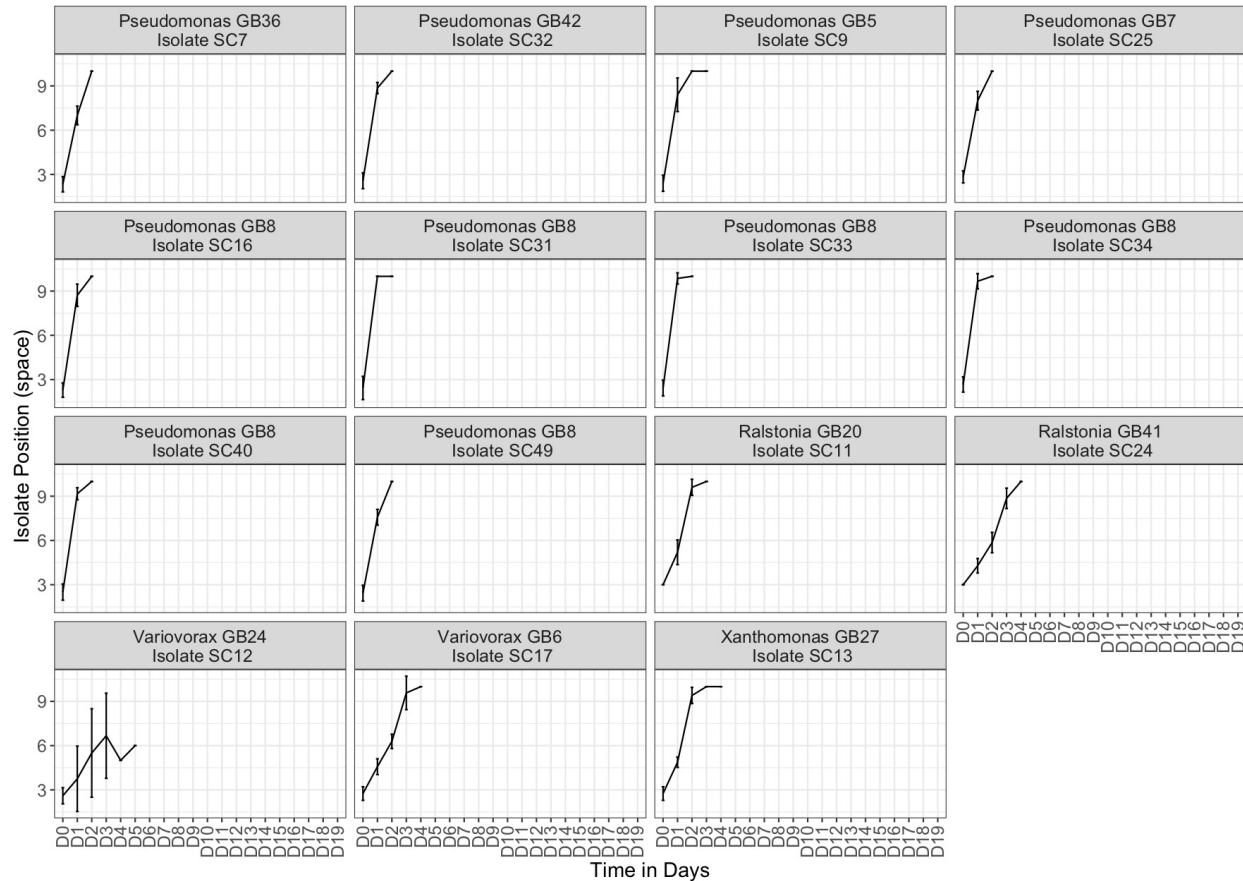
(d) Soil colonization over time for individual isolates, set 4.

Figure 4.11

Most isolates colonize the soil at roughly linear rates, and are capable of colonizing the soil matrix within 26 days. Each panel shows through-soil colonization rates of individual SynCom isolates. Panel titles list the species complex name and the isolate name underneath. Isolates were inoculated at position 1. The liquid inoculum diffused during inoculation, thus measurement immediately after inoculation (D0) are at position 2 or 3. Positions were evenly spaced 9 mm apart, with position 10 was the most distant site. Some trials were truncated due to external contamination. Error bars are standard deviation of biological replicates. Multiple isolates may represent a single species, see Table 4.1 for details. In species complexes encompassed many isolates, not all isolates were assayed, particularly if isolates had extremely similar genomes.
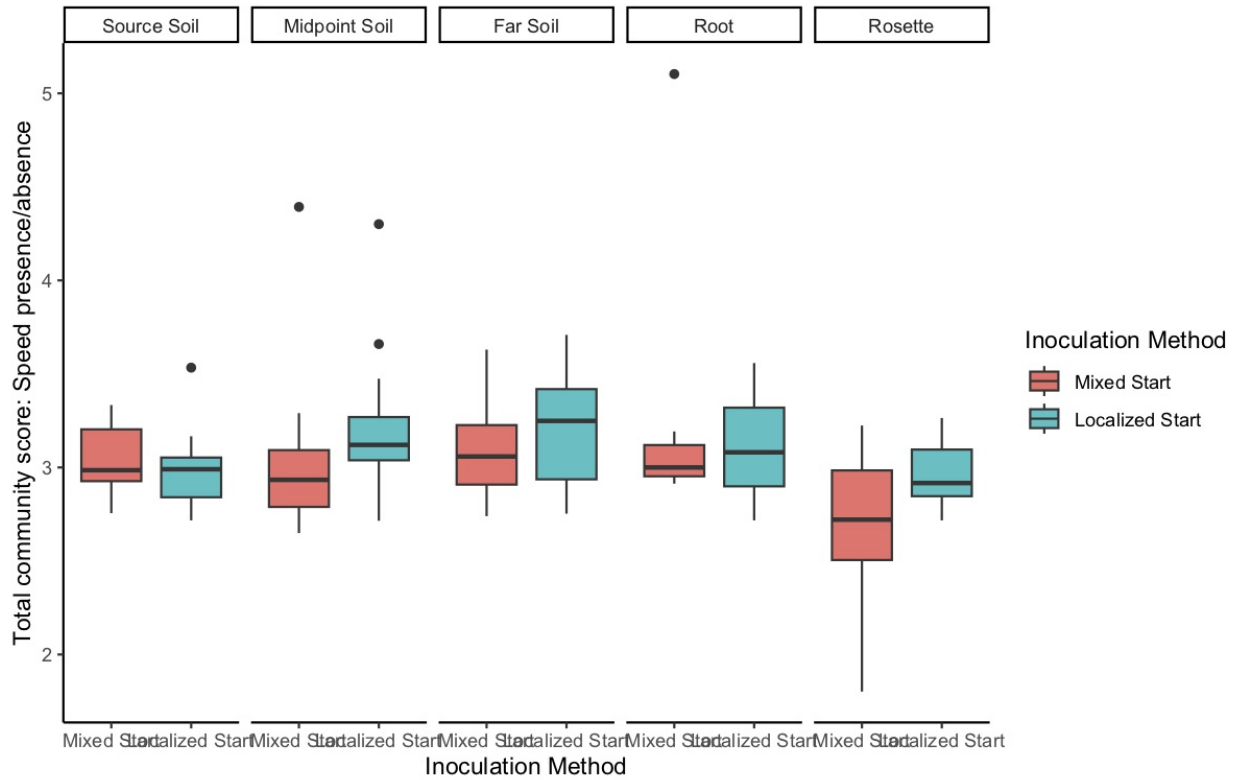
Figure 4.12
Mean colonization rate of species present in communities. After five weeks,
increased dispersal speed did not translate into increased presence in Localized Start
communities compared to Mixed Start communities. Community unweighted speed was
calculated by adding the dispersal rate of all species present in the community and dividing
by the species richness. Faster taxa were not more likely to be present in Localized Start
communities in soil or within plants (Kruskal-Wallis rank sum, p < 0.05).
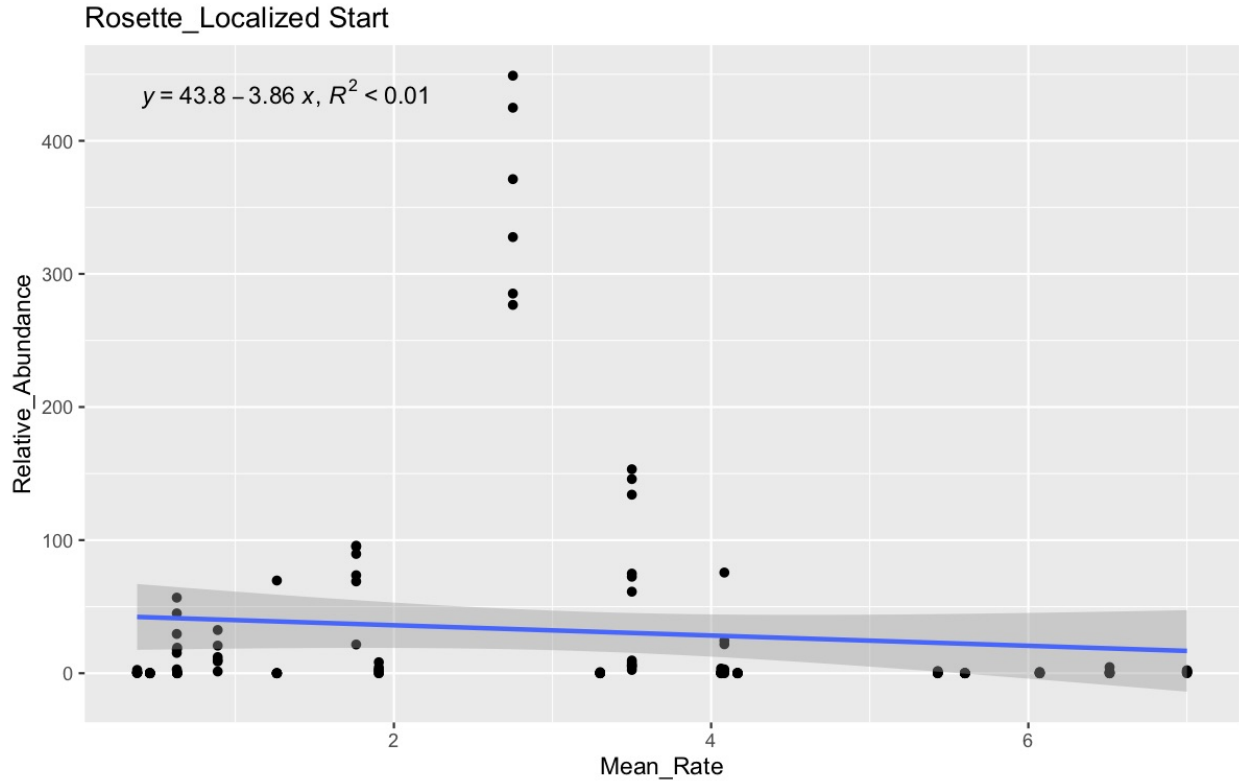
Figure 4.13

Correlation between species' soil colonization speed and community dominance in rosettes at Day 35. Individual soil colonization speed is not predictive of relative abundance in Localized Start rosettes after five weeks. Colonization speed was not correlated with taxa relative abundance in rosettes, roots, or any soil location, in either dispersal treatment.
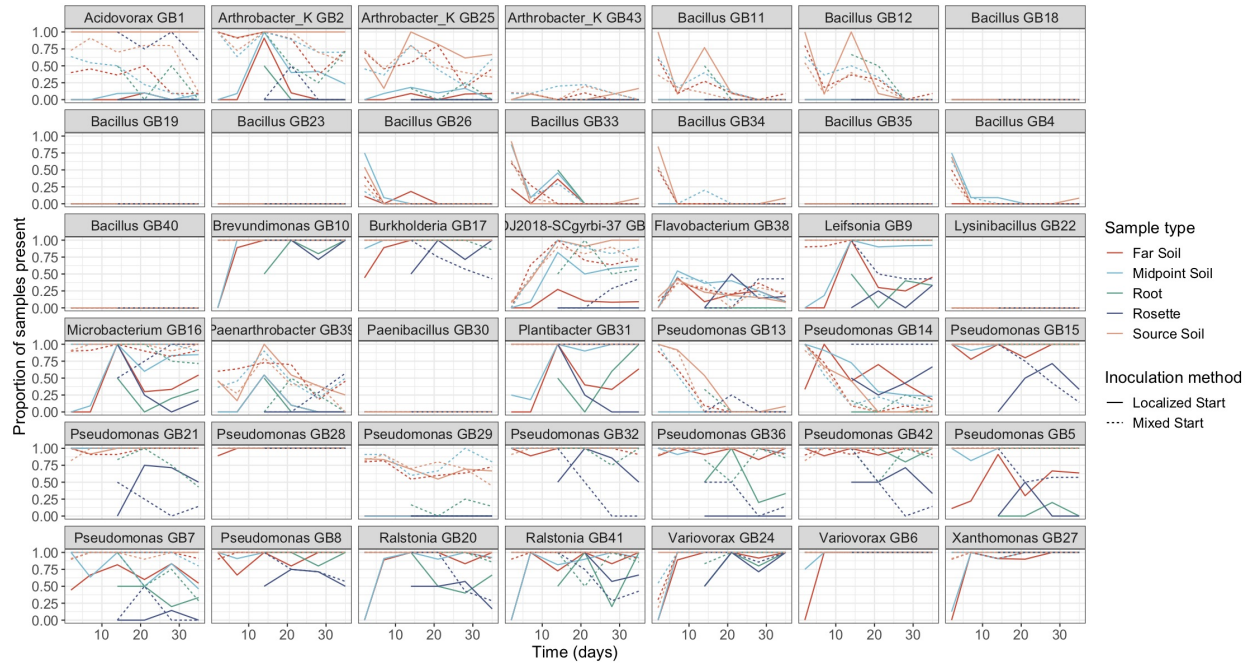
Figure 4.14
Prevalence of each SynCom species is affected by inoculation method, time and sample type. The proportion of samples where the species is present (>4 reads within a sample) is tracked on the y axis. Sample types are represented by line color. Some species showed identical prevalence patterns in colonized (solid lines) and directly inoculated (dashed lines) sites, whereas others did not.
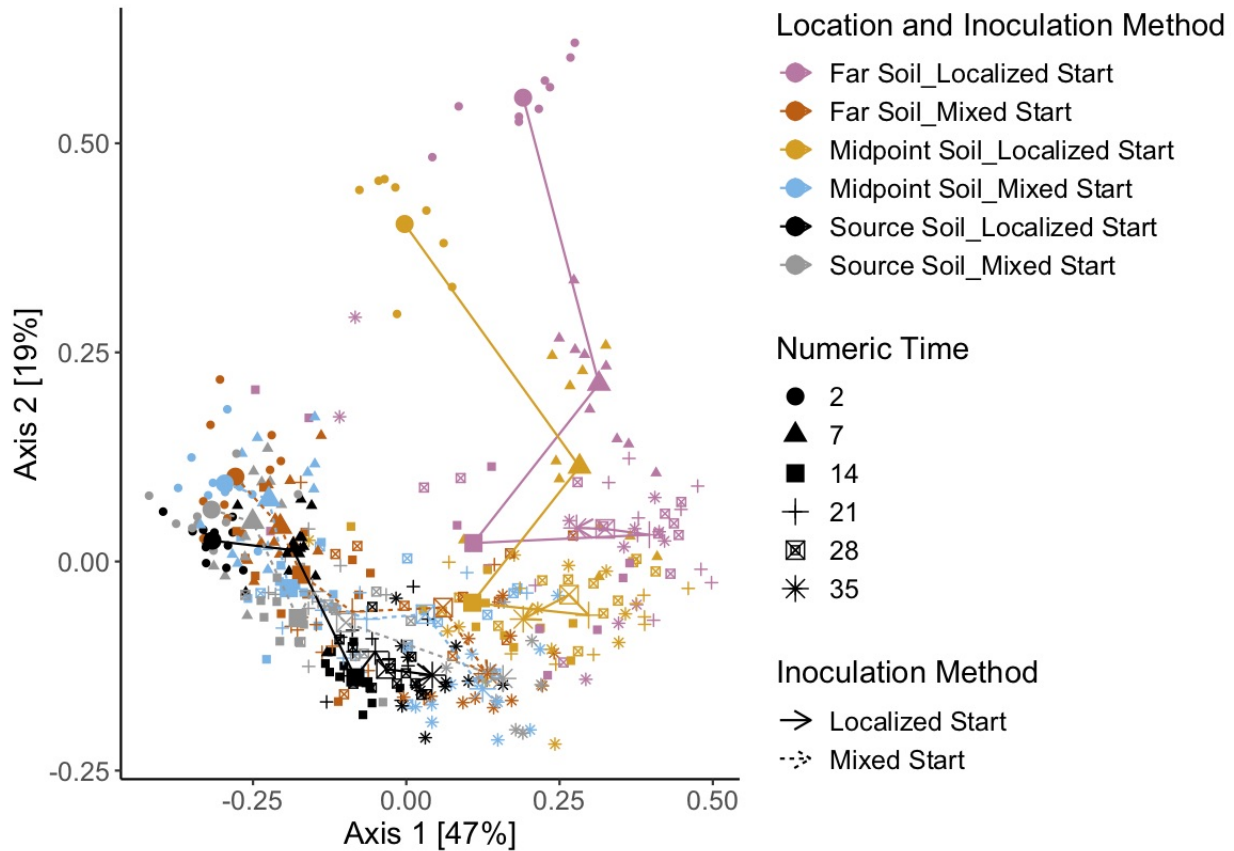
Figure 4.15
Midpoint and Far Soil sites follow distinct successional trajectories when through-soil dispersal is required to arrive on site. Principal Coordinate Analysis of Bray-Curtis dissimilarity. Localized Start Far Soil (pink points) and Midpoint Soil (orange points) remain distinct from directly inoculated soils at Day 35 (Localized Start Source Soil and all Mixed Start sites). Color represents a combination of site and dispersal treatment categories. Shapes show community change over time. Large points are group medians of each site/time/dispersal combination. Arrows follow these group medians over time, solid lines follow Localized Start dispersal treatments, whereas dashed lines follow Mixed Start dispersal treatments.

Factor	R^2	p
Time	0.25541	0.001
Inoculation method	0.29233	0.001
Plant presence	0.01163	0.004
Time x Inoculation method	0.15668	0.001
Time x Plant presence	0.01862	0.066
Inoculation Method x Plant presence	0.00443	0.105
Time x Inoculation method x Plant Presence	0.02336	0.019
Residual	0.23754	

Table 4.3
Plant presence has a small affect on Far Soil community composition.

4.1 Methods

4.1.1 Collection and isolation of Synthetic Community members

Collection of rhizosphere samples

The SynCom was derived from the rhizospheres of three mature, field-grown *Arabidopsis thaliana* collected in southwest Michigan in Spring 2018. Rhizosphere samples were collected by gently patting roots with a small, sterilized spatula to remove loosely associated soil. Roots were separated from aerial tissues with a flame-sterilized razor blade and vortexed in a microtube of Nutrient Broth (NB) media for 15 seconds. Root tissues were removed from the tube, leaving behind rhizosphere microbes. An equal volume of sterile 50% glycerol was added to the NB/rhizosphere slurry, and stored at -80°C until isolation.

Isolation of rhizosphere bacteria

25 μL of rhizosphere slurry was plated on 5 agar media types: tryptone yeast extract glucose agar, tryptone soy agar, and Reasoner's 2A agar (R2A) to target bacteria, and malt extract agar + 100 ug/mL ampicillin and potato dextrose agar+ 100 ug/mL ampicillin to target fungi. Individual colonies were picked and grown in liquid NB or the liquid version of their isolation media. Cultures were grown at 28°C, 200 RPM, until turbidity or visible growth, mixed with an equal volume of 50% gylcerol, and stored at -80°C. A 500 μL aliquot of each culture without glycerol was stored at -20°C for sequencing.

4.1.2 Library preparation

DNA was extracted using a double enzyme digest, chloroform/isopropanol precipitation (Appendix 6.1.1, modified from Perisin (2016)). Amplicon libraries were generated using KAPA HotStart HiFi PCR kits (Roche), with custom Illumina primers containing inline barcodes. Barcodes were factorially combined with Illumina dual indexes in a dual amplification processes to allow for ultra-high throughput sequencing (Appendix 6.2.2, barcodes based on

Bartoli et al. (2018)). Briefly, in the first amplification round, the V5-V7 region of 16S ribosomal gene (Bodenhausen et al., 2013) and a fragment of the DNA gyrase β subunit (Bartoli et al., 2018) of putative bacterial isolates were amplified separately. ITS-1 (Horton et al., 2014) and V8 18S (van Hannen et al., 1998) were amplified from suspected fungal isolates (Appendix 6.3). PCR products were purified with magnetic beads (Appendix 6.1.2) and indexed with custom Illumina MiSeq indexing primers (Appendix 6.3, Tables 6.13 & 6.12, Appendix 6.2.2, Table 6.4). The bacterial (16S and gyrB) or fungal (ITS1 and 18S) amplicons of each isolate were coamplified in the indexing PCR. PCR products were bead purified and quantified with Quant-iT PicoGreen ds DNA reagents (Invitrogen) according to manufacturer's instructions (3 μL PCR product in 200 μL total volume). PCR products were pooled with equal nucleic acid content from each sample and concentrated (Speed-Vac, ThermoFisher). Concentrated pools were size selected between 200-700 bp on a 1.5% agarose gel on a BluePippin (Sage Science) to remove primer dimers. Size selected libraries were bead-cleaned and quality checked on a Bioanalyzer (Agilent). Final libraries were sequenced on an Illumina MiSeq with a v3 2x 300 kit with $\sim$ 12% PhiX. Over 1000 isolates were marker gene sequenced.

4.1.3   Taxonomic identification

Libraries were demultiplexed and indexes removed using both onboard MiSeq software (indices) and cutadapt (barcodes) (Martin, 2011). Sequences were denoised and merged in DADA2 (Callahan et al., 2016). 16S and ITS1 were classified using custom-trained Naive-Bayes classifiers (Bolyen et al., 2019), built from the SILVA-138 database (Quast et al., 2013) and the UNITE database (Nilsson et al., 2018), respectively. gyrB and 18S were classified in BLAST (Sayers et al., 2020). Data was organized in R using phyloseq (McMurdie and Holmes, 2013).

4.1.4 Genomic sequencing of the Synthetic Community

83 bacterial isolates from the rhizosphere isolate collection were selected to maximize bacterial diversity based on 16S and gyrB sequences. Fungal isolates were excluded to simplify downstream assays. The effect of each isolate on plant growth (beneficial, pathogenic or commensal) was not assessed before inclusion within the SynCom. First, I verified that the community was stable over time: the SynCom remained diverse and assembled in a repeatable manner across biological replicates in soil and plant tissues in small peat-based microcosms over 3 weeks. SynCom genomes were sequenced to elucidate the taxonomic classification and functional capabilities of the SynCom members. Isolate DNA was fragmented and tagged using Illumina TDE1 enzyme kits. Libraries were amplified and indexed using custom primers and bead purified (Additional details: (Appendix 6.4), primers: Table 6.4). Libraries were quantified, pooled, and concentrated as described above. Libraries were size selected (330 - 1000 bp) on a 1.5% agarose cassette using a BluePippin (Sage Science). Size selected libraries were purified, quantified, quality checked, and sequenced on several MiSeq v3 2x 300 bp lanes.

Genomes were assembled in SPAdes (Bankevich et al., 2012). Taxonomy was assigned to the genus level in anvi'o (Eren et al., 2021) by aligning 22 single copy core genes from the Genome Taxonomy Database (Parks et al., 2018; Buchfink et al., 2015) (Appendix 6.6). Taxonomy was modified to match SILVA-138 taxonomy for downstream classification (Quast et al., 2013). I then defined species as containing a unique allele of a fraction of gyrB gene (Bartoli et al., 2018). Ultimately, the 83 SynCom members spanned 4 phyla, 14 genera, and 42 species (Supplemental Table 4.1). Finally, two sets of isolates within the *Arthrobacter K* GB2 species complex were distinguishable by a single nucleotide polymorphism in *topoisomerse IV* (*parE*), a gene that co-amplifies with *gyrB* (Poirier et al., 2018). This is denoted by the asterisk in the table.

4.1.5   Plant material and sterilization

Arabidopsis thaliana Columbia-0 (6909) seeds were sterilized with chlorine gas (Lindsey et al., 2017). Sterility was confirmed by germinating seeds on 1/2x Murashige and Skoog (MS) agar plates (pH 5.7) in growth chambers. Sterile seeds were stratified in sterile DI water for 3 days in the dark at 4°C prior to planting.

4.1.6   Synthetic Community generation

SynCom isolates were grown separately in R2B (28°C, 200 RPM) for up to 48 hours. Cultures were checked regularly for turbidity and transferred to 4°C if significant growth was observed. At 48h, OD_{600} of each stock was measured on a plate reader (Tecan SparkControl; 200 μL isolate stock in clear 96- well plate (Corning Costar 3370)). Isolates were pooled, with an equal amount of each isolate as determined by OD_{600}, to a final total community concentration of $OD_{600} = 0.4$ in R2B. The community slurry was immediately mixed by inversion, aliquoted into 50 mL tubes, combined with an equal volume of 40% glycerol, and stored at -80°C. For consistency across replicates and over time, all community inoculations used an aliquot of this original pool. Final community inoculum was $OD_{600} = 0.2$ in 20% glycerol in R2B; the concentration of each isolate within the community was $OD_{600} = 0.0024$.
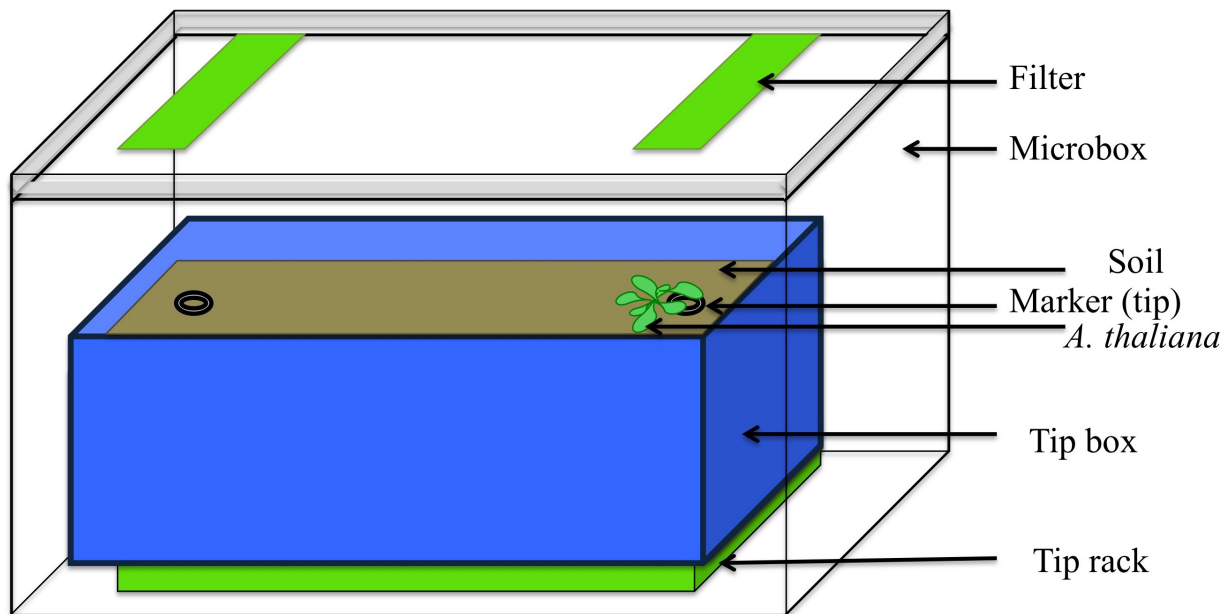
Figure 4.16
Microcosm design. A clear, polypropylene microbox engineered for sterile plant cultivation was used to house the experimental system (SacO$_2$, TP1600+TPD1600 #40 NG/NP). Microboxes have two HEPA filters on the lid to allow gas exchange, but prevent microorganisms from infiltrating the box. An empty, lidless tip box (ThermoFisher SureOne 10 μL - 200 μL tip boxes or similar) with 11 drainage holes was filled with soil, and sits atop an empty tip rack. Two sterile 10 μL pipette tips were placed 90 mm apart within the box. *A. thaliana* seeds were planted near one marker.

Microcosms and soil sterilization procedures were modified from Kremer *et al.* (2021). Microboxes designed for sterile plant cultivation encapsulated the microcosms (Fig. 4.16). Microboxes (SacO$_2$, TP1600+TPD1600 #40 [NG/NP]) had two HEPA filters on the lid to allow gas exchange, but prevent microorganisms from infiltrating the box. Empty 10 μL to 200 μL polypropylene tip boxes were used as pots (ThermoFisher SureOne 10 μL - 200 μL or similar). Empty tip boxes were cleaned, lids removed, and 11 8-mm drainage holes were drilled into the bottom of each box. The tip box filled with soil was placed atop an empty tip rack to allow excess water to drain from the soil (Fig. 4.16).

4.1.8   Soil substrate and sterilization

Pre-autoclaved tip boxes were loosely filled with soil. In community assembly assays, a 50:50 mix of Berger BM-1 and BM-2 (75 - 80% peat Moss, 20 - 25% vermiculite and perlite) was used. In Individual Movement assays, a 50:50 mix of ProMix PBX and coarse vermiculite was used to improve long-term sterility. Eight soil-filled tip boxes were placed on a stack (3-4) of tip racks in polypropylene containers (Sterilite). Boxes were watered to saturation with DI water and allowed to drain for 30 minutes. The polypropylene containers were covered and autoclaved for 65 minutes (Liquids exhaust, 121 C, 15 psi). Polypropylene boxes were allowed to rest for 48 hours at room temperature. In community assembly assays, soil was undisturbed during this period. In Individual Movement assays, polypropylene containers were transferred to a biological safety cabinet, where the soil within each tip box was mixed with a sterilize wooden applicator sticks during the rest period. After the rest period, boxes were autoclaved a second time for 65 minutes.

4.1.9   Microcosm sterilization and assembly

Microboxes with a pre-autoclaved tip rack inside were autoclaved for 35 minutes (Gravity and dry, 121 C, 15 psi). Autoclaved soil-filled tip boxes were transferred to a sterile polypropylene rinse stand using flame sterilized tweezers in a biological safety cabinet. Each soil box was flushed with ~ 300 mL sterilized DI water to remove phytotoxic byproducts generated by autoclaving and allowed to drain for 30 minutes. Soil pots were placed into prepared microboxes by using flame sterilized tweezers. Sterilized 10 μL pipette tips were placed into each box 90 mm apart using an autoclaved multichannel pipette to mark locations for consistent sampling distances.

If microcosms contained plants, five sterilized, stratified *A. thaliana* seeds were planted into soil-filled tip boxes in a shallow V shape with the base of the V near one marker (Fig. 4.1). Microcosms were housed in walk-in growth chambers (Percival) at 23°C, 20% RH, 70%

white light LED setting on a 14:10 hour light:dark cycle. Microcosms were rotated every two days.

4.1.10 SynCom inoculation

Experimental Overview
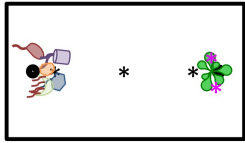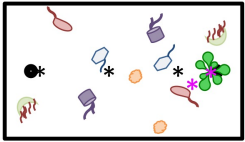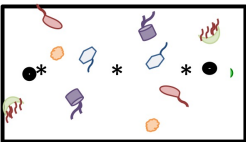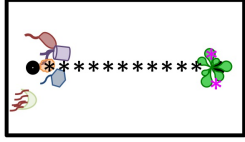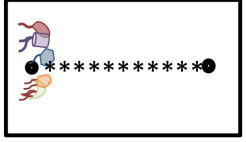
Experiment	Microcosm Types	Set-up
A **Community Assembly** Whole SynCom colonization using two inoculation methods. *Localized Start* – SynCom is inoculated at a singe location adjacent to the Source Soil marker. All other locations are colonized by bacterial movement/growth. *Mixed Start* – SynCom is inoculated throughout the soil box. All locations receive the same starting community.	Localized start with plant Localized start without plant Mixed start with plant Mixed start without plant	**Sample Types:** *3 soil locations* (Source Soil, Midpoint Soil, Far Soil) *3 plant types* (Whole Young Plants, Roots and Rosettes) **Repeat Sampling:** No **Presence determined by:** Sequencing *Intensively Sampled Time Points* *Both Localized and Mixed Start* **Sampling Time:** 2, 7, 14, 21, 28, & 35 days post-inoculation **Replicates:** 4-7 *Minimally Sampled Time Points* *Localized Start only* **Sampling Time:** Every 24 hours from immediately post-inoculation to 20 days post infection **Replicates:** 3
B **Individual Movement** Single isolates tracked as they colonize soil box individually	Localized start with plant Localized start without plant	**Replicates:** 3+ **Samples:** 10 soil locations **Sampling Time:** Every 24 hours for 26 days or microbe reaches far marker **Repeat Sampling:** Yes **Presence determined by:** Colony growth
Legend -- Plant (*A. thaliana*) ● -- Pipette tip (start and end marker) ✱ -- Soil sampling site ✱ -- Plant sampling site		

Figure 4.17
Experimental design overview.

The full community was inoculated into prepared microcosms three days after *A. thaliana* seeds were planted. Newly emerged cotelydons were present at the time of inoculation. The two inoculation methods are as follows. In Mixed Start microcosms, 500 μL of the community slurry was added to 12 mL 1/2x MS media and mixed well. 12.5 mL of the slurry-MS mix was distributed evenly over the soil box with a multichannel pipette, including directly onto

cotelydons (Fig. 4.17). In Localized Start microcosms, 12 mL 1/2x MS was first distributed over the soil using a multichannel pipette. Then, 500 μL of undiluted SynCom slurry was added immediately adjacent to the starting pipette tip marker (Fig. 4.17).

4.1.11 General microcosm characteristics
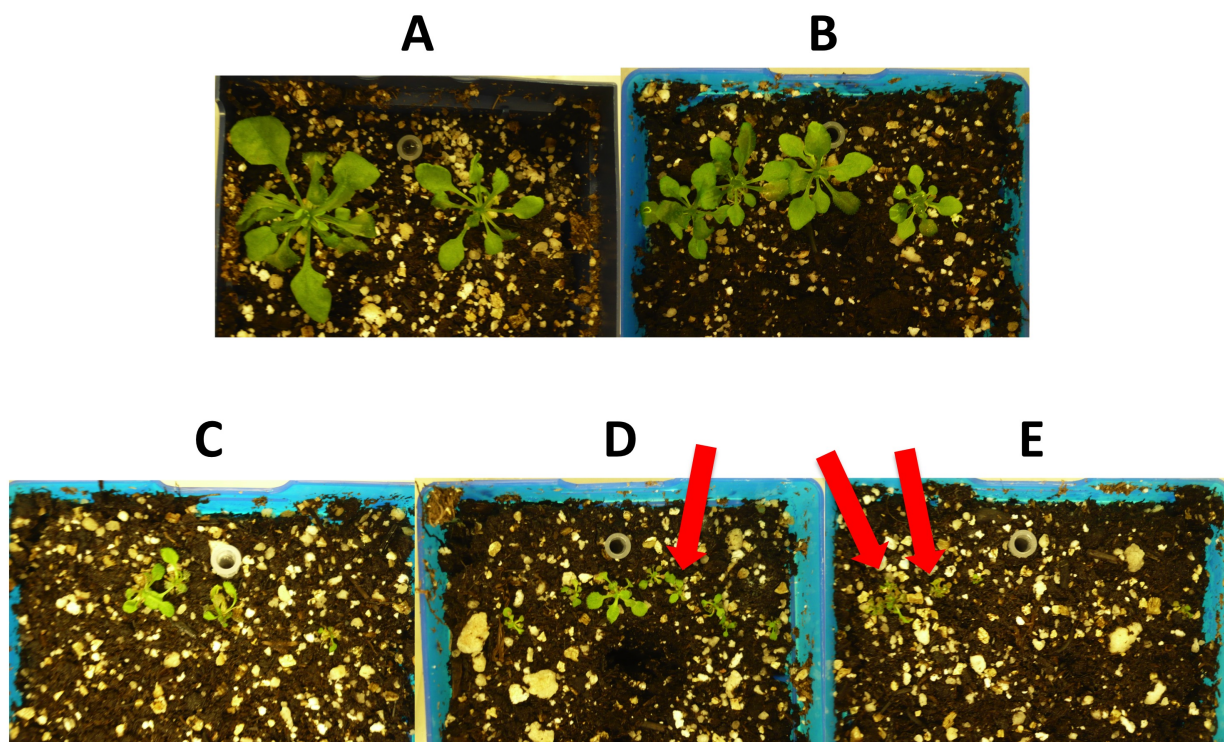
Figure 4.18
The SynCom is detrimental to plant health. Representative plant phenotypes 38 days after planting and 35 days after SynCom inoculation in the microcosm. Photos A and B represent typical plant phenotypes after growth in microcosms without any added microbes. Photos C, D and E represent typical phenotypes when grown in the presence of the SynCom. C is representative of the best phenotypes typically observed when plants were grown in the presence of the SynCom, with some growth and generally green leaves. In D the red arrow indicates a representative plant of this class, where little growth occurred, but some leaves appeared green. Other plants showed little to no growth from seedling size and diseased leaves that were brown, yellow and/or translucent (E, red arrows). The white circle in the center top of each box is a 10 μL pipette tip head.

Condensation was persistent within the microboxes, indicating a high-humidity environment throughout the experiment. The only nutrient added beyond the initial soil mix was 12 mL

of 1/2 MS distributed throughout the soil box during inoculation. *A. thaliana* grew well in the control microcosms, albeit slower than greenhouse-grown *A. thaliana*. The SynCom was detrimental to plant health, delaying or arresting rosette growth (Figure 4.18).

4.1.12   Sampling procedure

Start Point	End Point	Distance
Start marker	End marker	90 mm
Inoculation center	Inoculation spread	$\sim$ 18 mm
Inoculation spread	Midpoint Soil	$\sim$ 14 mm
	Far Soil	$\sim$ 50 mm
	A. thaliana	$\sim$ 59 mm
	Final individual movement position	$\sim$ 63 mm
Midpoint Soil	Far Soil	$\sim$ 36 mm
Individual movement step		9 mm

Table 4.4
Distances between points in the soil environment. Approximate distances are denoted with a tilde.

Mixed Start and Localized Start microcosms with and without plants (n = 4 - 7), were destructively harvested at 2, 7, 14, 21, 28, and 35 days post inoculation. Additionally, to capture early assembly dynamics, three Localized Start microcosms with *A. thaliana* were harvested daily for 20 days post-inoculation. Soil cores were extracted from three locations in

the soil: Source Soil - the inoculation site in Localized Start microcosms and the equivalent location in Mixed Start microcosms; Far Soil - on the opposite side of the box to Source Soil and adjacent plants if present; and Midpoint Soil - the halfway point between the two sites (Fig. 4.1). Distances between sampling sites are described in Table 4.4. If present, the plant(s) and surrounding soil was scooped out of the box with flame-sterilized tweezers and transferred to a flame-sterilized glass surface. Roots were gently patted with tweezers to remove excess and loosely associated soil. Between Day 0 - Day 13, plant tissues were not separated to maintain sufficient tissue mass for DNA extraction, henceforth referred to as Whole Young Plants. From Day 14 - Day 35, roots and rosettes were separated with a flame sterilized razor blade. Both endophytes and epiphytes were included in the community characterization, i.e. plant tissues were not washed or manipulated further. Plants from the same microcosm were combined into a single sample. Samples were stored in at -80°C in 1.4 mL Matrix tubes (ThermoFisher) until further processing.

4.1.13 Sample processing, library preparation, and sequencing

Frozen soil cores and plant samples were lyophilized overnight (LABCONCO FreeZone 4.5). Dry weight was recorded, samples randomized, and then stored at room temperature for several days until DNA extraction. DNA extraction was performed as described in Appendix 6.1.1), except DNA precipitation was performed in 100% ethanol with an overnight incubation at -20°C. Library preparation was performed as described in section 4.1.2 with the following modifications. The *gyrB* gene was amplified using custom primer mixes based on the gyrB sequences of the SynCom members to reduce the degeneracy of the primers and improve PCR performance (Appendix 6.2.2, Tables 6.5 and 6.6). A synthetic spike-in, a plasmid with synthetic DNA that co-amplifies with *gyrB*, was added before each PCR amplification to allow abundance normalization (Appendix 6.7). The first PCR amplification was performed in triplicate, pooled, and bead purified. Specific library preparation parameters

119

are described in Appendix 6.3. Libraries were sequenced on two MiSeq v3 2x 300 bp lanes.

4.1.14   Data processing

Sequencing data was demultiplexed with onboard MiSeq software. Indices and primers were removed using cutadapt (Martin, 2011). Sequences were denoised and merged in DADA2 (Callahan et al., 2016) with trimming parameters determined by FIGARO (Sasada et al., 2020). A custom database of gyrB sequences was built from the JGI database (Nordberg et al., 2014), the NCBI database (Sayers et al., 2020), and SynCom genomes. A Naive-Bayes classifier in QIIME2 (Bolyen et al., 2019) was trained on this data set and used to classify sequences. Synthetic spike-in and *Escherichia coli gyrB* sequences (used to replicate the spike-in plasmid) were separated from the rest of the data set using BLAST in QIIME2 (Bolyen et al., 2019). Data was then exported to R for analysis.

4.1.15   Data filtering

Analysis was performed in R (R Core Team, 2022), primarily using the phyloseq package (McMurdie and Holmes, 2013). ASVs with less than 10 reads and samples with less than 500 sequences were removed. Most non-SynCom ASVs and negative control samples were removed by these filters. Several high prevalence ASVs were manually identified as off-target contamination by BLAST and removed. Since the custom classifier defined sequences as belonging to SynCom species, ASVs were glommed at the species level. Any experimental samples with less than 75% of reads assigned to SynCom members were removed; it should be noted that most samples contained well over 90% SynCom reads. A 95% SynCom threshold was also tested with similar results. For most downstream analysis, only reads classified as SynCom members were considered.

4.1.16   Data transformation

Two data normalization and transformation methods were assessed with similar results.

1) *Rarefying:*

Data was rarefied to control for spurious effects derived from sampling depth variation, which spanned three orders of magnitude (Weiss et al., 2017). Communities were repeat rarefied without replacement 100 times (629 read depth) using custom scripts (McMurdie and Holmes, 2013) based on Cameron et al. (2021).

2) *Aitchison transformation:*

I also considered the composition nature of the samples and additionally analyzed the data with metrics appropriate for compositional data sets (Gloor et al., 2017). Separately, community compositions were transformed with a robust Aitchison transformation (centered log-ratio, ignoring zeros) using vegan (Oksanen, 2021). β-diversity analyses were repeated using the Aitchison distance with similar results to repeat rarefying.

4.1.17   Statistical analysis

All statistical analyses were performed in R (R Core Team, 2022). Plotting was performed using ggplot2 (Wickham, 2016) and numerous other accessory packages.

α-diversity

α-diversity was calculated using repeat rarefied data using the microbiome R package (Lahti and Shetty, 2017). Species richness was calculated for each iteration of rarefied communities, and mean richness of all iterations was used in downstream analysis (Cameron et al., 2021). Statistical analysis (Kruskal-Wallis rank sum and Wilcoxon tests) were calculated in base R (R Core Team, 2022).

β-diversity and community composition

If a rarefied community was used, the mean ASV table generated by repeat rarefying was used in β-diversity analyses. Bray-Curtis, Jaccard and UniFrac distances were calculated in phyloseq (McMurdie and Holmes, 2013) and robust Aitchison distance was calculated in vegan (Oksanen, 2021). Permutational multivariate analysis of variance was used to calculate statistical significance with 999 permutations unless otherwise noted. (PERMANOVA, (Anderson, 2017) *adonis2* function in vegan).

All factors were assessed individually in PERMANOVA for statistical significance and then combined into an overall model to assess the impact of these factors on general community structure, where $\times$ denotes an interaction:

$$distance \sim SoilLocation \times TimePoint \times InoculationMethod + PlateID \qquad (4.1)$$

To determine what time points and sample types were impacted by these factors post-hoc PERMANOVAs were performed on subsets of these data as described in the results (i.e. within a time point, within a sample types, inoculation type, or combination of the three), with appropriate adjustments to the model. Plant only models were also calculated.

To test the effect of plant presence on soil community structure, all soil samples were tested with the PERMANOVA run with the following formula:

$$distance \sim SampleType \times TimePoint \times InoculationMethod \times PlantPresence \qquad (4.2)$$

For post-hoc analysis, only Far Soil samples (the soil near plants) were considered. Analyses were performed separately on Localized Start and Mixed Start samples with the formula:

$$distance \sim TimePoint \times PlantPresence \qquad (4.3)$$

Community convergence with Principal Coordinate Analysis (PCoA)

Ordination of distance matrices were performed using phyloseq (Bray-Curtis, Jaccard, UniFrac) or qiime2 (Aitchison) (Bolyen et al., 2019)). Ordinations were plotted using ggplot2 (Wickham, 2016), and assessed on the top 5 axes. Since sample type was a major explanatory factor (soil vs. roots vs. rosettes), distance calculations and ordinations were constrained within sample type for community convergence assays. Whole community PCoAs had similar patterns to subsetted PCoAs.

Differential abundance

Differentially abundant microbes in the rarefied data set at Day 35 were identified with DESeq2 ($\alpha < 0.01$) (Love et al., 2014) and ANCOM (Mandal et al., 2015). Species present in 3 or fewer samples were excluded. ANCOM was run both with and without structural zeros.

4.1.18   Individual movement assays
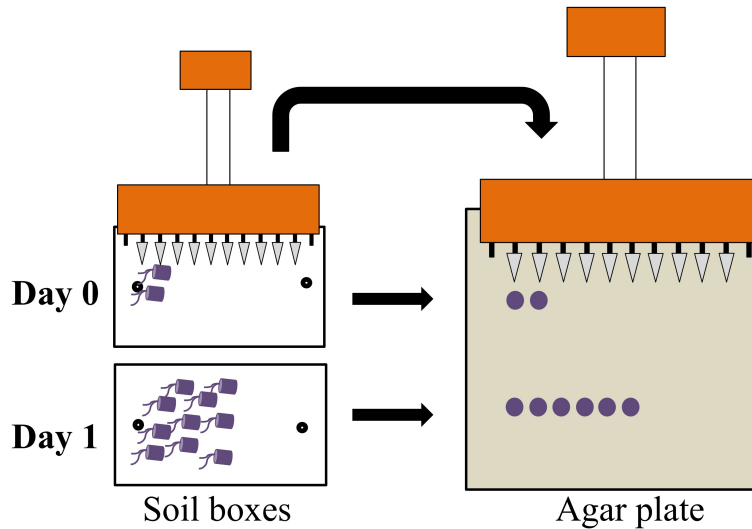
Figure 4.19
To measure isolate colonization progress, a multichannel pipette with 10 sterile 10 μL tips is dipped into the soil box, and then immediately touched onto R2A agar plates. Progress is determined by presence of CFUs at increasing distances from the inoculation point. Colony forming units were maintained at previous locations, suggesting concurrent bacterial movement and growth. Microcosms were sampled daily to obtain a per day colonization rate.

Individual colonization rates of SynCom members were measured using a method modified from (Bashan, 1986). Individual isolates were grown in R2B (28°C, 200 RPM) until turbid, pelleted and resuspended in 1/2 MS media at $OD_{600} = 0.2$. 12 mL 1/2x MS was distributed over the soil of prepared microcosms using a multichannel pipette. 500 μL of the individual isolate was slowly inoculated adjacent to the starting marker. Immediately following inoculation, ten evenly spaced locations were sampled by dipping a pipette with sterile 10 μL tips into the soil and immediately tapping onto R2B plates (Figures 4.19 and 4.1). Microcosms were repeatedly sampled every 24 hours until the isolate reached the final sampling site, 26 days post inoculation, or box contamination, whichever came first. Soil colonization rates were calculated by averaging the per day movement rate for the first three days of the assay.

If the isolate reached the final soil sampling site in less than three days, mean movement rates were calculated from the daily movement rates of one or two days.

Individual colonization dynamics were tested in microcosms both with and without a 25-day-old *A. thaliana* plant near the end marker for approximately half of the isolates. Because the presence of a plant had no discernible effect on the colonization rate of any of these microbes, the colonization rates of the remaining microbes were tested only in microcosms without plants. I did not distinguish between microcosms with and without plants while calculating the colonization rates.

CHAPTER 5

CONCLUSIONS

Microbiome assembly is a complex, multifaceted process. This dissertation investigated several aspects of microbial assembly processes and contributes to an improved understanding of the forces drive plant microbiome assembly. In Chapter 2, I asked if plant pattern recognition receptors (PRRs), which detect microbe-associated molecular patterns (MAMPs), affect endophytic bacterial and fungal microbiome assembly in the field using knockout mutants. I found that the loss of a PRR had little effect on endophytic microbiome structure. In Chapter 3, I tested if two native pathogens of *A. thaliana* triggered transgenerational induced resistance in *A. thaliana* rosettes, but found that the disease status of previous generations had no impact on the growth and pathogenesis of these native pathogens. In Chapter 4, I tested if bacterial dispersal rates affected plant microbiome structure using a synthetic bacterial community in a closed system. I found that substantial variation in bacterial movement through soil generated priority effects that had an enduring impact on both soil and plant microbiome structure.

Selective processes, including abiotic conditions, host effects, and microbe-microbe interactions, are important factors in plant microbiome assembly. One way host effects can manifest is through plant immunity, which can alter important features of the host environment and regulate the growth of many microbes (Hacquard et al., 2017). Plant immunity is thus thought to widely affect plant-associated microbiomes (Hacquard et al., 2017). In Chapter 2 and 3, I investigated how two arms of plant immunity affected members of the plant microbiome.

In Chapter 2, I tested the impact of MAMP-detecting PRRs on endophytic microbiome assembly in the field. I found that the loss of a MAMP-detecting PRR had little effect on endophytic fungal and bacterial microbiome structure. This result was unanticipated, since extensive previous work demonstrated that plants initiate substantial antimicrobial

responses to diverse MAMPs (Boller and Felix, 2009; Tang et al., 2017) and immunogenic MAMPs are prevalent across microbial taxa (Garrido-Oter et al., 2018; Teixeira et al., 2019). Based on these observations, it was widely presumed that most microbial encounters would stimulate MAMP-detecting PRRs and plant immunity to a certain extent, thus influencing plant microbiome composition or total load (Hacquard et al., 2017). My results did not support this hypothesis when individual MAMP-detecting PRRs and endophytic microbiomes are considered. This general lack of effect is observed in numerous plant tissues and across several developmental stages. However, MAMP-detecting PRRs could still impact other facets of plant microbiome assembly that this experiment did not address. For example, epiphytes were excluded from the data set. Since epiphytes are affected by plant immunity (Lee et al., 2012), it is possible that MAMP-detecting PRRs influence this subsection of the community. Furthermore, it is possible that MAMP-detecting PRRs act redundantly/in concert with each other to influence microbiome structure, rather than as individual receptors. Since I used single locus knockout lineages to test the effects of MAMP-detecting PRRs on microbiome assembly, the group effect of largely redundant receptors may not be detectable.

In Chapter 3, I tested if two bacterial pathogens isolated from wild *A. thaliana* in the Midwest USA (*Pseudomonas syringae* NP29.1a and *P. viridiflava* RMX3.1b, Jakob et al., 2002), could produce long-term, cross-generational immunity. Transgenerational induced resistance could potentially affect many members of the microbiome because it affects the growth and/or pathogenicity of microbes not present during the inducing infection (Luna et al., 2012; Slaughter et al., 2012; López Sánchez et al., 2021). However, I found no evidence that either of these two native bacterial pathogens triggered transgenerational induced resistance in *A. thaliana* rosettes. Previous work demonstrated that infection intensity, tested by manipulating the number of sequential exposures over the lifetime of the plant, affects the strength of transgenerational induced resistance phenotypes (López Sánchez et al., 2021). Additionally, previous studies that generated transgenerational resistance phenotypes used

high initial titers of virulent *P. syringae* DC3000 that cause significant growth reduction in the plant (Luna et al., 2012; López Sánchez et al., 2021), or avirulent *P. syringae* DC3000 *avrRpt2* that induced rapid, widespread cell death via hypersensitive response (Slaughter et al., 2012), respectively. In my experiments, *P. syringae* NP29.1a and *P. viridiflava* RMX3.1b never grew to the microbial titers measured in these works. Thus, these infections may not have sufficient strength to induce transgenerational induced resistance. If this is the case, it is likely that bacterial infections in the field rarely reach the titers or disease severity necessary to trigger transgenerational induced resistance (Dunning, 2008; Karasov et al., 2019). Thus, I speculate that infections in previous plant generations rarely influence *in planta* growth of bacterial pathogens, important members of the plant microbiome.

In Chapter 4, I pivoted from exploring the role of immunity in plant microbiome assembly to test the importance of another community assembly process: microbial dispersal. Little is known concerning the role or relative importance of dispersal in microbial community assembly (Fitzpatrick et al., 2020). To address this gap in knowledge, I developed a closed microcosm and synthetic bacterial community (SynCom). Using this system, I demonstrated that microbial dispersal has a large impact on microbiome assembly, even in a continuous environment. Plant microbiome membership and relative abundance profiles were strongly affected by dispersal treatment, i.e. if the SynCom was required to disperse through the soil to colonize a plant or directly inoculated onto plants. Importantly, this difference was driven by phenomena likely to apply in other assembly contexts. I found that plant-associated bacteria have significant variation in through-soil dispersal rates, which generates priority effects in both soil and plant microbiome assembly. Interestingly, priority effects in soil communities quickly created established restrictive communities that acted as "biological barriers" over centimeters of soil, preventing some bacteria from colonizing the plant. This chapter reveals unexpected mechanisms of microbiome assembly mediated by variation in microbial dispersal dynamics. Microbial dispersal is clearly a critical process in plant microbiome assembly

and deserves increased recognition and attention.

5.0.1 Improvements and lessons learned

The design and execution of these experiments could be significantly improved in several ways. If I performed these experiments again, I would design experiments to more definitively show that results in Chapter 2 and 3 are a true negative by increasing my statistical power. In the future, I will carefully consider the specific requirements and limitations statistical tests I expect to use in the analysis of the data to help guide experimental design. For example, in Chapter 2 (MAMP-detecting PRRs in microbiome assembly), I designed my experiment to test a wide breadth of plant tissues and developmental stages at the expense of sample size in each tissue and stage category. While this choice was both intentional and justified, it weakened some components of the analysis in unanticipated ways (e.g. small sample sizes substantially limit the power of differential abundance tests using ANCOM-BC2; Lin and Peddada, 2020). Small sample sizes are a recurrent limitation in my experiments. If I performed these experiments again, I would prioritize *a priori* power analyses based on previous data in the literature and/or pilot studies to ensure meaningful negative results. I would also consider ways to increase sample size by adjusting the motivating question to reduce the breadth and/or ameliorate laborious protocols.

5.0.2 Future directions

While the importance of host effects in plant microbiome assembly should not be dismissed, microbial dispersal is a critical, yet poorly understood, assembly process that demands further investigation. The experimental system I developed in Chapter 4 could easily be used to address further questions concerning the role of microbial dispersal in microbial community assembly. First, the synthetic community I used in Chapter 4 was detrimental to plant health (Figure 4.18). By using different SynComs, one could determine if dispersal plays an equally

important role in growth-promoting or commensal community assembly. Second, targeted manipulation of the plant microbiome by adding beneficial microbes is an important agricultural goal (King and Bell, 2022). This microcosm could be used to test if can beneficial target microbes freely disperse through the soil to reach the plant or if are they immobile or stymied by biological barriers. Can the addition of specific substrates like nutrients, water, or other substances help focal microbes successfully overcome biological barriers and travel through the soil? Third, this system is amenable to testing the interaction of dispersal with other selective factors like abiotic conditions (soil salinity, pH, nutrient concentrations, etc.) and microbe-microbe interactions. Lastly, recent work shows that bacterial populations in *A. thaliana* leaves are maintained at a constant level through birth/death cycling (Velásquez et al., 2022). Given the rapid generation time of bacteria, microbes associated *A. thaliana* for 5 weeks would cycle through many generations, allowing for rapid adaptation and possibly speciation. Metagenomic analysis of the existing (or augmented) data in Chapter 4 could unveil a role of adaptation/speciation or drift in plant microbiomes. These experiment are a fraction of the exciting possibilities offered by this experimental system. In conclusion, my dissertation helps delineate the impact of plant immunity on members of the plant microbiome and demonstrates that the role of microbial dispersal cannot be ignored. Further efforts to disentangle microbial dispersal processes may yield unanticipated insights into plant microbiome assembly rules and potentially uncover new strategies to more effectively engineer microbiomes.

CHAPTER 6

APPENDICES

6.1 General Protocols

6.1.1 DNA extraction

Isolate cultures were pelleted at 6600 x g for 15 minutes, the supernatant removed, and pellets resuspended in 150 μL TES (10 mM Tris-Cl, 1mM EDTA, 100mM NaCl). 2-3 2.33 mm sterilized, silica beads were added to each tube, and tubes were homogenized for 2 minutes at 1750 RPM in a Spex GenoGrinder2000. 100 μL lysozyme mix (EpiCenter ReadyLyse lysozyme diluted to 125 U/μL in TES) was added to each well, gently vortexted for 10 seconds, and incubated at room temperature for 30 minutes. 250 μL Proteinase-K mix (0.5 mg/mL Proteinase-K, 1% SDS, to volume in TES) was added to each well, vortexed for 10 seconds to mix, and incubated at 55°C for 4 hours. 500 μL 24:1 chloroform:isoamyl was mixed into each well, and plates were centrifuged for 15 minutes at 6600 x g at 4°C. The top 350 μL of each well was added to plates with 500 μL cold 100% isopropanol, mixed, and then incubated at -20 C for 1 hour. Plates were centrifuged for 15 minutes (4°C, 6600 x g), isopropanol removed, and DNA pellets were washed with 400 μL 70% ethanol. Ethanol was removed and samples were dried in a biological safety cabinet using a 96-well blower to remove any remaining ethanol. DNA was then resuspended in 100 μL TE (10 mM Tris-Cl, 1mM EDTA) by vortexting for 2 minutes. To remove excess carbohydrates, plates were incubated on ice for 5 minutes and then centrifuged for 12 minutes (4°C, 6600 x g). 75 μL of the supernatant containing the DNA was removed and placed into fresh plates for further analysis.

6.1.2   Bead clean up

Bead clean ups were performed with in-house Solid Phase Reversible Immobilization (SPRI) beads (Rohland and Reich, 2012), which contain:

0.1% SpeedBead Carboxylate-Modified Magnetic Particles (Hydrophobic) (rinsed in TE buffer)

18% PEG-8000 (w/v)

1M NaCl

10mM Tris-HCl pH 8.0

1 mM EDTA, pH 8.0.

Clean up was performed as described in Rohland and Reich (2012) with the following parameters: beads were added at 1:1 PCR volume, two rinses 80% EtOH were used, and the purified DNA was eluted in molecular-grade, sterile water.

6.2 Primers

6.2.1 PRR mutant confirmation primers

Genotype	Primer	Sequence
efr	Forward	CTGTGGTGGTTAGGGATTCG
	Reverse	GATGGGTTACCATCACTGGC
	Insert	LBb1.3: ATTTTGCCGATTTCGGAAC
fls2	Forward	AGGGCTTCTTACAAACCTTCG
	Reverse	CGTTGATGTTTTTGAACACCC
	Insert	LBb1.3: ATTTTGCCGATTTCGGAAC
lore	Forward	CATTTTCATCCATCGATGGAC
	Reverse	TTCCCTTTCACAACAATCCTG
	Insert	SAIL-LB1short: TGGATAAATAGCCTTGCTTCC
lyk4	Forward	GAAGAATGGTTTTGAACGACAAG
	Reverse	AGAAAAGGAAACAGGGAAGTGTC
	Insert	p745: AACGTCCGCAATGTGTTATTAAGTTGTC

6.2.2 Illumina 16S, gyrB, 18S and ITS1 sequencing

Barcoded primers for 16S, gyrB, 18S and ITS1 amplification (PCR1) for library preparation on the Illumina MiSeq Platform:

Forward amplification primer description:

Field number (space-delimited), description:

1. 5' Illumina overlap region

2. forward inline barcode (Table 6.1)

3. gene specific forward primer (Table 6.2)

133

TCGTCGGCAGCGTCAGATGTGTATAAGAGACAG NNNNNN LENGTHVARIES

Reverse amplification primer description:

Field number (space-delimited), description:

1. 3' Illumina overlap region

2. inline forward barcode (Table 6.1)

3. gene specific reverse primer (Table 6.3)

GTCTCGTGGGCTCGGAGATGTGTATAAGAGACAG NNNNNN LENGTHVARIES

Forward barcode name	Forward barcode sequence	Reverse barcode name	Reverse barcode sequence
t1 forward	GACTAC	t1 reverse	AAGGCC
t2 forward	CTGGTT	t2 reverse	GTCAGG
t3 forward	ACTCGA	t3 reverse	CCTCTT
t4 forward	TGCTGT	t4 reverse	TCGTAG

Table 6.1
Barcodes used with gene specific amplification primers in Illumina library prep.

Forward name	Forward sequence
16S 799F forward	AACMGGATTAGATACCCKG
gyrB forward	MGNCCNGSNATGTAYATHGG
18S 1427F forward	TCTGTGATGCCCTTAGATGTTCTGGG
ITS1 forward	CTTGGTCATTTAGAGGAAGTAA

Table 6.2
Forward primers used in gene specific amplification for Illumina library preparation. Name includes target and primer name.

Reverse name	Reverse sequence
16S 1193R reverse	ACGTCATCCCCACCTTCC
gyrB reverse	ACNCCRTGNARDCCDCCNGA
18S 1616R reverse	GCGGTGTGTACAAAGGGCAGGG
ITS1 reverse	GCTGCGTTCTTCATCGATGC

Table 6.3
Reverse primers used in gene specific amplification for Illumina library preparation. Name includes target and primer name.

Primers for library indexing (PCR2) on the Illumina MiSeq Platform:

P5 (forward) indexing primer description:

Field number (space-delimited), description:

1. 5' Illumina adapter

2. i5 index (Table 6.4)

3. PCR 1 overlap region

AATGATACGGCGACCACCGAGATCTACAC NNNNNNNN TCGTCGGCAGCGTC

P7 (reverse) indexing primer description:

Field number (space-delimited), description:

1. 3' Illumina adapter

2. i7 index (Table 6.4)

3. PCR 1 overlap region

CAAGCAGAAGACGGCATACGAGAT NNNNNNNN GTCTCGTGGGCTCGG

i5 name	i5 index	i7 name	i7 index
SA501	ATCGTACG	NA701	AACTCTCG
SA502	ACTATCTG	NA702	ACTATGTC
SA503	TAGCGAGT	NA703	AGTAGCGT
SA504	CTGCGTGT	NA704	CAGTGAGT
SA505	TCATCGAG	NA705	CGTACTCA
SA506	CGTGAGTG	NA706	CTACGCAG
SA507	GGATATCT	NA707	GGAGACTA
SA508	GACACCGT	NA708	GTCGCTCG
		NA709	GTCGTAGT
SB501	CTACTATA	NA710	TAGCAGAC
SB502	CGTTACTA	NA711	TCATAGAC
SB503	AGAGTCAC	NA712	TCGCTATA
SB504	TACGAGAC		
SB505	ACGTCTCG	NB701	AAGTCGAG
SB506	TCGACGAG	NB702	ATACTTCG
SB507	GATCGTGT	NB703	AGCTGCTA
SB508	GTCAGATA	NB704	CATAGAGA
		NB705	CGTAGATC
SC501	ACGACGTG	NB706	CTCGTTAC
SC502	ATATACAC	NB707	GCGCACGT
SC503	CGTCGCTA	NB708	GGTACTAT
SC504	CTAGAGCT	NB709	GTATACGC
SC505	GCTCTAGT	NB710	TACGAGCA
SC506	GACACTGA	NB711	TCAGCGTT
SC507	TGCGTACG	NB712	TCGCTACG
SC508	TAGTGTAG		
SD501	AAGCAGCA		
SD502	ACGCGTGA		
SD503	CGATCTAC		
SD504	TGCGTCAC		
SD505	GTCTAGTG		
SD506	CTAGTATG		
SD507	GATAGCGT		
SD508	TCTACACT		

Table 6.4
Illumina indices used in library amplification.

Custom primers for Synthetic Community gyrase B library amplification

Forward gyrB SynCom mix primer description:

Field number (space-delimited), description:

1. 5' Illumina adapter

2. Forward gyrB targeting sequence (Table 6.5)

TCGTCGGCAGCGTCAGATGTGTATAAGAGACAG NNNNNNNNNNNNNNNNNNNN

Reverse gyrB SynCom mix primer description:

Field number (space-delimited), description:

1. 3' Illumina adapter

2. Reverse gyrB targeting sequence (Table 6.6)

GTCTCGTGGGCTCGGAGATGTGTATAAGAGACAG

NNNNNNNNNNNNNNNNNNNN

Forward Name	Sequence	Mix Fraction
gyrBF consensus	CGNCCSGGBATGTAYATYGG	101/117
gyrBF add1	CGTCCATCGATGTATATTGG	2/117
gyrBF add2	C GTCCAGGAATGTACATTGG	4/117
gyrBF add3	CGACCCGGAATGTACATCGG	5/117
gyrBF add4	CGTCCCGGAATGTACATCGG	2/117
gyrBF add5	CGGCCAGGGATGTATATTGG	1/117
gyrBF add6	AGACCAGGGATGTATATCGG	1/117
gyrBF spike	CGTCCGGCTATGTACATAGG	1/117

Table 6.5
Forward primers used in custom Synthetic Community gyrase B amplification mix and their proportion in the final primer mix.

Reverse Name	Sequence	Mix Fraction
gyrBR consensus	ACRCCRTGSARRCCRCCRGA	77/117
gyrBR 18T	ACACCATGAAGACCGCCTGA	1/117
gyrBR 15T	ACTCCGTGAAGTCCTCCCGA	2/117
gyrBR 9T	ACACCGTGTAATCCACCAGA	3/117
gyrBR 3C1	ACCCCGTGCAAGCCGCCGGA	2/117
gyrBR 3C2	ACCCCGTGCAATCCACCGGA	2/117
gyrBR 9A	ACACCGTGAAGGCCGCCGGA	1/117
gyrBR spike	ACTCCGTGAAGTCCGCCAGA	1/117
gyrBR 18C	ACGCCGTGCAGKCCGCCCGA	10/117
gyrBR 12T	ACACCGTGCAATCCGCCGGA	1/117
gyrBR 12C	ACGCCGTGSAGCCCGCCGGA	5/117
gyrBR 3T	ACTCCGTGCAAACCACCGGA	11/117

Table 6.6
Reverse primers used in custom Synthetic Community gyrase B amplification mix and their proportion in the final primer mix.

6.3 PCR recipes and cycling parameters for Synthetic Community isolate characterization

Ingredient	Volume
HiFi Buffer	3 μL
10 mm dNTPs	0.45 μL
10 uM forward primer	0.45 μL
10 uM reverse primer	0.45 μL
HiFi HotStart enzyme	0.2 μL
PCR water	9.45 μL
Template	1 μL
Total Volume	15 μL

Table 6.7
PCR recipe for 16S, 18S, and ITS1 library amplification.

Ingredient	Volume
HiFi Buffer	3 μL
10 mm dNTPs	0.45 μL
10 uM forward primer	1.8 μL
10 uM reverse primer	1.8 μL
HiFi HotStart enzyme	0.2 μL
DMSO	0.75 μL
MgCl2	1.67 μL
PCR water	4.33 μL
Template	1 μL
Total Volume	15 μL

Table 6.8

PCR recipe for gyraseB library amplification with highly degenerate primers.

Temperature	Time	Step number
95°C	3:00	1
98°C	0:20	2
69°C	0:15	3
72°C	0:15	4
		Repeat steps 2-4 30x
72°C	1:00	5
4°C	hold	6

Table 6.9

Isolate PCR1: cycling for amplification and inline barcoding for 16S and 18S sequences in isolate identification

Temperature	Time	Step number
95°C	3:00	1
98°C	0:20	2
69°C	0:20	3
72°C	0:20	4
		Repeat steps 2-4 35x
72°C	1:00	5
4°C	hold	6

Table 6.10

Isolate PCR1: cycling for amplification and inline barcoding for ITS1 sequences in isolate identification

Temperature	Time	Step number
95°C	3:00	1
98°C	0:20	2
65°C	0:20	3
72°C	0:20	4
Repeat steps 2-4 20x, decrease annealing temperature (Step 3) 0.5 C each time.		
98°C	0:20	5
55°C	0:20	6
72°C	0:20	7
		Repeat steps 5-7 22x
72°C	1:00	5
4°C	hold	6

Table 6.11

Isolate PCR1: Touchdown PCR cycling for gyrB amplification and inline barcoding in isolate identification

Temperature	Time	Step number
Temperature Time Step Number 95°C	3:00	1
95°C	0:30	2
69°C	0:30	3
72°C	0:30	4
		Repeat steps 2-4 8x
72°C	5:00	5
4°C	hold	6

Table 6.12

Isolate identification PCR2: PCR cycling for Illumina indexing of PCR1 amplicons in isolate marker gene amplicons.

Ingredient	Volume
HiFi Buffer	3 μL
10 mm dNTPs	0.45 μL
5 uM i5 Index	1.5 μL
5 uM i7 Index	1.5 μL
HiFi HotStart enzyme	0.2 μL
PCR water	6.35 μL
Template 1	1 μL
Template 2	1 μL
Total Volume	15 μL

Table 6.13
PCR recipe for Illumina indexing isolate marker gene sequencing. Two amplicons were indexed in each sample. Template 1 and 2 represent either 16S and gyrB amplicons or ITS1 and 18S amplicons.

6.4 Library preparation for genomic sequencing of SynCom isolates

Reagent	Volume
TDE1	0.5
TD	2.5
Water	0.3
Template (1 ng/μL)	1.7

Table 6.14
Recipe for tagmentation of isolate DNA for genomic sequencing.

Reagent	Volume
HiFi Buffer	3 μL
10 mm dNTPs	0.45 μL
HiFi HotStart enzyme	0.2 μL
PCR water	3.35 μL
Tagmentation product	5 μL
5 uM i5 index	1.5 μL
5 uM i7 index	1.5 μL
Total Volume	15 μL

Table 6.15
Recipe for indexing of tagmented DNA for genomic sequencing.

6.5   Library preparation protocols for Synthetic Community assembly experiments

Ingredient	Volume
HiFi Buffer	3 μL
10 mm dNTPs	0.45 μL
10 uM forward mix	0.9 μL
10 uM reverse mix	0.9 μL
HiFi HotStart enzyme	0.2 μL
PCR water	7.55 μL
Spike (0.58 pg/μL)	1 μL
Template	1 μL
Total Volume	15 μL

Table 6.16
PCR1 recipe for SynCom gyrB amplification for Illumina library preparation.

Ingredient	Volume
HiFi Buffer	4 μL
10 mm dNTPs	0.6 μL
5 uM i5 Index	2 μL
5 uM i7 Index	2 μL
HiFi HotStart enzyme	0.26 μL
PCR water	9.14 μL
Template	2 μL
Total Volume	20 μL

Table 6.17
PCR2, Illumina indexing, recipe for SynCom gyrB in Illumina library preparation.

Temperature	Time	Step number
95°C	3:00	1
98°C	0:20	2
53°C	0:15	3
72°C	0:15	4
		Repeat steps 2-4 30x
72°C	1:00	5
4°C	hold	6

Table 6.18
SynCom PCR1: cycling for gyrB amplification of SynCom community assembly.

6.6 Core genes used to classify isolate genomes

Single copy core genes used to classify SynCom genomes
Ribosomal L1
Ribosomal L13
Ribosomal L16
Ribosomal L17
Ribosomal L2
Ribosomal L20
Ribosomal L21p
Ribosomal L22
Ribosomal L27A
Ribosomal L3
Ribosomal L4
Ribosomal L6
Ribosomal L9 C
Ribosomal S11
Ribosomal S2
Ribosomal S20p
Ribosomal S3 C
Ribosomal S6
Ribosomal S7
Ribosomal S8
Ribosomal S9
ribosomal L24

Table 6.19
The Genome Taxonomy Database 22 single-copy core genes used to define Synthetic Community genome taxonomy to the genus level.

6.7 Synthetic spike sequences

All spike sequences were carried on a plasmid in *E. coli* TOP10 cells. Spike plasmids were purified using a QIAGEN MiniPrep following manufacturer's instructions. Spikes gyrB and 16S were designed in house, the spike for ITS1 was designed by Tkacz et al. (2018).

Spike target sequences

Field number (space-delimited), description:

1) Forward primer for co-amplification.

2) Synthetic filler region.

3) Reverse complement of reverse primer for co-amplification.

gyrB: CGTCCGGCTATGTACATAGG gacggagtgccgacgccccatccggcggtggccaaccggtttc tctcggcgagttgtagcggtgcacggcctgcccctcaaaagtactgcagtgccccgacgccagggtgtagggtccagtctgacggg ccagaagcagggcccatcgtcatgatgctgggagctggctcacagttaagacatgtgtttcagtttgcgcacacgaactcgcggggg gccctatcccgaactgtaccagtgttgtgccgcctcta TCTGGCGGACTTCACGGAGT

16S, 799F-1193R: AACCGGATTAGATACCCGG gtgacccccgttcgccttcgatcggctcaccat attaatcttggtggcagaccttttagaggattgtgttgctcgactatgaccgactttgtacttcaccgtttgggggagaagcctacct tggccttgcccaccggctgcggtcacggagaagcgagaccgttgacgccgtcagagaaagaatcgagaactggcaaatcgggtgg gatagctaactagtggcggctgaccaataggcagtgagaatgcttccgggtccacagccgcttcggttccgttattggtctatacag agctcctggctcaggaactgacacataccccact GGAAGGTGGGGATGACGT

ITS1: (Tkacz et al., 2018) CTTGGTCATTTAGAGGAAGTAA tcccttgtctcctaaaaaaca aagatttactatgcacagaggaacgtctatctaacggttggtatcttgaatgctcggtcccttttgtcattccggattaattcatttcc ctcattcacaagcttgcgaagtctatattgatatatgaatgcaatctagaagagggcacttaaaattagcagtagttaatatttttaa actccatttggtttattcgttacgagactgatt GCATCGATGAAGAACGCAGC

REFERENCES

Araz S. Abdullah, Caroline S. Moffat, Francisco J. Lopez-Ruiz, Mark R. Gibberd, John Hamblin, and Ayalsew Zerihun. Host–multi-pathogen warfare: Pathogen interactions in co-infected plants. *Frontiers in Plant Science*, 8(October):1–12, 2017. ISSN 1664462X. doi: 10.3389/fpls.2017.01806.

Matthew T. Agler, Jonas Ruhe, Samuel Kroll, Constanze Morhenn, Sang Tae Kim, Detlef Weigel, and Eric M. Kemen. Microbial Hub Taxa Link Host and Abiotic Factors to Plant Microbiome Variation. *PLoS Biology*, 14(1):1–31, 2016. ISSN 15457885. doi: 10.1371/journal.pbio.1002352.

J. Aitchison. *The Statistical Analysis of Compositional Data.* Chapman and Hall, London, 1986.

Marti J. Anderson. Permutational Multivariate Analysis of Variance (PERMANOVA). In *Wiley StatsRef: Statistics Reference Online*, pages 1–15. John Wiley & Sons, Ltd, 11 2017. doi: 10.1002/9781118445112.stat07841.

Marti J. Anderson, Kari E. Ellingsen, and Brian H. McArdle. Multivariate dispersion as a measure of beta diversity. *Ecology Letters*, 9(6):683–693, 2006. ISSN 1461023X. doi: 10.1111/j.1461-0248.2006.00926.x.

Gontran Arnault, Cendrine Mony, and Philippe Vandenkoornhuyse. Plant microbiota dysbiosis and the Anna Karenina Principle. *Trends in Plant Science*, 28(1):18–30, 2022. ISSN 13601385. doi: 10.1016/j.tplants.2022.08.012. URL `https://doi.org/10.1016/j.tplants.2022.08.012`.

Yang Bai, Daniel B. Müller, Girish Srinivas, Ruben Garrido-Oter, Eva Potthoff, Matthias Rott, Nina Dombrowski, Philipp C. Münch, Stijn Spaepen, Mitja Remus-Emsermann, Bruno Hüttel, Alice C. McHardy, Julia A. Vorholt, and Paul Schulze-Lefert. Functional overlap of the Arabidopsis leaf and root microbiota. *Nature*, 528(7582):364–369, 12 2015. ISSN 14764687. doi: 10.1038/nature16192.

Daniel J. Ballhorn, Stefanie Kautz, and Jessie May Laumann. Herbivore damage induces a transgenerational increase of cyanogenesis in wild lima bean (Phaseolus lunatus). *Chemoecology*, 26(1):1–5, 2016. ISSN 09377409. doi: 10.1007/s00049-015-0201-x.

David A. Baltrus. Bacterial dispersal and biogeography as underappreciated influences on phytobiomes, 8 2020. ISSN 13695266.

Anton Bankevich, Sergey Nurk, Dmitry Antipov, Alexey A. Gurevich, Mikhail Dvorkin, Alexander S. Kulikov, Valery M. Lesin, Sergey I. Nikolenko, Son Pham, Andrey D. Prjibelski, Alexey V. Pyshkin, Alexander V. Sirotkin, Nikolay Vyahhi, Glenn Tesler, Max A. Alekseyev, and Pavel A. Pevzner. SPAdes: A new genome assembly algorithm and its applications to single-cell sequencing. *Journal of Computational Biology*, 19(5):455–477, 2012. ISSN 10665277. doi: 10.1089/cmb.2012.0021.

Kristin M. Barbour, Alberto Barrón-Sandoval, Kendra E. Walters, and Jennifer B.H. Martiny. Towards quantifying microbial dispersal in the environment. *Environmental Microbiology*, 25(1):137–142, 2023. ISSN 14622920. doi: 10.1111/1462-2920.16270.

Claudia Bartoli, Léa Frachon, Matthieu Barret, Mylène Rigal, Carine Huard-Chauveau, Baptiste Mayjonade, Catherine Zanchetta, Olivier Bouchez, Dominique Roby, Sébastien Carrère, and Fabrice Roux. In situ relationships between microbiota and potential pathobiota in Arabidopsis thaliana. *ISME Journal*, 12(8):2024–2038, 2018. ISSN 17517370. doi: 10.1038/s41396-018-0152-7. URL http://dx.doi.org/10.1038/s41396-018-0152-7.

Yoav Bashan. Migration of the Rhizosphere Bacteria Azospirillum brusilense and Pseudomonas fluorescens Towards Wheat Roots in the Soil. Technical report, 1986.

Martina Beck, Ines Wyrsch, James Strutt, Rinukshi Wimalasekera, Alex Webb, Thomas Boller, and Silke Robatzek. Expression patterns of FLAGELLIN SENSING 2 map to bacterial entry sites in plant shoots and roots. *Journal of Experimental Botany*, 65(22):6487–98, 2014. ISSN 1460-2431. doi: 10.1093/jxb/eru366. URL http://www.pubmedcentral.nih.gov/articlerender.fcgi?artid=4246182&tool=pmcentrez&rendertype=abstract.

Kathleen Beilsmith. *Spatiotemporal patterns in the colonization of Arabidopsis thaliana by native bacterial communities and pathogens*. PhD thesis, University of Chicago, 2020.

Kathleen Beilsmith, Matthew Perisin, and Joy Bergelson. Natural bacterial assemblages in Arabidopsis thaliana tissues become more distinguishable and diverse during host development. *mBio*, 12(1):1–16, 2021. ISSN 21507511. doi: 10.1128/mBio.02723-20.

Matthias L. Berens, Katarzyna W. Wolinska, Stijn Spaepen, Jörg Ziegler, Tatsuya Nobori, Aswin Nair, Verena Krüler, Thomas M. Winkelmüller, Yiming Wang, Akira Mine, Dieter Becker, Ruben Garrido-Oter, Paul Schulze-Lefert, and Kenichi Tsuda. Balancing trade-offs between biotic and abiotic stress responses through leaf age-dependent variation in stress hormone cross-talk. *Proceedings of the National Academy of Sciences of the United States of America*, 116(6):2364–2373, 2019. ISSN 10916490. doi: 10.1073/pnas.1817233116.

Joy Bergelson, Jana Mittelstrass, and Matthew W. Horton. Characterizing both bacteria and fungi improves understanding of the Arabidopsis root microbiome. *Scientific Reports*, 9(1):1–11, 2019. ISSN 20452322. doi: 10.1038/s41598-018-37208-z.

Natacha Bodenhausen, Matthew W. Horton, and Joy Bergelson. Bacterial Communities Associated with the Leaves and the Roots of Arabidopsis thaliana. *PLoS ONE*, 8(2): e56329, 2013. ISSN 1932-6203. doi: 10.1371/journal.pone.0056329. URL http://dx.plos.org/10.1371/journal.pone.0056329.

Natacha Bodenhausen, Miriam Bortfeld-Miller, Martin Ackermann, and Julia A Vorholt. A Synthetic Community Approach Reveals Plant Genotypes Affecting the Phyllosphere Microbiota. *PLoS Genetics*, 10(4), 2014. doi: 10.1371/journal.pgen.1004283.

Thomas Boller and Georg Felix. A Renaissance of Elicitors: Perception of Microbe-Associated Molecular Patterns and Danger Signals by Pattern-Recognition Receptors. *Annual Review of Plant Biology*, 60(1):379–406, 2009. ISSN 1543-5008. doi: 10.1146/annurev.arplant.57.032905.105346. URL `http://www.annualreviews.org/doi/abs/10.1146/annurev.arplant.57.032905.105346`.

Evan Bolyen, Jai Ram Rideout, Matthew R. Dillon, Nicholas A. Bokulich, Christian C. Abnet, Gabriel A. Al-Ghalith, Harriet Alexander, Eric J. Alm, Manimozhiyan Arumugam, Francesco Asnicar, Yang Bai, Jordan E. Bisanz, Kyle Bittinger, Asker Brejnrod, Colin J. Brislawn, C. Titus Brown, Benjamin J. Callahan, Andrés Mauricio Caraballo-Rodríguez, John Chase, Emily K. Cope, Ricardo Da Silva, Christian Diener, Pieter C. Dorrestein, Gavin M. Douglas, Daniel M. Durall, Claire Duvallet, Christian F. Edwardson, Madeleine Ernst, Mehrbod Estaki, Jennifer Fouquier, Julia M. Gauglitz, Sean M. Gibbons, Deanna L. Gibson, Antonio Gonzalez, Kestrel Gorlick, Jiarong Guo, Benjamin Hillmann, Susan Holmes, Hannes Holste, Curtis Huttenhower, Gavin A. Huttley, Stefan Janssen, Alan K. Jarmusch, Lingjing Jiang, Benjamin D. Kaehler, Kyo Bin Kang, Christopher R. Keefe, Paul Keim, Scott T. Kelley, Dan Knights, Irina Koester, Tomasz Kosciolek, Jorden Kreps, Morgan G. I. Langille, Joslynn Lee, Ruth Ley, Yong-Xin Liu, Erikka Loftfield, Catherine Lozupone, Massoud Maher, Clarisse Marotz, Bryan D. Martin, Daniel McDonald, Lauren J. McIver, Alexey V. Melnik, Jessica L. Metcalf, Sydney C. Morgan, Jamie T. Morton, Ahmad Turan Naimey, Jose A. Navas-Molina, Louis Felix Nothias, Stephanie B. Orchanian, Talima Pearson, Samuel L. Peoples, Daniel Petras, Mary Lai Preuss, Elmar Pruesse, Lasse Buur Rasmussen, Adam Rivers, Michael S. Robeson, Patrick Rosenthal, Nicola Segata, Michael Shaffer, Arron Shiffer, Rashmi Sinha, Se Jin Song, John R. Spear, Austin D. Swafford, Luke R. Thompson, Pedro J. Torres, Pauline Trinh, Anupriya Tripathi, Peter J. Turnbaugh, Sabah Ul-Hasan, Justin J. J. van der Hooft, Fernando Vargas, Yoshiki Vázquez-Baeza, Emily Vogtmann, Max von Hippel, William Walters, Yunhu Wan, Mingxun Wang, Jonathan Warren, Kyle C. Weber, Charles H. D. Williamson, Amy D. Willis, Zhenjiang Xu, Jesse R. Zaneveld, Yilong Zhang, Qiyun Zhu, Rob Knight, and J. Gregory Caporaso. Reproducible, interactive, scalable and extensible microbiome data science using QIIME 2. *Nature Biotechnology*, 37(8):852–857, 2019. doi: 10.1038/s41587-019-0209-9.

Alex Boyko, Todd Blevins, Youli Yao, Andrey Golubov, Andriy Bilichak, Yaroslav Ilnytskyy, Jens Hollander, Frederick Meins, and Igor Kovalchuk. Transgenerational adaptation of Arabidopsis to stress requires DNA methylation and the function of dicer-like proteins. *PLoS ONE*, 5(3), 2010. ISSN 19326203. doi: 10.1371/journal.pone.0009514.

Primrose J Boynton and Celeste N Peterson. Superior Dispersal Ability Can Lead to Persistent Ecological Dominance throughout Succession. *Applied and Environmental Microbiology*, 85(6):1–16, 2019.

Zoltan Bozsoki, Jeryl Cheng, Feng Feng, Kira Gysel, Maria Vinther, Kasper R. Andersen, Giles Oldroyd, Mickael Blaise, Simona Radutoiu, and Jens Stougaard. Receptor-mediated chitin perception in legume roots is functionally separable from Nod factor perception.

Proceedings of the National Academy of Sciences of the United States of America, 114 (38):E8118–E8127, 2017. ISSN 10916490. doi: 10.1073/pnas.1706795114.

Benjamin Brachi, Daniele Filiault, Hannah Whitehurst, Paul Darme, Pierre Le Gars, Marine Le Mentec, Timothy C. Morton, Envel Kerdaffrec, Fernando Rabanal, Alison Anastasio, Mathew S. Box, Susan Duncan, Feng Huang, Riley Leff, Polina Novikova, Matthew Perisin, Takashi Tsuchimatsu, Roderick Woolley, Caroline Dean, Magnus Nordborg, Svante Holm, and Joy Bergelson. Plant genetic effects on microbial hubs impact host fitness in repeated field trials. *Proceedings of the National Academy of Sciences of the United States of America*, 119(30), 2022. ISSN 10916490. doi: 10.1073/pnas.2201285119.

J. Roger Bray and J. T. Curtis. An Ordination of the Upland Forest Communities of Southern Wisconsin. *Ecological Monographs*, 27(4):326–349, 1957.

B. Buchfink, C. Xie, and D. Huson. Fast and sensitive protein alignment using DIAMOND. *Nature Methods*, 12:59–60, 2015. doi: https://doi.org/10.1038/nmeth.3176.

Davide Bulgarelli, Matthias Rott, Klaus Schlaeppi, Emiel Ver Loren van Themaat, Nahal Ahmadinejad, Federica Assenza, Philipp Rauf, Bruno Huettel, Richard Reinhardt, Elmon Schmelzer, Joerg Peplies, Frank Oliver Gloeckner, Rudolf Amann, Thilo Eickhorst, and Paul Schulze-Lefert. Revealing structure and assembly cues for Arabidopsis root-inhabiting bacterial microbiota. *Nature*, 488(7409):91–95, 2012. ISSN 1476-4687. doi: 10.1038/nature11336. URL http://www.ncbi.nlm.nih.gov/pubmed/22859207.

B. J. Callahan, P. J. McMurdie, M. J. Rosen, A. W. Han, A. J. Johnson, and S. P. Holmes. DADA2: High-resolution sample inference from Illumina amplicon data. *Nature Methods*, 13:581–583, 2016. doi: https://doi.org/10.1038/nmeth.3869.

Ellen S. Cameron, Philip J. Schmidt, Benjamin J.M. Tremblay, Monica B. Emelko, and Kirsten M. Müller. Enhancing diversity analysis by repeatedly rarefying next generation sequencing data describing microbial communities. *Scientific Reports*, 11(1):1–13, 2021. ISSN 20452322. doi: 10.1038/s41598-021-01636-1. URL https://doi.org/10.1038/s41598-021-01636-1.

Charlotte I. Carlström, Christopher M. Field, Miriam Bortfeld-Miller, Barbara Müller, Shinichi Sunagawa, and Julia A. Vorholt. Synthetic microbiota reveal priority effects and keystone strains in the Arabidopsis phyllosphere. *Nature Ecology and Evolution*, 3 (10):1445–1454, 10 2019. ISSN 2397334X. doi: 10.1038/s41559-019-0994-z.

Lilia C. Carvalhais, Paul G. Dennis, Dayakar V. Badri, Brendan N. Kidd, Jorge M. Vivanco, and Peer M. Schenk. Linking jasmonic acid signaling, root exudates, and rhizosphere microbiomes. *Molecular Plant-Microbe Interactions*, 28(9):1049–1058, 2015. ISSN 08940282. doi: 10.1094/MPMI-01-15-0016-R.

Gabriel Castrillo, Paulo José, Pereira Lima, Sur Herrera Paredes, Theresa F Law, Laura De Lorenzo, Piotr Mieczkowski, Corbin D Jones, Meghan E Feltcher, Omri M Finkel,

and W Natalie. Root microbiota drive direct integration of phosphate stress and immunity. *Nature Publishing Group*, 543(7646):513–518, 2017. ISSN 0028-0836. doi: 10.1038/nature21417. URL http://dx.doi.org/10.1038/nature21417.

Jonathan M. Chase. Community assembly: When should history matter? *Oecologia*, 136 (4):489–498, 2003. ISSN 00298549. doi: 10.1007/s00442-003-1311-7.

Tao Chen, Kinya Nomura, Xiaolin Wang, Reza Sohrabi, Jin Xu, Lingya Yao, Bradley C. Paasch, Li Ma, James Kremer, Yuti Cheng, Li Zhang, Nian Wang, Ertao Wang, Xiu Fang Xin, and Sheng Yang He. A plant genetic network for preventing dysbiosis in the phyllosphere. *Nature*, 580(7805):653–657, 4 2020. ISSN 14764687. doi: 10.1038/s41586-020-2185-0.

Cheng Cheng, Xiquan Gao, Baomin Feng, Jen Sheen, Libo Shan, and Ping He. Plant immune response to pathogens differs with changing temperatures. *Nature Communications*, 4 (May):1–9, 2013. ISSN 20411723. doi: 10.1038/ncomms3530.

Chai Hao Chiu, Pawel Roszak, Martina Orvošová, and Uta Paszkowski. Arbuscular mycorrhizal fungi induce lateral root development in angiosperms via a conserved set of MAMP receptors. *Current Biology*, 32(20):4428–4437, 2022. ISSN 18790445. doi: 10.1016/j.cub.2022.08.069.

Kyoung Hee Choi and Herbert P. Schweizer. mini-Tn7 insertion in bacteria with single attTn7 sites: Example Pseudomonas aeruginosa. *Nature Protocols*, 1(1):153–161, 6 2006. ISSN 17542189. doi: 10.1038/nprot.2006.24.

Kyoung Hee Choi, Jared B. Gaynor, Kimberly G. White, Carolina Lopez, Catharine M. Bosio, Rox Ann R. Karkhoff-Schweizer, and Herbert P. Schweizer. A Tn7-based broad-range bacterial cloning and expression system. *Nature Methods*, 2(6):443–448, 6 2005. ISSN 15487091. doi: 10.1038/nmeth765.

Nicholas R. Colaianni, Katarzyna Parys, Ho Seok Lee, Jonathan M. Conway, Nak Hyun Kim, Natalie Edelbacher, Tatiana S. Mucyn, Mathias Madalinski, Theresa F. Law, Corbin D. Jones, Youssef Belkhadir, and Jeffery L. Dangl. A complex immune response to flagellin epitope variation in commensal communities. *Cell Host and Microbe*, 29(4):635–649, 4 2021. ISSN 19346069. doi: 10.1016/j.chom.2021.02.006.

Devin Coleman-Derr, Damaris Desgarennes, Citlali Fonseca-Garcia, Stephen Gross, Scott Clingenpeel, Tanja Woyke, Gretchen North, Axel Visel, Laila P. Partida-Martinez, and Susannah G. Tringe. Plant compartment and biogeography affect microbiome composition in cultivated and native Agave species. *New Phytologist*, 209(2):798–811, 2016. ISSN 14698137. doi: 10.1111/nph.13697.

Uwe Conrath, Gerold J.M. Beckers, Victor Flors, Pilar García-Agustín, Gábor Jakab, Felix Mauch, Mari Anne Newman, Corné M.J. Pieterse, Benoit Poinssot, María J. Pozo, Alain Pugin, Ulrich Schaffrath, Jurriaan Ton, David Wendehenne, Laurent Zimmerli, and

Brigitte Mauch-Mani. Priming: Getting ready for battle. *Molecular Plant-Microbe Interactions*, 19(10):1062–1071, 2006. ISSN 08940282. doi: 10.1094/MPMI-19-1062.

Peter A. Crisp, Diep Ganguly, Steven R. Eichten, Justin O. Borevitz, and Barry J. Pogson. Reconsidering plant memory: Intersections between stress recovery, RNA turnover, and epigenetics. *Science Advances*, 2(2), 2016. ISSN 23752548. doi: 10.1126/sciadv.1501340.

Haitao Cui, Kenichi Tsuda, and Jane E. Parker. Effector-Triggered Immunity: From Pathogen Perception to Robust Defense. *Annual Review of Plant Biology*, 66:487–511, 2015. ISSN 1543-5008. doi: 10.1146/annurev-arplant-050213-040012. URL `http://www.annualreviews.org/doi/abs/10.1146/annurev-arplant-050213-040012`.

Gordon F. Custer, Luana Bresciani, and Francisco Dini-Andreote. Ecological and Evolutionary Implications of Microbial Dispersal. *Frontiers in Microbiology*, 13(April):1–13, 2022. ISSN 1664302X. doi: 10.3389/fmicb.2022.855859.

M. De Cáceres and P. Legendre. Associations between species and groups of sites: indices and statistical inference. *Ecology*, 90:3566–3574, 2009.

Francisco J. de Lamo, Margarita Šimkovicová, David H. Fresno, Tamara de Groot, Nico Tintor, Martijn Rep, and Frank L.W. Takken. Pattern-triggered immunity restricts host colonization by endophytic fusaria, but does not affect endophyte-mediated resistance. *Molecular Plant Pathology*, 22(2):204–215, 2021. ISSN 13643703. doi: 10.1111/mpp.13018.

Martin De Vos, Vivian R. Van Oosten, Remco M.P. Van Poecke, Johan A. Van Pelt, Maria J. Pozo, Martin J. Mueller, Antony J. Buchala, Jean Pierre Métraux, L. C. Van Loon, Marcel Dicke, and Corné M.J. Pieterse. Signal signature and transcriptome changes of Arabidopsis during pathogen and insect attack. *Molecular Plant-Microbe Interactions*, 18(9):923–937, 2005. ISSN 08940282. doi: 10.1094/MPMI-18-0923.

Reena Debray, Robin A. Herbert, Alexander L. Jaffe, Alexander Crits-Christoph, Mary E. Power, and Britt Koskella. Priority effects in microbiome assembly. *Nature Reviews Microbiology*, 20(2):109–121, 2022. ISSN 17401534. doi: 10.1038/s41579-021-00604-w.

Peter N. Dodds and John P. Rathjen. Plant immunity: towards an integrated view of plant–pathogen interactions. *Nature Reviews Genetics*, 11(8):539–548, 2010. ISSN 1471-0056. doi: 10.1038/nrg2812. URL `http://www.nature.com/doifinder/10.1038/nrg2812`.

Megan T. Albert Dunning. *Host genotype and population structure in the interaction between Arabidopsis thaliana and its natural bacterial pathogens*. PhD thesis, University of Chicago, 2008.

Paloma Durán, Thorsten Thiergart, Ruben Garrido-Oter, Matthew Agler, Eric Kemen, Paul Schulze-Lefert, and Stéphane Hacquard. Microbial Interkingdom Interactions in Roots Promote Arabidopsis Survival. *Cell*, 175(4):973–983, 11 2018. ISSN 10974172. doi: 10.1016/j.cell.2018.10.020.

Aurélia Emonet, Feng Zhou, Jordan Vacheron, Clara Margot Heiman, Valérie Dénervaud Tendon, Ka Wai Ma, Paul Schulze-Lefert, Christoph Keel, and Niko Geldner. Spatially Restricted Immune Responses Are Required for Maintaining Root Meristematic Activity upon Detection of Bacteria. *Current Biology*, 31(5):1012–1028, 2021. ISSN 18790445. doi: 10.1016/j.cub.2020.12.048.

A. Murat Eren, Evan Kiefl, Alon Shaiber, Iva Veseli, Samuel E. Miller, Matthew S. Schechter, Isaac Fink, Jessica N. Pan, Mahmoud Yousef, Emily C. Fogarty, Florian Trigodet, Andrea R. Watson, Özcan C. Esen, Ryan M. Moore, Quentin Clayssen, Michael D. Lee, Veronika Kivenson, Elaina D. Graham, Bryan D. Merrill, Antti Karkman, Daniel Blankenberg, John M. Eppley, Andreas Sjödin, Jarrod J. Scott, Xabier Vázquez-Campos, Luke J. McKay, , Elizabeth A. McDaniel, Sarah L. R. Stevens, Rika E. Anderson, Jessika Fuessel, Antonio Fernandez-Guerra, Lois Maignien, Tom O. Delmont, and Amy D. Willis. Community-led, integrated, reproducible multi-omics with anvi'o. *Nature Microbiology*, 6 (1):3–6, 2021. doi: 10.1038/s41564-020-00834-3.

Moises Exposito-Alonso, Claude Becker, Verena J. Schuenemann, Ella Reiter, Claudia Setzer, Radka Slovak, Benjamin Brachi, Jörg Hagmann, Dominik G. Grimm, Jiahui Chen, Wolfgang Busch, Joy Bergelson, Rob W. Ness, Johannes Krause, Hernán A. Burbano, and Detlef Weigel. The rate and potential relevance of new mutations in a colonizing plant lineage. *PLoS Genetics*, 14(2):1–21, 2018. ISSN 15537404. doi: 10.1371/journal.pgen.1007155.

Daniel P. Faith. Conservation evaluation and phylogenetic diversity. *Biological Conservation*, 61:1–10, 1992. ISSN 10960309. doi: https://doi.org/10.1016/0006-3207(92)91201-3.

Jun Fan, Casey Crooks, and Chris Lamb. High-throughput quantitative luminescence assay of the growth in planta of Pseudomonas syringae chromosomally tagged with Photorhabdus luminescens luxCDABE. *Plant Journal*, 53(2):393–399, 2008. ISSN 09607412. doi: 10.1111/j.1365-313X.2007.03303.x.

Feng Feng, Jongho Sun, Guru V. Radhakrishnan, Tak Lee, Zoltán Bozsóki, Sébastien Fort, Aleksander Gavrin, Kira Gysel, Mikkel B. Thygesen, Kasper Røjkjær Andersen, Simona Radutoiu, Jens Stougaard, and Giles E.D. Oldroyd. A combination of chitooligosaccharide and lipochitooligosaccharide recognition promotes arbuscular mycorrhizal associations in Medicago truncatula. *Nature Communications*, 10(1), 12 2019. ISSN 20411723. doi: 10.1038/s41467-019-12999-5.

Connor R Fitzpatrick, Isai Salas-González, Jonathan M Conway, Omri M Finkel, Sarah Gilbert, Dor Russ, Paulo José Pereira Lima Teixeira, and Jeffery L Dangl. The Plant Microbiome : From Ecology to Reductionism and Beyond. *Annual Review of Microbiology*, 74:81–100, 2020.

Jose P. Fonseca, Venkatachalam Lakshmanan, Clarissa Boschiero, and Kirankumar S. Mysore. The Pattern Recognition Receptor FLS2 Can Shape the Arabidopsis Rhizo-

sphere Microbiome β-Diversity but Not EFR1 and CERK1. *Plants*, 11(10):1–11, 2022. ISSN 22237747. doi: 10.3390/plants11101323.

Tadashi Fukami. Historical Contingency in Community Assembly: Integrating Niches, Species Pools, and Priority Effects. *Annual Review of Ecology, Evolution, and Systematics*, 46:1–23, 2015. ISSN 15452069. doi: 10.1146/annurev-ecolsys-110411-160340.

Ruben Garrido-Oter, Ryohei Thomas Nakano, Nina Dombrowski, Ka Wai Ma, Alice C. McHardy, and Paul Schulze-Lefert. Modular Traits of the Rhizobiales Root Microbiota and Their Evolutionary Relationship with Symbiotic Rhizobia. *Cell Host and Microbe*, 24 (1):155–167, 7 2018. ISSN 19346069. doi: 10.1016/j.chom.2018.06.006.

Chrystel Gibelin-Viala, Emilie Amblard, Virginie Puech-Pages, Maxime Bonhomme, Magali Garcia, Adeline Bascaules-Bedin, Judith Fliegmann, Jiangqi Wen, Kirankumar S. Mysore, Christine le Signor, Christophe Jacquet, and Clare Gough. The Medicago truncatula LysM receptor-like kinase LYK9 plays a dual role in immunity and the arbuscular mycorrhizal symbiosis. *New Phytologist*, 223(3):1516–1529, 2019. ISSN 14698137. doi: 10.1111/nph. 15891.

Jane Glazebrook. Contrasting mechanisms of defense against biotrophic and necrotrophic pathogens. *Annual Review of Phytopathology*, 43:205–227, 2005. ISSN 00664286. doi: 10.1146/annurev.phyto.43.040204.135923.

Gregory B. Gloor, Jean M. Macklaim, Vera Pawlowsky-Glahn, and Juan J. Egozcue. Microbiome datasets are compositional: And this is not optional, 11 2017. ISSN 1664302X.

Stéphane Hacquard, Stijn Spaepen, Ruben Garrido-Oter, and Paul Schulze-Lefert. Interplay Between Innate Immunity and the Plant Microbiota. *Annual Review of Phytopathology*, 55 (24):1–25, 2017. doi: 10.1146/annurev-phyto-080516. URL `https://doi.org/10.1146/annurev-phyto-080516-035623`.

Adam Hannan Parker, Samuel W. Wilkinson, and Jurriaan Ton. Epigenetics: a catalyst of plant immunity against pathogens. *New Phytologist*, 233(1):66–83, 2022. ISSN 14698137. doi: 10.1111/nph.17699.

M. Amine Hassani, Paloma Durán, and Stéphane Hacquard. Microbial interactions within the plant holobiont, 3 2018. ISSN 20492618.

J. Henrichsen. Bacterial surface translocation: a survey and a classification. *Bacteriological reviews*, 36(4):478–503, 1972. ISSN 00053678. doi: 10.1128/mmbr.36.4.478-503.1972.

Matthew W Horton, Natacha Bodenhausen, Kathleen Beilsmith, Dazhe Meng, Brian D Muegge, Sathish Subramanian, M Madlen Vetter, Bjarni J Vilhjálmsson, Magnus Nordborg, Jeffrey I Gordon, and Joy Bergelson. Genome-wide association study of Arabidopsis thaliana leaf microbial community. *Nature Communications*, 5(May):5320, 2014. ISSN 2041-1723. doi: 10.1038/ncomms6320. URL `http://www.ncbi.nlm.nih.gov/pubmed/25382143`.

Stephen P. Hubbell. *The Unified Neutral Theory of Biodiversity and Biogeography*. Princeton University Press, Princeton, 2001.

Bethany Huot, Jian Yao, Beronda L. Montgomery, and Sheng Yang He. Growth-defense tradeoffs in plants: A balancing act to optimize fitness. *Molecular Plant*, 7(8):1267–1287, 2014. ISSN 17529867. doi: 10.1093/mp/ssu049. URL `http://dx.doi.org/10.1093/mp/ssu049`.

Mayumi Iwasaki. Chromatin resetting mechanisms preventing transgenerational inheritance of epigenetic states. *Frontiers in Plant Science*, 6(MAY):1–5, 2015. ISSN 1664462X. doi: 10.3389/fpls.2015.00380.

Paul Jaccard. The distribution of the flora in the alpine zone. *New Phytologist*, 11(2):37–50, 1912.

Katrin Jakob, Erica M Goss, Hitoshi Araki, Tam Van, Martin Kreitman, and Joy Bergelson. Pseudomonas viridiflava and P. syringae - Natural Pathogens of Arabidopsis thaliana. Technical Report 12, 2002.

Katrin Jakob, Joel M. Kniskern, and Joy Bergelson. The role of pectate lyase and the jasmonic acid defense response in Pseudomonas viridiflava virulence. *Molecular Plant-Microbe Interactions*, 20(2):146–158, 2007. ISSN 08940282. doi: 10.1094/MPMI-20-2-0146.

Jonathan D G Jones and Jeffery L Dangl. The plant immune system. *Nature Reviews*, 444 (November):323–329, 2006. ISSN 0028-0836. doi: 10.1038/nature05286.

Talia L. Karasov, Joel M. Kniskern, Liping Gao, Brody J. DeYoung, Jing Ding, Ullrich Dubiella, Ruben O. Lastra, Sumitha Nallu, Fabrice Roux, Roger W. Innes, Luke G. Barrett, Richard R. Hudson, and Joy Bergelson. The long-term maintenance of a resistance polymorphism through diffuse interactions. *Nature*, 512(7515):436–440, 2014. ISSN 0028-0836. doi: 10.1038/nature13439. URL `http://www.nature.com/doifinder/10.1038/nature13439`.

Talia L. Karasov, Juliana Almario, Claudia Friedemann, Wei Ding, Michael Giolai, Darren Heavens, Sonja Kersten, Derek S. Lundberg, Manuela Neumann, Julian Regalado, Richard A. Neher, Eric Kemen, and Detlef Weigel. Arabidopsis thaliana and Pseudomonas Pathogens Exhibit Stable Associations over Evolutionary Timescales. *Cell Host and Microbe*, 24(1):168–179, 2018. ISSN 19346069. doi: 10.1016/j.chom.2018.06.011. URL `http://dx.doi.org/10.1016/j.chom.2018.06.011`.

Talia L. Karasov, Manuela Neumann, Alejandra Duque-Jaramillo, Sonja Kersten, Ilja Bezrukov, Birgit Schröppel, Efthymia Symeonidi, Derek S. Lundberg, Julian Regalado, Gautam Shirsekar, Joy Bergelson, and Detlef Weigel. The relationship between microbial population size and disease in the Arabidopsis thaliana phyllosphere. *bioRxiv*, 2019. ISSN 2692-8205. doi: 10.1101/828814.

Talia L Karasov, Manuela Neumann, Gautam Shirsekar, Grey Monroe, Pathodopsis Team, Detlef Weigel, Rebecca Schwab, Cristina Barragan, Ilja Bezrukov, Alba González Hernando, Julia Hildebrandt, Sonja Kersten, Patricia Lang, Sergio Latorre, Miriam Lucke, Anette Habring, Claudia Friedemann, Fiona Paul, Derek Lundberg, Ulrich Lutz, Fernando Rabanal, Julian Regalado, Thanvi Srikant, Bridgit Waithaka, Anjar Wibowo, and Wei Yuan. Drought selection on Arabidopsis populations and their microbiomes. *bioRxiv*, page 2022.04.08.487684, 2022. URL `https://www.biorxiv.org/content/10.1101/2022.04.08.487684v1%0Ahttps://www.biorxiv.org/content/10.1101/2022.04.08.487684v1.abstract`.

Fumiaki Katagiri, Roger Thilmony, and Sheng Yang He. The Arabidopsis Thaliana-Pseudomonas Syringae Interaction. In *The Arabidopsis Book*, volume 1, page e0039. BioOne, 1 2002. doi: 10.1199/tab.0039.

Steven W. Kembel, Peter D. Cowan, Matthew R. Helmus, William K. Cornwell, Helene Morlon, David D. Ackerly, Simon P. Blomberg, and Campbell O. Webb. Picante: R tools for integrating phylogenies and ecology. *Bioinformatics*, 26(11):1463–1464, 2010. ISSN 13674803. doi: 10.1093/bioinformatics/btq166.

William L King and Terrence H Bell. Can dispersal be leveraged to improve microbial inoculant success ? *Trends in Biotechnology*, 40(1):12–21, 2022. ISSN 0167-7799. doi: 10.1016/j.tibtech.2021.04.008. URL `https://doi.org/10.1016/j.tibtech.2021.04.008`.

Joel M. Kniskern, M. Brian Traw, and Joy Bergelson. Salicylic acid and jasmonic acid signaling defense pathways reduce natural bacterial diversity on Arabidopsis thaliana. *Molecular Plant-Microbe Interactions*, 20(12):1512–1522, 2007. ISSN 08940282. doi: 10.1094/MPMI-20-12-1512.

Joel M Kniskern, Luke G Barrett, and Joy Bergelson. Maladaptation in wild populations of the generalist plant pathogen Pseudomonas syringae. *Evolution*, 65(3):818–830, 2011. doi: 10.1111/j.1558-5646.2010.01157.x.Maladaptation.

James M. Kremer, Reza Sohrabi, Bradley C. Paasch, David Rhodes, Caitlin Thireault, Paul Schulze-Lefert, James M. Tiedje, and Sheng Yang He. Peat-based gnotobiotic plant growth systems for Arabidopsis microbiome research, 5 2021. ISSN 17502799.

U. S. Krüger, F. Bak, J. Aamand, O. Nybroe, N. Badawi, B. F. Smets, and A. Dechesne. Novel method reveals a narrow phylogenetic distribution of bacterial dispersers in environmental communities exposed to lowhydration conditions. *Applied and Environmental Microbiology*, 84(7):1–16, 2018. ISSN 10985336. doi: 10.1128/AEM.02857-17.

Enoch Narh Kudjordjie, Rumakanta Sapkota, and Mogens Nicolaisen. Arabidopsis assemble distinct root-associated microbiomes through the synthesis of an array of defense metabolites. *PLoS ONE*, 16(10 October):1–19, 2021. ISSN 19326203. doi: 10.1371/journal.pone.0259171. URL `http://dx.doi.org/10.1371/journal.pone.0259171`.

Bram Kuijper, Rufus A. Johnstone, and Stuart Townley. The Evolution of Multivariate Maternal Effects. *PLoS Computational Biology*, 10(4), 2014. ISSN 15537358. doi: 10.1371/journal.pcbi.1003550.

Alexander Kutschera, Corinna Dawid, Nicolas Gisch, Christian Schmid, Lars Raasch, Tim Gerster, Milena Schäffer, Elwira Smakowska-Luzan, Youssef Belkhadir, A. Corina Vlot, Courtney E. Chandler, Romain Schellenberger, Dominik Schwudke, Robert K. Ernst, Stéphan Dorey, Ralph Hückelhoven, Thomas Hofmann, and Stefanie Ranf. Bacterial medium-chain 3-hydroxy fatty acid metabolites trigger immunity in Arabidopsis plants. *Science*, 364(6436):178–181, 2019. ISSN 10959203. doi: 10.1126/science.aau1279.

Séverine Lacombe, Alejandra Rougon-Cardoso, Emma Sherwood, Nemo Peeters, Douglas Dahlbeck, H Peter van Esse, Matthew Smoker, Ghanasyam Rallapalli, Bart P H J Thomma, Brian Staskawicz, Jonathan D G Jones, and Cyril Zipfel. Interfamily transfer of a plant pattern-recognition receptor confers broad-spectrum bacterial resistance. *Nature Biotechnology*, 28(4):365–369, 2010. ISSN 1087-0156. doi: 10.1038/nbt.1613. URL http://www.nature.com/doifinder/10.1038/nbt.1613.

Leo Lahti and Sudarshan Shetty. microbiome R package, 2017.

Christian Lampei. Multiple simultaneous treatments change plant response from adaptive parental effects to within-generation plasticity, in Arabidopsis thaliana. *Oikos*, 128(3): 368–379, 2019. ISSN 16000706. doi: 10.1111/oik.05627.

Christina Lang-Mladek, Olga Popova, Kathrin Kiok, Marc Berlinger, Branislava Rakic, Werner Aufsatz, Claudia Jonak, Marie Theres Hauser, and Christian Luschnig. Transgenerational inheritance and resetting of stress-induced loss of epigenetic gene silencing in Arabidopsis. *Molecular Plant*, 3(3):594–602, 2010. ISSN 17529867. doi: 10.1093/mp/ssq014. URL http://dx.doi.org/10.1093/mp/ssq014.

Jennifer A Lau and Jay T Lennon. Evolutionary ecology of plant – microbe interactions: soil microbial structure alters selection on plant traits. *New Phytologist*, 192:215–224, 2011.

Sarah Lebeis, Sur Herrera Parades, Derek S. Lundberg, Natalie Breakfield, Jase Gehring, Meredith McDonald, Stephanie Malfatti, Tijana Glavina del Rio, Corbin D. Jones, Susannah G. Tringe, and Jeffery L. Dangl. Salicylic acid modulates colonization of the root microbiome by specific bacterial species. *Science*, 349(6250):860–864, 2015. doi: 10.5061/dryad.238b2.

Jiyoung Lee, Gail M. Teitzel, Kathy Munkvold, Olga del Pozo, Gregory B. Martin, Richard W. Michelmore, and Jean T. Greenberg. Type III secretion and effectors shape the survival and growth pattern of Pseudomonas syringae on leaf surfaces. *Plant Physiology*, 158(4):1803–1818, 2012. ISSN 15322548. doi: 10.1104/pp.111.190686.

Asaf Levy, Isai Salas Gonzalez, Maximilian Mittelviefhaus, Scott Clingenpeel, Sur Herrera Paredes, Jiamin Miao, Kunru Wang, Giulia Devescovi, Kyra Stillman, Freddy Monteiro, Bryan Rangel Alvarez, Derek S. Lundberg, Tse Yuan Lu, Sarah Lebeis, Zhao

Jin, Meredith McDonald, Andrew P. Klein, Meghan E. Feltcher, Tijana Glavina Rio, Sarah R. Grant, Sharon L. Doty, Ruth E. Ley, Bingyu Zhao, Vittorio Venturi, Dale A. Pelletier, Julia A. Vorholt, Susannah G. Tringe, Tanja Woyke, and Jeffery L. Dangl. Genomic features of bacterial adaptation to plants. *Nature Genetics*, 50(1):138–150, 2018. ISSN 15461718. doi: 10.1038/s41588-017-0012-9. URL `http://dx.doi.org/10.1038/s41588-017-0012-9`.

I. M. Lewis. Bacterial antagonism with special reference to the effect of Pseuodmonas fluorescens on spore forming bacteria in soil. *Journal of Bacteriology*, 17(2):89–103, 1929.

Huang Lin and Shyamal Das Peddada. Analysis of compositions of microbiomes with bias correction. *Nature Communications*, 11(1):1–11, 2020. ISSN 20411723. doi: 10.1038/s41467-020-17041-7. URL `http://dx.doi.org/10.1038/s41467-020-17041-7`.

Benson E. Lindsey, Luz Rivero, Chistopher S. Calhoun, Erich Grotewold, and Jelena Brkljacic. Standardized method for high-throughput sterilization of Arabidopsis seeds. *Journal of Visualized Experiments*, 2017(128):1–7, 2017. ISSN 1940087X. doi: 10.3791/56587.

Xueru Liu, Kevin Ao, Jia Yao, Yuelin Zhang, and Xin Li. Engineering plant disease resistance against biotrophic pathogens. *Current Opinion in Plant Biology*, 60:101987, 2021. ISSN 13695266. doi: 10.1016/j.pbi.2020.101987. URL `https://doi.org/10.1016/j.pbi.2020.101987`.

Ana López Sánchez, David Pascual-Pardo, Leonardo Furci, Michael R. Roberts, and Jurriaan Ton. Costs and Benefits of Transgenerational Induced Resistance in Arabidopsis. *Frontiers in Plant Science*, 12(February), 2021. ISSN 1664462X. doi: 10.3389/fpls.2021.644999.

Michael I. Love, Wolfgang Huber, and Simon Anders. Moderated estimation of fold change and dispersion for RNA-seq data with DESeq2. *Genome Biology*, 15(12):1–21, 2014. ISSN 1474760X. doi: 10.1186/s13059-014-0550-8.

Catherine Lozupone, Manuel E. Lladser, Dan Knights, Jesse Stombaugh, and Rob Knight. UniFrac: An effective distance metric for microbial community comparison, 2 2011. ISSN 17517362.

E. Luna, T. J. A. Bruce, M. R. Roberts, V. Flors, and J. Ton. Next-Generation Systemic Acquired Resistance. *Plant Physiology*, 158(2):844–853, 2012. ISSN 0032-0889. doi: 10.1104/pp.111.187468. URL `http://www.plantphysiol.org/cgi/doi/10.1104/pp.111.187468`.

Derek S Lundberg, Sarah L Lebeis, Sur Herrera Paredes, Scott Yourstone, Jase Gehring, Stephanie Malfatti, Julien Tremblay, Anna Engelbrektson, Victor Kunin, Tijana Glavina, Robert C Edgar, Thilo Eickhorst, and Ruth E Ley. Defining the core Arabidopsis thaliana root microbiome. *Nature*, 488(7409):86–90, 2012. ISSN 0028-0836. doi: 10.1038/nature11237. URL `http://dx.doi.org/10.1038/nature11237`.

Ka Wai Ma, Yulong Niu, Yong Jia, Jana Ordon, Charles Copeland, Aurélia Emonet, Niko Geldner, Rui Guan, Sara Christina Stolze, Hirofumi Nakagami, Ruben Garrido-Oter, and Paul Schulze-Lefert. Coordination of microbe–host homeostasis by crosstalk with plant innate immunity. *Nature Plants*, 7(6):814–825, 2021. ISSN 20550278. doi: 10.1038/s41477-021-00920-2. URL http://dx.doi.org/10.1038/s41477-021-00920-2.

Alberto P. Macho and Cyril Zipfel. Plant PRRs and the activation of innate immune signaling. *Molecular Cell*, 54(2):263–272, 2014. ISSN 10974164. doi: 10.1016/j.molcel.2014.03.028. URL http://dx.doi.org/10.1016/j.molcel.2014.03.028.

Siddhartha Mandal, Will Van Treuren, Richard A. White, Merete Eggesbo, Rob Knight, and Shyamal Das Peddada. Analysis of composition of microbiomes: a novel method for studying microbial composition. *Microbial Ecology in Health and Disease*, 26:27663, 2015. ISSN 00987484. doi: 10.3401/mehd.v26.27663.

B. F. J. Manly. *Randomization, Bootstrap, and Monte Carlo Methods in Biology*. Chapman & Hall, London, 2007.

Marcel Martin. Cutadapt removes adapter sequences from high-throughput sequencing reads. *EMBnet.journal*, 17(1):10–12, 2011. doi: https://doi.org/10.14806/ej.17.1.200.

Esteban Martínez-García, Pablo I. Nikel, Max Chavarría, and Víctor de Lorenzo. The metabolic cost of flagellar motion in Pseudomonas putidaKT2440. *Environmental Microbiology*, 16(1):291–303, 2014. ISSN 14622912. doi: 10.1111/1462-2920.12309.

Cameron Martino, James T. Morton, Clarisse A. Marotz, Luke R. Thompson, Anupriya Tripathi, Rob Knight, and Karsten Zengler. A novel sparse compositional technique reveals microbial perturbations. *mSystems*, 4(1), 2019.

Brigitte Mauch-Mani, Ivan Baccelli, Estrella Luna, and Victor Flors. Defense Priming: An Adaptive Part of Induced Resistance. *Annual Review of Plant Biology*, 68:485–512, 2017. ISSN 15452123. doi: 10.1146/annurev-arplant-042916-041132.

PJ McMurdie and S Holmes. An R Package for Reproducible Interactive Analysis and Graphics of Microbiome Census Data. *PLoS ONE*, 8((4):e61217, 2013. doi: https://doi.org/10.1371/journal.pone.0061217.

Yves A. Millet, Cristian H. Danna, Nicole K. Clay, Wisuwat Songnuan, Matthew D. Simon, Danièle Werck-Reichhart, and Frederick M. Ausubel. Innate immune responses activated in Arabidopsis roots by microbe-associated molecular patterns. *Plant Cell*, 22(3):973–990, 2010. ISSN 1532298X. doi: 10.1105/tpc.109.069658.

Diogo Mina, José Alberto Pereira, Teresa Lino-Neto, and Paula Baptista. Epiphytic and Endophytic Bacteria on Olive Tree Phyllosphere: Exploring Tissue and Cultivar Effect. *Microbial Ecology*, 80(1):145–157, 2020. ISSN 1432184X. doi: 10.1007/s00248-020-01488-8.

Tatiana E. Mishina and Jürgen Zeier. Pathogen-associated molecular pattern recognition rather than development of tissue necrosis contributes to bacterial induction of systemic acquired resistance in Arabidopsis. *Plant Journal*, 50(3):500–513, 2007. ISSN 09607412. doi: 10.1111/j.1365-313X.2007.03067.x.

Kana Miyata, Toshinori Kozaki, Yusuke Kouzai, Kenjirou Ozawa, Kazuo Ishii, Erika Asamizu, Yoshihiro Okabe, Yosuke Umehara, Ayano Miyamoto, Yoshihiro Kobae, Kohki Akiyama, Hanae Kaku, Yoko Nishizawa, Naoto Shibuya, and Tomomi Nakagawa. The bifunctional plant receptor, OsCERK1, regulates both chitin-triggered immunity and arbuscular mycorrhizal symbiosis in rice. *Plant and Cell Physiology*, 55(11):1864–1872, 2014. ISSN 14719053. doi: 10.1093/pcp/pcu129.

Carey D. Nadell, Knut Drescher, Ned S. Wingreen, and Bonnie L. Bassler. Extracellular matrix structure governs invasion resistance in bacterial biofilms. *ISME Journal*, 9(8): 1700–1709, 2015. ISSN 17517370. doi: 10.1038/ismej.2014.246.

Dan Naylor, Stephanie Degraaf, Elizabeth Purdom, and Devin Coleman-Derr. Drought and host selection influence bacterial community dynamics in the grass root microbiome. *ISME Journal*, 11(12):2691–2704, 2017. ISSN 17517370. doi: 10.1038/ismej.2017.118. URL http://dx.doi.org/10.1038/ismej.2017.118.

Vladimir Nekrasov, Jing Li, Martine Batoux, Milena Roux, Zhao Hui Chu, Severine Lacombe, Alejandra Rougon, Pascal Bittel, Marta Kiss-Papp, Delphine Chinchilla, H. Peter Van Esse, Lucia Jorda, Benjamin Schwessinger, Valerie Nicaise, Bart P.H.J. Thomma, Antonio Molina, Jonathan D.G. Jones, and Cyril Zipfel. Control of the pattern-recognition receptor EFR by an ER protein complex in plant immunity. *EMBO Journal*, 28(21):3428–3438, 2009. ISSN 14602075. doi: 10.1038/emboj.2009.262. URL http://dx.doi.org/10.1038/emboj.2009.262.

Bruno Pok Man Ngou, Hee Kyung Ahn, Pingtao Ding, and Jonathan D.G. Jones. Mutual potentiation of plant immunity by cell-surface and intracellular receptors. *Nature*, 592 (7852):110–115, 2021. ISSN 14764687. doi: 10.1038/s41586-021-03315-7. URL http://dx.doi.org/10.1038/s41586-021-03315-7.

RH Nilsson, K-H Larsson, AFS Taylor, J Bengtsson-Palme, TS Jeppesen, D Schigel, P Kennedy, K Picard, FO Glöckner, L Tedersoo, I Saar, U Kõljalg, and K. Abarenkov. The UNITE database for molecular identification of fungi: handling dark taxa and parallel taxonomic classifications. *Nucleic Acids Research*, 47(D1):D259–D264, 2018. doi: https://doi.org/10.1093/nar/gky1022.

H Nordberg, M Cantor, S Dusheyko, S Hua, A Poliakov, I Shabalov, T Smirnova, IV Grigoriev, and I. Dubchak. The genome portal of the Department of Energy Joint Genome Institute: 2014 updates. *Nucleic Acids Research*, 42(1):26–31, 2014.

Sarah L. O'Brien, Sean M. Gibbons, Sarah M. Owens, Jarrad Hampton-Marcell, Eric R. Johnston, Julie D. Jastrow, Jack A. Gilbert, Folker Meyer, and Dionysios A. Antonopoulos.

Spatial scale drives patterns in soil bacterial diversity. *Environmental microbiology*, 18(6): 2039–2051, 2016. ISSN 14622920. doi: 10.1111/1462-2920.13231.

Steve L. O'Kane and Ihsan A. Al-Shehbaz. A synopsis of Arabidopsis (Brassicaceae), 1997. ISSN 10553177.

Jari Oksanen. Vegan: ecological diversity. 2021.

Donovan H Parks, Maria Chuvochina, David W Waite, Christian Rinke, Adam Skarshewski, Pierre-Alain Chaumeil, and Philip Hugenholtz. A standardized bacterial taxonomy based on genome phylogeny substantially revises the tree of life. *Nature Biotechnology*, 36(10): 996–1004, 2018. doi: 10.1038/nbt.4229.

Katarzyna Parys, Nicholas R. Colaianni, Ho Seok Lee, Ulrich Hohmann, Natalie Edelbacher, Alen Trgovcevic, Zuzana Blahovska, Duhwa Lee, Alexander Mechtler, Zsuzsanna Muhari-Portik, Mathias Madalinski, Niklas Schandry, Isaac Rodríguez-Arévalo, Claude Becker, Elisabeth Sonnleitner, Arthur Korte, Udo Bläsi, Niko Geldner, Michael Hothorn, Corbin D. Jones, Jeffery L. Dangl, and Youssef Belkhadir. Signatures of antagonistic pleiotropy in a bacterial flagellin epitope. *Cell Host and Microbe*, 29(4):620–634, 2021. ISSN 19346069. doi: 10.1016/j.chom.2021.02.008.

Ales Pecinka and Ortrun Mittelsten Scheid. Stress-induced chromatin changes: A critical view on their heritability. *Plant and Cell Physiology*, 53(5):801–808, 2012. ISSN 00320781. doi: 10.1093/pcp/pcs044.

Ales Pecinka, Marisa Rosa, Adam Schikora, Marc Berlinger, Heribert Hirt, Christian Luschnig, and Ortrun Mittelsten Scheid. Transgenerational stress memory is not a general response in Arabidopsis. *PLoS ONE*, 4(4), 2009. ISSN 19326203. doi: 10.1371/journal.pone.0005202.

Matthew Perisin. The Dynamics of Bacterial Communities Associated with Arabidopsis thaliana. *University of Chicago- PhD Dissertation*, (March), 2016.

E. C. Pielou. The measurement of diversity in different types of biological collections. *Journal of Theoretical Biology*, 13:131–144, 1966. ISSN 10958541. doi: 10.1016/0022-5193(66) 90013-0.

Corné M.J. Pieterse, Antonio Leon-Reyes, Sjoerd Van Der Ent, and Saskia C.M. Van Wees. Networking by small-molecule hormones in plant immunity. *Nature Chemical Biology*, 5 (5):308–316, 2009. ISSN 15524469. doi: 10.1038/nchembio.164.

Corné M.J. Pieterse, Christos Zamioudis, Roeland L. Berendsen, David M. Weller, Saskia C.M. Van Wees, and Peter A.H.M. Bakker. Induced Systemic Resistance by Beneficial Microbes. *Annual Review of Phytopathology*, 52(1):347–375, 2014. ISSN 0066-4286. doi: 10.1146/annurev-phyto-082712-102340. URL http://www.annualreviews.org/doi/abs/10.1146/annurev-phyto-082712-102340.

Alexander Platt, Matthew Horton, Yu S. Huang, Yan Li, Alison E. Anastasio, Ni Wayan Mulyati, Jon Ågren, Oliver Bossdorf, Diane Byers, Kathleen Donohue, Megan Dunning, Eric B. Holub, Andrew Hudson, Valérie Le Corre, Olivier Loudet, Fabrice Roux, Norman Warthmann, Detlef Weigel, Luz Rivero, Randy Scholl, Magnus Nordborg, Joy Bergelson, and Justin O. Borevitz. The scale of population structure in Arabidopsis thaliana. *PLoS Genetics*, 6(2), 2010. ISSN 15537390. doi: 10.1371/journal.pgen.1000843.

Simon Poirier, Olivier Rué, Raphaëlle Peguilhan, Gwendoline Coeuret, Monique Zagorec, Marie Christine Champomier-Vergès, Valentin Loux, and Stéphane Chaillou. Deciphering intra-species bacterial diversity of meat and seafood spoilage microbiota using gyrB amplicon sequencing: A comparative analysis with 16S rDNA V3-V4 amplicon sequencing. *PLoS ONE*, 13(9):1–26, 2018. ISSN 19326203. doi: 10.1371/journal.pone.0204629.

Christian Quast, Elmar Pruesse, Pelin Yilmaz, Jan Gerken, Timmy Schweer, Pablo Yarza, Jörg Peplies, and Frank Oliver Glöckner. The SILVA ribosomal RNA gene database project: improved data processing and web-based tools. *Nucleic Acids Research*, 41(D1): D590–D596, 2013. doi: https://doi.org/10.1093/nar/gks1219.

Thomas P. Quinn, Ionas Erb, Greg Gloor, Cedric Notredame, Mark F. Richardson, and Tamsyn M. Crowley. A field guide for the compositional analysis of any-omics data. *GigaScience*, 8(9):1–14, 2019. ISSN 2047217X. doi: 10.1093/gigascience/giz107.

R Core Team. R: A Language and Environment for Statistical Computing, 2022. URL `https://www.r-project.org/`.

Josep Ramoneda, Johannes J. Le Roux, Emmanuel Frossard, Beat Frey, and Hannes Andres Gamper. Experimental assembly reveals ecological drift as a major driver of root nodule bacterial diversity in a woody legume crop. *FEMS Microbiology Ecology*, 96(6), 5 2020. ISSN 15746941. doi: 10.1093/femsec/fiaa083.

Stefanie Ranf, Nicolas Gisch, Milena Schäffer, Tina Illig, Lore Westphal, Yuriy A Knirel, Patricia M Sánchez-Carballo, Ulrich Zähringer, Ralph Hückelhoven, Justin Lee, and Dierk Scheel. A lectin S-domain receptor kinase mediates lipopolysaccharide sensing in Arabidopsis thaliana. *Nature Immunology*, 16(4):426–433, 2015. ISSN 1529-2908. doi: 10.1038/ni.3124. URL `http://www.nature.com/doifinder/10.1038/ni.3124`.

Charlotte Rich-Griffin, Ruth Eichmann, Marco U. Reitz, Sophie Hermann, Katherine Woolley-Allen, Paul E. Brown, Kate Wiwatdirekkul, Eddi Esteban, Asher Pasha, Karl Heinz Kogel, Nicholas J. Provart, Sascha Ott, and Patrick Schäfer. Regulation of cell type-specific immunity networks in Arabidopsis roots. *Plant Cell*, 32(9):2742–2762, 2020. ISSN 1532298X. doi: 10.1105/TPC.20.00154.

Rusty J. Rodriguez, Joan Henson, Elizabeth Van Volkenburgh, Marshal Hoy, Leesa Wright, Fleur Beckwith, Yong Ok Kim, and Regina S. Redman. Stress tolerance in plants via habitat-adapted symbiosis. *ISME Journal*, 2(4):404–416, 2008. ISSN 17517362. doi: 10.1038/ismej.2007.106.

Matthew B. Rogers, Brian Firek, Min Shi, Andrew Yeh, Rachel Brower-Sinning, Victoria Aveson, Brittany L. Kohl, Anthony Fabio, Joseph A. Carcillo, and Michael J. Morowitz. Disruption of the microbiota across multiple body sites in critically ill children. *Microbiome*, 4(1):66, 2016. ISSN 20492618. doi: 10.1186/s40168-016-0211-0. URL `http://dx.doi.org/10.1186/s40168-016-0211-0`.

Nadin Rohland and David Reich. Cost-effective, high-throughput DNA sequencing libraries for multiplexed target capture. *Genome Research*, 22(5):939–946, 2012. ISSN 10889051. doi: 10.1101/gr.128124.111.

Fabrice Roux, Liping Gao, and Joy Bergelson. Impact of initial pathogen density on resistance and tolerance in a polymorphic disease resistance gene system in Arabidopsis thaliana. *Genetics*, 185(1):283–291, 2010. ISSN 00166731. doi: 10.1534/genetics.109. 112383.

Fabrice Roux, Léa Frachon, and Claudia Bartoli. The Genetic Architecture of Adaptation to Leaf and Root Bacterial Microbiota in Arabidopsis thaliana. *Molecular Biology and Evolution*, 40(5):1–21, 2023. ISSN 15371719. doi: 10.1093/molbev/msad093. URL `https://doi.org/10.1093/molbev/msad093`.

Yusuke Saijo and Eliza Po iian Loo. Plant immunity in signal integration between biotic and abiotic stress responses. *New Phytologist*, 225(1):87–104, 2020. ISSN 14698137. doi: 10.1111/nph.15989.

Isai Salas-González, Guilhem Reyt, Paulina Flis, Valéria Custódio, David Gopaulchan, Niokhor Bakhoum, Tristan P. Dew, Kiran Suresh, Rochus Benni Franke, Jeffery L. Dangl, David E. Salt, and Gabriel Castrillo. Coordination between microbiota and root endodermis supports plant mineral nutrient homeostasis. *Science*, 371(6525), 2021. ISSN 10959203. doi: 10.1126/science.abd0695.

Christian Santos-Medellín, Joseph Edwards, Zachary Liechty, Bao Nguyen, and Venkatesan Sundaresan. Drought Stress Results in a Compartment-Specific Restructuring of Rice Root-Associated Microbiomes. *mBio*, 8(4):1–15, 2017. ISSN 2150-7511. URL `http://www.ncbi.nlm.nih.gov/pubmed/28720730%0Ahttp://www.pubmedcentral.nih.gov/articlerender.fcgi?artid=PMC5516253`.

Ryan Sasada, Michael Weinstein, Aishani Prem, Mingda Jin, and Jeffrey Bhasin. FIGARO: An efficient and objective tool for optimizing microbiome rRNA gene trimming parameters. *Journal of Biomolecular Techniques*, 31(S2), 2020.

Eric W. Sayers, Jeff Beck, J. Rodney Brister, Evan E. Bolton, Kathi Canese, Donald C. Comeau, Kathryn Funk, Anne Ketter, Sunghwan Kim, Avi Kimchi, Paul A. Kitts, Anatoliy Kuznetsov, Stacy Lathrop, Zhiyong Lu, Kelly McGarvey, Thomas L. Madden, Terence D. Murphy, Nuala O'Leary, Lon Phan, Valerie A. Schneider, Françoise Thibaud-Nissen, Bart W. Trawick, Kim D. Pruitt, and James Ostell. Database resources of the National Center for Biotechnology Information. *Nucleic Acids Research*, 48(D1):D9–D16, 2020. ISSN 13624962. doi: 10.1093/nar/gkz899.

Romain Schellenberger, Jérôme Crouzet, Arvin Nickzad, Lin Jie Shu, Alexander Kutschera, Tim Gerster, Nicolas Borie, Corinna Dawid, Maude Cloutier, Sandra Villaume, Sandrine Dhondt-Cordelier, Jane Hubert, Sylvain Cordelier, Florence Mazeyrat-Gourbeyre, Christian Schmid, Marc Ongena, Jean Hugues Renault, Arnaud Haudrechy, Thomas Hofmann, Fabienne Baillieul, Christophe Clément, Cyril Zipfel, Charles Gauthier, Eric Déziel, Stefanie Ranf, and Stephan Dorey. Bacterial rhamnolipids and their 3-hydroxyalkanoate precursors activate Arabidopsis innate immunity through two independent mechanisms. *Proceedings of the National Academy of Sciences of the United States of America*, 118(39): 1–10, 2021. ISSN 10916490. doi: 10.1073/PNAS.2101366118.

C. E. Shannon. The Bell system technical journal. *Journal of the Franklin Institute*, 27(3): 379–423, 1948. ISSN 00160032. doi: 10.1016/s0016-0032(23)90506-5.

Chikako Shindo, Giorgina Bernasconi, and Christian S. Hardtke. Natural genetic variation in arabidopsis: Tools, traits and prospects for evolutionary ecology. *Annals of Botany*, 99 (6):1043–1054, 2007. ISSN 03057364. doi: 10.1093/aob/mcl281.

Gautam Shirsekar, Jane Devos, Sergio M. Latorre, Andreas Blaha, Maique Queiroz Dias, Alba Gonzalez Hernando, Derek S. Lundberg, Hernan A. Burbano, Charles B. Fenster, and Detlef Weigel. Multiple Sources of Introduction of North American Arabidopsis thaliana from across Eurasia. *Molecular Biology and Evolution*, 38(12):5328–5344, 2021. ISSN 15371719. doi: 10.1093/molbev/msab268.

Ana Slaughter, Xavier Daniel, Victor Flors, Estrella Luna, Barbara Hohn, and Brigitte Mauch-Mani. Descendants of primed Arabidopsis plants exhibit resistance to biotic stress. *Plant Physiology*, 158(2):835–843, 2012. ISSN 15322548. doi: 10.1104/pp.111.191593.

Reza Sohrabi, Bradley C. Paasch, Julian A. Liber, and Sheng Yang He. Phyllosphere Microbiome. *Annual Review of Plant Biology*, 74(1), 2023. ISSN 1543-5008. doi: 10.1146/annurev-arplant-102820-032704.

Steven H. Spoel, Jessica S. Johnson, and Xinnian Dong. Regulation of tradeoffs between plant defenses against pathogens with different lifestyles. *Proceedings of the National Academy of Sciences of the United States of America*, 104(47):18842–18847, 2007. ISSN 00278424. doi: 10.1073/pnas.0708139104.

Pavel Svoboda, Eva S. Lindström, Omneya Ahmed Osman, and Silke Langenheder. Dispersal timing determines the importance of priority effects in bacterial communities. *ISME Journal*, 12(2):644–646, 2018. ISSN 17517370. doi: 10.1038/ismej.2017.180. URL `http://dx.doi.org/10.1038/ismej.2017.180`.

Dingzhong Tang, Guoxun Wang, and Jian Min Zhou. Receptor kinases in plant-pathogen interactions: More than pattern recognition. *Plant Cell*, 29(4):618–637, 2017. ISSN 1532298X. doi: 10.1105/tpc.16.00891.

Paulo José PL Teixeira, Nicholas R. Colaianni, Connor R. Fitzpatrick, and Jeffery L. Dangl. Beyond pathogens: microbiota interactions with the plant immune system.

Current Opinion in Microbiology, 49(September):7–17, 2019. ISSN 18790364. doi: 10.1016/j.mib.2019.08.003.

Paulo J.P.L. Teixeira, Nicholas R. Colaianni, Theresa F. Law, Jonathan M. Conway, Sarah Gilbert, Haofan Li, Isai Salas-González, Darshana Panda, Nicole M. Del Risco, Omri M. Finkel, Gabriel Castrillo, Piotr Mieczkowski, Corbin D. Jones, and Jeffery L. Dangl. Specific modulation of the root immune system by a community of commensal bacteria. *Proceedings of the National Academy of Sciences of the United States of America*, 118(16), 2021. ISSN 10916490. doi: 10.1073/pnas.2100678118.

The Arabidopsis Genome Initiative. Analysis of the genome sequence of the flowering plant Arabidopsis thaliana. *Nature*, 408:796–815, 2000. ISSN 10227954. doi: 10.1134/S1022795411020074.

Andrzej Tkacz, Marion Hortala, and Philip S. Poole. Absolute quantitation of microbiota abundance in environmental samples. *Microbiome*, 6(1):1–13, 2018. ISSN 20492618. doi: 10.1186/s40168-018-0491-7.

Andrzej Tkacz, Eloïne Bestion, Zhiyan Bo, Marion Hortala, and Philip S. Poole. Influence of plant fraction, soil, and plant species on microbiota: A multikingdom comparison. *mBio*, 11(1), 2020. ISSN 21507511. doi: 10.1128/mBio.02785-19.

Hirokazu Toju, Rachel L. Vannette, Marie Pierre L. Gauthier, Manpreet K. Dhami, and Tadashi Fukami. Priority effects can persist across floral generations in nectar microbial metacommunities. *Oikos*, 127(3):345–352, 2018. ISSN 16000706. doi: 10.1111/oik.04243.

Charlotte Tollenaere, Hanna Susi, and Anna Liisa Laine. Evolutionary and Epidemiological Implications of Multiple Infection in Plants. *Trends in Plant Science*, 21(1):80–90, 2016. ISSN 13601385. doi: 10.1016/j.tplants.2015.10.014. URL `http://dx.doi.org/10.1016/j.tplants.2015.10.014`.

M. Brian Traw, Joel M. Kniskern, and Joy Bergelson. SAR increases fitness of Arabidopsis thaliana in the presence of natural bacterial pathogens. *Evolution*, 61(10):2444–2449, 2007. ISSN 00143820. doi: 10.1111/j.1558-5646.2007.00211.x.

Elhanan Tzipilevich, Dor Russ, Jeffery L. Dangl, and Philip N. Benfey. Plant immune system activation is necessary for efficient root colonization by auxin-secreting beneficial bacteria. *Cell Host and Microbe*, 29(10):1507–1520, 2021. ISSN 19346069. doi: 10.1016/j.chom.2021.09.005. URL `https://doi.org/10.1016/j.chom.2021.09.005`.

T. Uller, S. Nakagawa, and S. English. Weak evidence for anticipatory parental effects in plants and animals. *Journal of Evolutionary Biology*, 26(10):2161–2170, 2013. ISSN 1010061X. doi: 10.1111/jeb.12212.

Erik J van Hannen, Miranda P van Agterveld, Herman J Gons, and Hendrikus J Laanbroek. Revealing genetic diversity of eukaryotic microorganisms in aquatic environments by denaturing gradient gel electrophoresis. *Journal of Phycology*, 213:206–213, 1998.

Marieke Van Hulten, Maaike Pelser, L. C. Van Loon, Corné M.J. Pieterse, and Jurriaan Ton. Costs and benefits of priming for defense in Arabidopsis. *Proceedings of the National Academy of Sciences of the United States of America*, 103(14):5602–5607, 2006. ISSN 00278424. doi: 10.1073/pnas.0510213103.

Rachel L. Vannette and Tadashi Fukami. Dispersal enhances beta diversity in nectar microbes. *Ecology Letters*, 20:901–910, 2017. doi: 10.1111/ele.12787.

Nathan Vannier, Matthew Agler, and Stéphane Hacquard. Microbiota-mediated disease resistance in plants. *PLoS Pathogens*, 15(6):1–7, 2019. ISSN 15537374. doi: 10.1371/journal.ppat.1007740.

André C. Velásquez, José C. Huguet-Tapia, and Sheng Yang He. Shared in planta population and transcriptomic features of nonpathogenic members of endophytic phyllosphere microbiota. *Proceedings of the National Academy of Sciences of the United States of America*, 119(14):1–12, 2022. ISSN 10916490. doi: 10.1073/pnas.2114460119.

Mark Vellend. Conceptual synthesis in community ecology. *Quarterly Review of Biology*, 85(2):183–206, 2010. ISSN 00335770. doi: 10.1086/652373.

Eline H. Verbon, Louisa M. Liberman, Jiayu Zhou, Jiayu Yin, Corné M.J. Pieterse, Philip N. Benfey, Ioannis A. Stringlis, and Ronnie de Jonge. Cell-type-specific transcriptomics reveals that root hairs and endodermal barriers play important roles in beneficial plant-rhizobacterium interactions. *Molecular Plant*, 16:1–18, 2023. doi: 10.1016/j.molp.2023.06.001.

J. Kevin Vessey. Plant growth promoting rhizobacteria as biofertilizers. *Plant and Soil*, 255(2):571–586, 2003. ISSN 0032079X. doi: 10.1023/A:1026037216893.

M. Madlen Vetter, Ilkka Kronholm, Fei He, Heidrun Häweker, Matthieu Reymond, Joy Bergelson, Silke Robatzek, and Juliette De Meaux. Flagellin perception varies quantitatively in arabidopsis thaliana and its relatives. *Molecular Biology and Evolution*, 29(6):1655–1667, 2012. ISSN 07374038. doi: 10.1093/molbev/mss011.

Madlen Vetter, Talia L. Karasov, and Joy Bergelson. Differentiation between MAMP Triggered Defenses in Arabidopsis thaliana. *PLoS Genetics*, 12(6), 6 2016. ISSN 15537404. doi: 10.1371/journal.pgen.1006068.

Cyrille Violle, Marie-Laure Navas, Denis Vile, Elena Kazakou, Claire Fortunel, Irène Hummel, and Eric Garnier. Let the concept of trait be functional! *Oikos*, 116(5):882–892, 2007. ISSN 0030-1299. doi: 10.1111/j.2007.0030-1299.15559.x.

Julia A. Vorholt. Microbial life in the phyllosphere, 12 2012. ISSN 17401526.

Navish Wadhwa and Howard C. Berg. Bacterial motility: machinery and mechanisms. *Nature Reviews Microbiology*, 20(3):161–173, 2022. ISSN 17401534. doi: 10.1038/s41579-021-00626-4.

Maggie R Wagner, Derek S. Lundberg, Devin Coleman-Derr, Susannah G. Tringe, Jeffery L. Dangl, and Thomas Mitchell-Olds. Natural soil microbes alter flowering phenology and the intensity of selection on flowering time in a wild Arabidopsis relative. *Ecology Letters*, 17:717–726, 2014. doi: 10.1111/ele.12276.

Dale R. Walters, Linda Paterson, David J. Walsh, and Neil D. Havis. Priming for plant defense in barley provides benefits only under high disease pressure. *Physiological and Molecular Plant Pathology*, 73(4-5):95–100, 11 2008. ISSN 08855765. doi: 10.1016/j. pmpp.2009.03.002.

J. Wan, K. Tanaka, X.-C. Zhang, G. H. Son, L. Brechenmacher, T. H. N. Nguyen, and G. Stacey. LYK4, a Lysin Motif Receptor-Like Kinase, Is Important for Chitin Signaling and Plant Innate Immunity in Arabidopsis. *Plant Physiology*, 160(September):396–406, 2012. ISSN 0032-0889. doi: 10.1104/pp.112.201699.

Jinrong Wan, Xue Cheng Zhang, David Neece, Katrina M. Ramonell, Steve Clough, Sung Yong Kim, Minviluz G. Stacey, and Gary Stacey. A LysM receptor-like kinase plays a critical role in chitin signaling and fungal resistance in Arabidopsis. *Plant Cell*, 20 (2):471–481, 2008. ISSN 1532298X. doi: 10.1105/tpc.107.056754.

Sophie Weiss, Zhenjiang Zech Xu, Shyamal Peddada, Amnon Amir, Kyle Bittinger, Antonio Gonzalez, Catherine Lozupone, Jesse R. Zaneveld, Yoshiki Vázquez-Baeza, Amanda Birmingham, Embriette R. Hyde, and Rob Knight. Normalization and microbial differential abundance strategies depend upon data characteristics. *Microbiome*, 5(1):1–18, 2017. ISSN 20492618. doi: 10.1186/s40168-017-0237-y.

Hadley Wickham. *ggplot2: Elegant Graphics for Data Analysis*. Springer-Verlag New York, 2016. URL `https://ggplot2.tidyverse.org`.

Roland Willmann, Heini M. Lajunen, Gitte Erbs, Mari Anne Newman, Dagmar Kolb, Kenichi Tsuda, Fumiaki Katagiri, Judith Fliegmann, Jean Jacques Bono, Julie V. Cullimore, Anna K. Jehle, Friedrich Götz, Andreas Kulik, Antonio Molinaro, Volker Lipka, Andrea A. Gust, and Thorsten Nürnberger. Arabidopsis lysin-motif proteins LYM1 LYM3 CERK1 mediate bacterial peptidoglycan sensing and immunity to bacterial infection. *Proceedings of the National Academy of Sciences of the United States of America*, 108(49): 19824–19829, 2011. ISSN 00278424. doi: 10.1073/pnas.1112862108.

Kathrin Wippel, Ke Tao, Yulong Niu, Rafal Zgadzaj, Niklas Kiel, Rui Guan, Eik Dahms, Pengfan Zhang, Dorthe B. Jensen, Elke Logemann, Simona Radutoiu, Paul Schulze-Lefert, and Ruben Garrido-Oter. Host preference and invasiveness of commensal bacteria in the Lotus and Arabidopsis root microbiota. *Nature Microbiology*, 6(9):1150–1162, 2021. ISSN 20585276. doi: 10.1038/s41564-021-00941-9.

Alexandra B Wolf, Max-bernhard Rudnick, Wietse De Boer, and George A Kowalchuk. Early colonizers of unoccupied habitats represent a minority of the soil bacterial community. *FEMS Microbiology Ecology*, 91(January):1–9, 2015. doi: 10.1093/femsec/fiv024.

Katarzyna W. Wolinska, Nathan Vannier, Thorsten Thiergart, Brigitte Pickel, Sjoerd Gremmen, Anna Piasecka, Mariola Piślewska-Bednarek, Ryohei Thomas Nakano, Youssef Belkhadir, Paweł Bednarek, and Stéphane Hacquard. Tryptophan metabolism and bacterial commensals prevent fungal dysbiosis in Arabidopsis roots. *Proceedings of the National Academy of Sciences of the United States of America*, 118(49), 2021. ISSN 10916490. doi: 10.1073/pnas.2111521118.

Ines Wyrsch, Ana Domínguez-Ferreras, Niko Geldner, and Thomas Boller. Tissue-specific FLAGELLIN-SENSING 2 (FLS2) expression in roots restores immune responses in Arabidopsis fls2 mutants. *New Phytologist*, 206(2):774–784, 2015. ISSN 14698137. doi: 10.1111/nph.13280.

Xiu-fang Xin, Kinya Nomura, Kyaw Aung, André C Velásquez, Jian Yao, Freddy Boutrot, and Jeff H Chang. Bacteria establish an aqueous living space in plants crucial for virulence. *Nature Publishing Group*, 539(7630):524–529, 2016. ISSN 0028-0836. doi: 10.1038/nature20166. URL `http://dx.doi.org/10.1038/nature20166`.

Koste A. Yadeta and Bart P.H.J. Thomma. The xylem as battleground for plant hosts and vascular wilt pathogens. *Frontiers in Plant Science*, 4(APR):1–12, 2013. ISSN 1664462X. doi: 10.3389/fpls.2013.00097.

Ke Yu, Corné M.J. Pieterse, Peter A.H.M. Bakker, and Roeland L. Berendsen. Beneficial microbes going underground of root immunity, 10 2019. ISSN 13653040.

Minhang Yuan, Zeyu Jiang, Guozhi Bi, Kinya Nomura, Menghui Liu, Boying Cai, Jianmin Zhou, Sheng Yang He, and Xiu-fang Xin. Pattern-recognition receptors are required for NLR-mediated plant immunity. *Nature*, 592(7852):105–109, 2021. doi: 10.1038/s41586-021-03316-6.Pattern-recognition.

Lu Zhang, Liangbin Yuan, Christian Staehelin, Yin Li, Jiuxiao Ruan, Zhenwei Liang, Zhiping Xie, Wei Wang, Jianghui Xie, and Shangzhi Huang. The LYSIN MOTIF-CONTAINING RECEPTOR-LIKE KINASE 1 protein of banana is required for perception of pathogenic and symbiotic signals. *New Phytologist*, 223(3):1530–1546, 2019. ISSN 14698137. doi: 10.1111/nph.15888.

Feng Zhou, Aurélia Emonet, Valérie Dénervaud Tendon, Peter Marhavy, Dousheng Wu, Thomas Lahaye, and Niko Geldner. Co-incidence of Damage and Microbial Patterns Controls Localized Immune Responses in Roots. *Cell*, 180(3):440–453, 2 2020. ISSN 10974172. doi: 10.1016/j.cell.2020.01.013.

Cyril Zipfel, Silke Robatzek, Lionel Navarro, Edward J Oakeley, Jonathan D G Jones, Georg Felix, and Thomas Boller. Bacterial disease resistance in Arabidopsis through flagellin perception. *Nature*, 428(6984):764–767, 2004. ISSN 0028-0836. doi: 10.1038/nature02485.

Cyril Zipfel, Gernot Kunze, Delphine Chinchilla, Anne Caniard, Jonathan D G Jones, Thomas Boller, and Georg Felix. Perception of the Bacterial PAMP EF-Tu by the Recep-

tor EFR Restricts Agrobacterium-Mediated Transformation. *Cell*, 125(4):749–760, 2006. ISSN 00928674. doi: 10.1016/j.cell.2006.03.037.